

## University Library



Author/Filing Title ..... *ECK, T.* .....

Class Mark ..... *T* .....

Please note that fines are charged on ALL  
overdue items.

--	--	--

0403694671





# A APPENDIX

The aim of this appendix is to complete the thesis. Novel and original work that was presented in the previous chapters is complemented by the appendix.

Additionally, well known essential theories, such as the beam's and plate's partial differential equations, are also presented herein to enable a fast understanding when deriving vibrational energy flow (VEF) of these structures. In particular the derivation of the internal forces and moments of a transversally vibrating beam and plate was included, in order to gain a better understanding when deriving the VEF expressions of beams and plates.

Further, results obtained on the theoretical and practical computation of VEF in beam and plate structures are presented using tables and figures.



Loughborough  
University

Pilkington Library

Date 24/2/09

Class

T

Acc

No.

0403694671

## Appendix A1

## Partial Differential Beam Equation

The partial differential beam equation is derived using classical Euler-Bernoulli theory. The beam is assumed to be homogenous and isotropic. The displacement is considered to be small, thus  $\tan(\alpha) \approx \alpha$ . As shown in

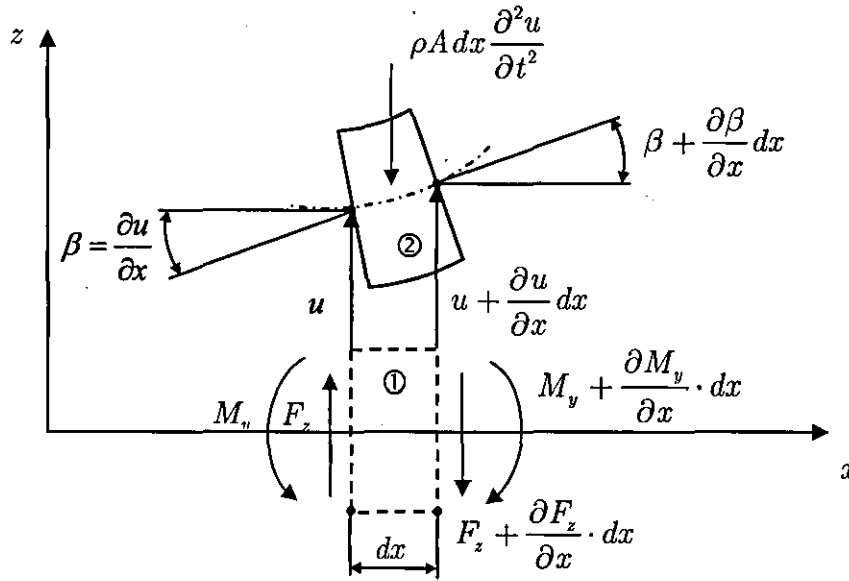


**Figure A1.1** Infinitesimal small beam element under bending.

Figure A1.1, the infinitesimal small increase in angle  $(\partial\beta/\partial x)dx$  at the right-hand side due to flexural wave motion of the small beam element is given as:

$$\frac{\partial^2 u}{\partial x^2} dx = -\frac{x}{z}. \quad (\text{A1.1})$$

Here,  $u$  is the lateral displacement, which is a function of space and time. Vibration behaviour is derived from the linear elastic stress-strain-displacement relations. Inserting the strain-displacement relation,  $\epsilon_x = x/dx$ ,

where  $\varepsilon_x$  is the normal strain in the  $x$  direction, into equation (A1.1), the normal tensile strain on the small beam element is defined as:

$$\varepsilon_x = -z \frac{\partial^2 u}{\partial x^2}. \quad (\text{A1.2})$$

Applying Hooke's law for a linear elastic medium, the normal linear stress distribution of the small beam element is given by:

$$\sigma_x = -Ez \frac{\partial^2 u}{\partial x^2}. \quad (\text{A1.3})$$

The material dependent constant  $E$  is known as Young's modulus. Multiplying the normal stress  $\sigma_x$  by a moment arm  $z$  that is perpendicular to the cross-sectional area  $A$  and integrating this product over the beam's cross-sectional area, the bending moment  $M_y$  can be found to be:

$$M_y = \int_A \sigma_x z dA = -E \frac{\partial^2 u(x,t)}{\partial x^2} \int_A z^2 dA = -EI \frac{\partial^2 u(x,t)}{\partial x^2}. \quad (\text{A1.4})$$

The material geometry dependent factor  $I$  is the second moment of area. By taking moment equilibrium on the small beam element (positive sign in clockwise direction):

$$-M_y + \left( M_y + \frac{\partial M_y}{\partial x} dx \right) + F_z dx = 0, \quad (\text{A1.5})$$

one can find the shear force  $F_z$  to be:

$$F_z = -\frac{\partial M_y}{\partial x} = EI \frac{\partial^3 u(x,t)}{\partial x^3}. \quad (\text{A1.6})$$

It can be seen that the shear force is the spatial derivative of the bending moment. The partial differential equation of motion may be derived by applying Newton's second law of motion on the infinitesimal small beam element as:

$$F_z - \left( F_z + \frac{\partial F_z}{\partial x} dx \right) = \rho A dx \frac{\partial^2 u}{\partial t^2}. \quad (\text{A1.7})$$

The relation given in equation (A1.7) is the internal reaction to external load application. Substituting equation (A1.6) into equation (A1.7), the general inhomogeneous partial differential equation of a transversally excited beam forced by a general load is given by:

$$EI \frac{\partial^4 u(x,t)}{\partial x^4} + \rho A \frac{\partial^2 u(x,t)}{\partial t^2} = p(x,t), \quad (\text{A1.8})$$

where  $p(x,t)$  is the load applied per unit length. In the case of a point force excitation, the applied load term can be written as:

$$p(x,t) = F_0 \delta(x - x_0) e^{j\omega t}. \quad (\text{A1.9})$$

Here,  $F_0$  is the applied force amplitude,  $j = \sqrt{-1}$ ,  $\omega/2\pi$  is the excitation frequency applied at excitation location  $x_0$  and  $\delta$  represents Dirac's delta function. The Euler-Bernoulli theory neglects shear deformation and rotary inertia effects. The upper frequency limit is given by  $\lambda \leq 6t$ , where  $\lambda$  is the wavelength and,  $t$  is the beam's thickness. Linear hysteretic damping can be introduced to the beam's partial differential equation straight forwardly by employing a loss factor  $\eta$  in the normal stress equation (A1.3) as [114]:

$$\sigma_x = -E(1 + j\eta) z \frac{\partial^2 u}{\partial x^2}. \quad (\text{A1.10})$$

## Appendix A2

### Time-Averaging of Complex Instantaneous Quantities

The time-averaged vibrational energy flow in a beam under sinusoidal load variation is given by:

$$\langle P(t) \rangle_t = \frac{1}{T} \left( \int_0^T F_s v_s dt - \int_0^T M_B \omega_B dt \right). \quad (\text{A2.1})$$

If one assumes the shear force  $F_s$  as a real quantity, the following can be written as:

$$F_s = F_{s_0} \cos(\omega t). \quad (\text{A2.2})$$

The respective translational velocity component  $v_s$ , which is also real, is given by:

$$v_s = v_{s_0} \cos(\omega t - \varphi). \quad (\text{A2.3})$$

Herein,  $\varphi$  is the phase difference between force and velocity. Analogously, the bending moment  $M_B$  is:

$$M_B = M_{B_0} \cos(\omega t), \quad (\text{A2.4})$$

and the angular velocity  $\omega_B$  is given by:

$$\omega_B = \omega_{B_0} \cos(\omega t - \varphi). \quad (\text{A2.5})$$



By substituting the above defined force and moment terms as well as its appropriate velocity components into equation (A2.1), the time-averaged energy flow of these real quantities is:

$$P_r = \frac{\cos(\varphi)}{2} (F_{s_0} v_{s_0} - M_{B_0} \omega_{B_0}). \quad (\text{A2.6})$$

Analogously, when using pure imaginary force, moments, and velocities, defined by the sine function, the time-averaged energy flow of imaginary quantities is given by:

$$P_i = \frac{\sin(\varphi)}{2} (F_{s_0} v_{s_0} - M_{B_0} \omega_{B_0}). \quad (\text{A2.7})$$

However, in this work the shear force, translational velocity, bending moment and angular velocity are employed as complex quantities and, thus,  $F_s = F_{s_0} e^{j\omega t}$ ,  $v_s = v_{s_0} e^{j(\omega t - \varphi)}$ ,  $M_B = M_{B_0} e^{j\omega t}$  and  $\omega_B = \omega_{B_0} e^{j(\omega t - \varphi)}$ . Neglecting the time independent amplitudes, it can be shown that:

$$\int_0^T \cos(\omega t) \cos(\omega t - \varphi) dt = \frac{1}{2} \Re \left\{ \int_0^T e^{j\omega t} (e^{j(\omega t - \varphi)})^* dt \right\}. \quad (\text{A2.8})$$

The asterisk \* denotes conjugate complex of the velocity term and,  $\Re$  denotes the real part of the complex energy flow expression. By solving the integral on the right-hand side of equation (A2.8), time-averaging of complex products can be written as:

$$\frac{1}{2} \Re \left\{ \int_0^T e^{j\omega t} (e^{j(\omega t - \varphi)})^* dt \right\} = \frac{1}{2} \Re \left\{ e^{j\omega t} (e^{j(\omega t - \varphi)})^* \right\} = \frac{1}{2} \Re \left\{ (e^{j\omega t})^* e^{j(\omega t - \varphi)} \right\}. \quad (\text{A2.9})$$

Thus, in general it can be written [102]:

$$\langle \Re \{A\} \Re \{B\} \rangle_t = \frac{1}{2} \Re \{AB^*\} = \frac{1}{2} \Re \{A^*B\}. \quad (\text{A2.10})$$

Here,  $\langle \rangle_t$  denotes the time-averaging of two complex quantities,  $A$  and  $B$ . Similarly, when the time-averaged product of the imaginary part is of interest:

$$\langle \Im \{A\} \Im \{B\} \rangle_t = \frac{1}{2} \Im \{AB^*\} = \frac{1}{2} \Im \{A^*B\}. \quad (\text{A2.11})$$

## Appendix A3

### Partial Differential Plate Equation

The derivation of the plate's differential equation is similar to the beam case. Also here, classical Euler-Bernoulli theory is employed. The plate is considered

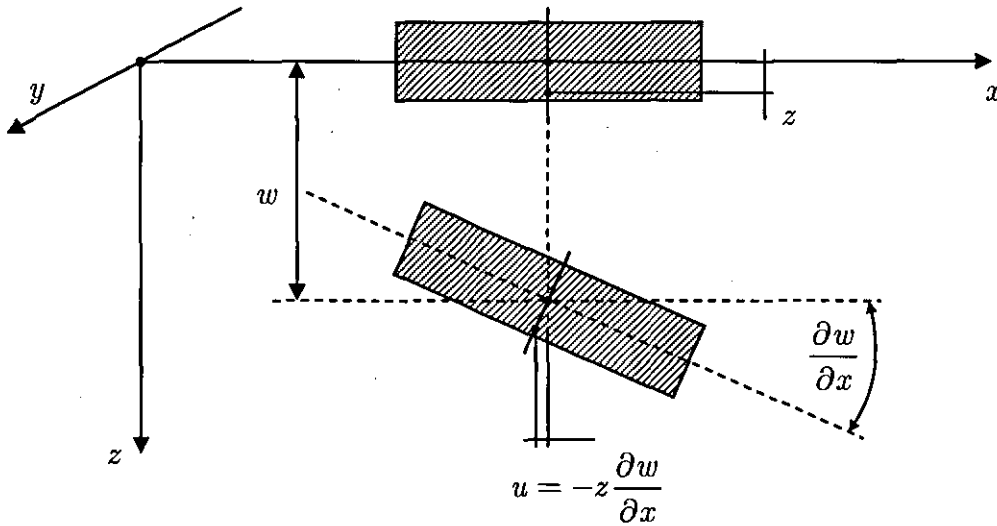


**Figure A3.1** Deflection and rotation of the plate element under lateral load.

to be homogeneous and isotropic. Thin plates are considered only. Thus,  $h \ll L_x$  and  $h \ll L_y$ , where  $L_x$  is the plate's length,  $L_y$  is the plate's width and,  $h$  is the plate's thickness. Further, it is assumed that the normal of the middle plane before bending is deformed into the normal of the middle plane after bending. The stress in direction of the plate's thickness  $\sigma_z$  is neglected. Finally, the middle plane remains unstrained after bending [136]. In contrast to the beam, the infinitesimal small plate element experiences deformation in longitudinal and lateral direction. By assuming linear elastic deformations, longitudinal strain, lateral strain, and shear strain components occur.

Figure A3.1 displays the deformation of a plate part under lateral loading. When loading the plate, the plate element experiences a deflection,  $w$ . If one assumes small deflections, the respective deformation angle  $\alpha$  is then

approximated by  $\tan(\alpha) \approx \alpha \approx \partial w / \partial x$ . If one considers the motion  $u$  of a point in the element and the strain is the partial derivative of this small point motion, i.e.  $\varepsilon_{xx} = \partial u / \partial x$ , then the strain-deflection relation is given as:

$$\varepsilon_{xx} = -z \frac{\partial^2 w}{\partial x^2}. \quad (\text{A3.1})$$

Similarly, the motion of a small point  $v$  into the  $y$  direction can be defined as:

$$\varepsilon_{yy} = -z \frac{\partial^2 w}{\partial y^2}. \quad (\text{A3.2})$$

It can be shown that the sum of  $\partial u / \partial y + \partial v / \partial x$  can be identified as shear strain  $\varepsilon_{xy}$  and, thus, it follows that:

$$\varepsilon_{xy} = -2z \frac{\partial^2 w}{\partial x \partial y}. \quad (\text{A3.3})$$

Using Hooke's law, the stress-strain relations of all three strain components are given by:

$$\varepsilon_{xx} = \frac{1}{E} (\sigma_{xx} - \nu \sigma_{yy}), \quad (\text{A3.4})$$

$$\varepsilon_{yy} = \frac{1}{E} (\sigma_{yy} - \nu \sigma_{xx}), \quad (\text{A3.5})$$

$$\varepsilon_{xy} = \frac{1}{G} \tau_{xy}. \quad (\text{A3.6})$$

Herein,  $\nu$  is Poisson's ratio,  $E$  is Young's modulus,  $G = E / 2(1 + \nu)$  is the shear modulus and,  $\tau_{xy}$  is the shear stress. Using equations (A3.1) to (A3.3)

and equations (A3.4) to (A3.6), the following stress-deflection relations can be obtained [136]:

$$\sigma_{xx} = -\frac{Ez}{1-\nu^2} \left( \frac{\partial^2 w}{\partial x^2} + \nu \frac{\partial^2 w}{\partial y^2} \right). \quad (\text{A3.7})$$

$$\sigma_{yy} = -\frac{Ez}{1-\nu^2} \left( \frac{\partial^2 w}{\partial y^2} + \nu \frac{\partial^2 w}{\partial x^2} \right). \quad (\text{A3.8})$$

$$\tau_{xy} = -\frac{Ez}{1+\nu} \frac{\partial^2 w}{\partial x \partial y}. \quad (\text{A3.9})$$

To obtain moments, occurring in a thin plate under lateral load, the above defined stresses are integrated over the plate's thickness. Thus [108]:

$$M_{xx} = \int_{-h/2}^{h/2} \sigma_{xx} z dz = -D \left( \frac{\partial^2 w}{\partial x^2} + \nu \frac{\partial^2 w}{\partial y^2} \right), \quad (\text{A3.10})$$

$$M_{yy} = \int_{-h/2}^{h/2} \sigma_{yy} z dz = -D \left( \frac{\partial^2 w}{\partial y^2} + \nu \frac{\partial^2 w}{\partial x^2} \right), \quad (\text{A3.11})$$

$$M_{xy} = -M_{yx} = -\int_{-h/2}^{h/2} \tau_{xy} z dz = D(1-\nu) \frac{\partial^2 w}{\partial x \partial y}, \quad (\text{A3.12})$$

with  $D$  being the flexural rigidity of the plate given as:

$$D = \frac{Eh^3}{12(1-\nu^2)}. \quad (\text{A3.13})$$

The negative sign in front of the integral expression in equation (A3.12) is due

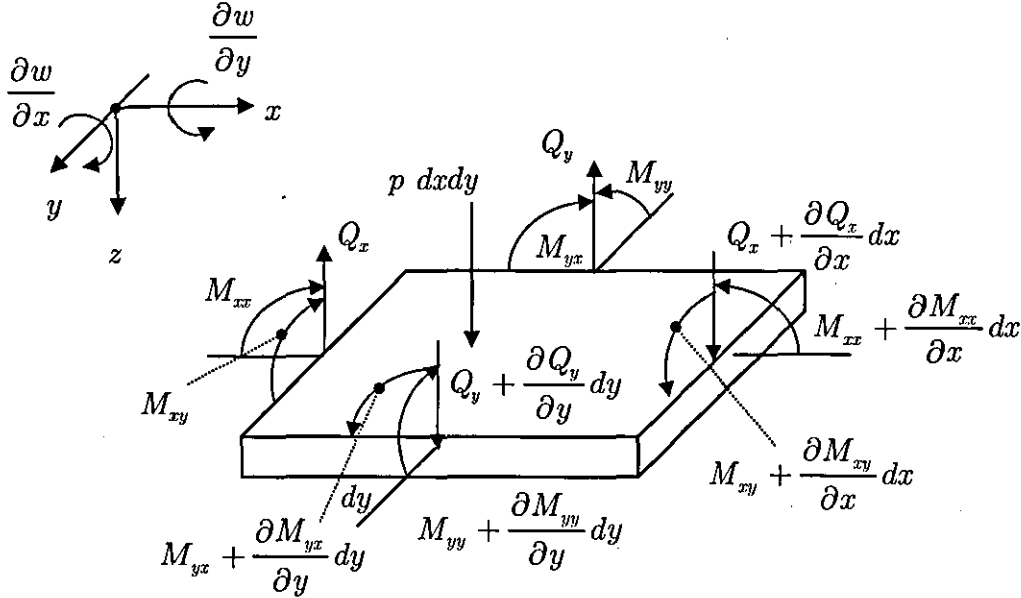


**Figure A3.2** Forces and moments on small plate element.

to equilibrium with the shear force, according to the sign conventions displayed in Figure A3.2. Figure A3.2 also displays all the moments and forces acting on an infinitesimal small plate element. To obtain the shear forces, one may take moment equilibrium about the  $x$ -axis and  $y$ -axis. By taking the moment equilibrium about the  $x$ -axis:

$$\frac{\partial M_{xy}}{\partial x} dxdy - \frac{\partial M_{yx}}{\partial y} dydx + Q_y dxdy = 0, \quad (\text{A3.14})$$

as well as about the  $y$ -axis:

$$\frac{\partial M_{yx}}{\partial y} dydx + \frac{\partial M_{xy}}{\partial x} dxdy - Q_x dydx = 0, \quad (\text{A3.15})$$

the shear forces  $Q_x$  and  $Q_y$  per unit length are given as:

$$Q_x = -D \frac{\partial}{\partial x} \left( \frac{\partial^2 w}{\partial x^2} + \frac{\partial^2 w}{\partial y^2} \right), \quad (\text{A3.16})$$

$$Q_y = -D \frac{\partial}{\partial y} \left( \frac{\partial^2 w}{\partial y^2} + \frac{\partial^2 w}{\partial x^2} \right). \quad (\text{A3.17})$$

It can be seen from equations (A3.16) and (A3.17) that the direction of the shear forces, as shown in Figure A3.2, is in opposite direction. From Figure A3.2 it can also be seen that the infinitesimal increment of the shear forces, bending moments, and twisting moments needs to be taken into account only. Applying Newton's second law of motion to the small plate element yields to:

$$\frac{\partial Q_x}{\partial x} dx dy + \frac{\partial Q_y}{\partial y} dy dx + p dx dy = \rho h dx dy \frac{\partial^2 w}{\partial t^2}. \quad (\text{A3.18})$$

Substituting equations (A3.16) and (A3.17) into (A3.18), the inhomogeneous partial differential equation of a plate, loaded laterally, may be written as:

$$D \left( \frac{\partial^4 w}{\partial x^4} + 2 \frac{\partial^4 w}{\partial x^2 \partial y^2} + \frac{\partial^4 w}{\partial y^4} \right) + \rho h \frac{\partial^2 w}{\partial t^2} = p. \quad (\text{A3.19})$$

By applying the biharmonic of the two-dimensional Laplace operator as:

$$\nabla^4 = \nabla^2 \cdot \nabla^2 = \frac{\partial^4}{\partial x^4} + 2 \frac{\partial^4}{\partial x^2 \partial y^2} + \frac{\partial^4}{\partial y^4}, \quad (\text{A3.20})$$

equation (A3.19) in its final form can be written as:

$$D \nabla^4 w(x, y, t) + \rho h \frac{\partial^2 w(x, y, t)}{\partial t^2} = p(x, y, t). \quad (\text{A3.21})$$

## Appendix A4

### Numerical Differentiation Using Finite Differences

The most common technique to obtain derivatives from tabulated data is the use of finite differences. A finite difference is the algebraic difference between data points of the function  $f(x)$  separated by the spacing  $\Delta x$ . The so-called forward difference is given by [137]:

$$\Delta f(x) = f(x + \Delta x) - f(x). \quad (\text{A4.1})$$

$\Delta$  is known as the forward difference operator. Analogously, the backward difference is defined as:

$$\nabla f(x) = f(x) - f(x - \Delta x). \quad (\text{A4.2})$$

Herein,  $\nabla$  is the backward difference operator. It can be seen that forward differences employ points upwards the point of interest and backward differences use points downwards the point of interest. The third type of differences is the so-called central differences  $\delta$ . Its first order form is given by [138]:

$$\delta f(x) = f\left(x + \frac{1}{2}\Delta x\right) - f\left(x - \frac{1}{2}\Delta x\right). \quad (\text{A4.3})$$

Central differences employ points upwards and downwards the point of interest. Finite differences can be of different order  $n$ . Forward differences of different order are related to each other as [137]:

$$\Delta^n f(x) = \Delta[\Delta^{n-1} f(x)]. \quad (\text{A4.4})$$



Analogously, equation (A4.4) can also be applied to backward and central differences. It can be shown that the so-called difference quotient [137] is related to the infinitesimal calculus of order  $n$  as [139]:

$$D^n f(x) = \lim_{\Delta x \rightarrow 0} \frac{\Delta^n f(x)}{(\Delta x)^n}. \quad (\text{A4.5})$$

Here,  $D_n$  is the differentiation operator of order  $n$ ,  $\Delta n$  is the forward difference operator of order  $n$  and  $\Delta x$  is the spacing between two adjacent points of the function  $f(x)$ . The same relationship holds true for the backward and central differences. When differentiating tabulated data numerically, the limit cannot be applied (unless the point ensemble is approximated, e.g. by an interpolation method). Thus, numerical differentiation using finite differences is an approximation to the true derivative value. The error made can be found using the Taylor expansion. Consider the two Taylor expansions of the two-dimensional function  $u(x,y)$  as [140]:

$$u(x+h,y) = \left( u(x,y) + h \frac{\partial u(x,y)}{\partial x} + \frac{1}{2!} h^2 \frac{\partial^2 u(x,y)}{\partial x^2} + \frac{1}{3!} h^3 \frac{\partial^3 u(x,y)}{\partial x^3} + \dots \right), \quad (\text{A4.6})$$

$$u(x-h,y) = \left( u(x,y) - h \frac{\partial u(x,y)}{\partial x} + \frac{1}{2!} h^2 \frac{\partial^2 u(x,y)}{\partial x^2} - \frac{1}{3!} h^3 \frac{\partial^3 u(x,y)}{\partial x^3} + \dots \right). \quad (\text{A4.7})$$

Herein,  $\Delta x = h$  is the constant spacing between adjacent points. The first partial derivative of  $u(x,y)$ , where  $u(x,y)$  is the point of interest, can be obtained in different ways. By truncating the Taylor series at the second term and rearranging equations (A4.6) and (A4.7), respectively, one may obtain the first partial derivative containing the forward  $\Delta$  and backward  $\nabla$  difference, as given below [140]:

$$\frac{\partial u(x, y)}{\partial x} = \frac{u(x + h, y) - u(x, y)}{h} - \frac{1}{2} h f''(\xi), \quad (\text{A4.8})$$

$$\frac{\partial u(x, y)}{\partial x} = \frac{u(x, y) - u(x - h, y)}{h} + \frac{1}{2} h f''(\xi). \quad (\text{A4.9})$$

It can be realised that the second term of equations (A4.8) and (A4.9) is the error made due to the truncation of the Taylor series. It can also be seen that this error is a function of the spacing  $h$ . The algebraic difference of equations (A4.6) and (A4.7) yields to [140]:

$$\frac{\partial u(x, y)}{\partial x} = \frac{u\left(x + \frac{1}{2}h, y\right) - u\left(x - \frac{1}{2}h, y\right)}{h} - \frac{1}{6} h^2 f'''(\xi). \quad (\text{A4.10})$$

It can be noticed that the error that is made when using the central difference is proportional to  $h^2$ . Thus, this expression is more accurate than the forward or backward difference approximation. Forward and backward differences are related to the central difference by employing a so-called shifting operator  $E_s u(x) = u(x + h)$  as [141]:

$$\delta^n f(x) = E_s^{-\frac{n}{2}} \Delta f(x) = E_s^{\frac{n}{2}} \nabla f(x). \quad (\text{A4.11})$$

Every further derivation can be found by employing equation (A4.4) and the right-hand side of equation (A4.5) to compute the respective forward and backward difference quotients of order  $n$ . Equation (A4.11) is employed to determine the central differences. Thus, the second order forward difference quotient is:

$$\frac{\partial^2 u(x, y)}{\partial x^2} \approx \frac{\Delta[\Delta u(x, y)]}{(\Delta x)^2} = \frac{u(x + 2h, y) - 2u(x + h, y) + u(x, y)}{h^2}. \quad (\text{A4.12})$$

The second order backward difference can be found to be:

$$\frac{\partial^2 u(x, y)}{\partial x^2} \approx \frac{\nabla[\nabla u(x, y)]}{(\Delta x)^2} = \frac{u(x, y) - 2u(x - h, y) + u(x - 2h, y)}{h^2}. \quad (\text{A4.13})$$

Finally, the second order central difference becomes to:

$$\frac{\partial^2 u(x, y)}{\partial x^2} \approx \frac{E\Delta^2}{(\Delta x)^2} = \frac{E\nabla^2}{(\Delta x)^2} = \frac{u(x + h, y) - 2u(x, y) + u(x - h, y)}{h^2}. \quad (\text{A4.14})$$

The third order difference quotients can be found analogously, as demonstrated above. The third order forward difference quotient is given by:

$$\frac{\Delta[\Delta^2 u(x, y)]}{(\Delta x)^3} = \frac{u(x + 3h, y) - 3u(x + 2h, y) + 3u(x + h, y) - u(x, y)}{h^3}. \quad (\text{A4.15})$$

The third order backward difference can be found to be:

$$\frac{\nabla[\nabla^2 u(x, y)]}{(\Delta x)^3} = \frac{u(x, y) - 3u(x - h, y) + 3u(x - 2h, y) - u(x - 3h, y)}{h^3}. \quad (\text{A4.16})$$

Finally, the third order central difference becomes to:

$$\frac{\partial^3 u}{\partial x^3} \approx \frac{u\left(x + \frac{3}{2}h, y\right) - 3u\left(x + \frac{1}{2}h, y\right) + 3u\left(x - \frac{1}{2}h, y\right) - u\left(x - \frac{3}{2}h, y\right)}{h^3}. \quad (\text{A4.17})$$

Also here, the error due to truncation is either proportional to  $h$  or  $h^2$ , depending on the use of the forward, backward or central differences. Thus, when using central differences and decreasing the point distance  $h$  by half, the error can be reduced by factor 4. However, the spacing between two adjacent points can not be decreased endlessly, since the error due to rounding of a

computer increases its influence with decreasing  $h$ . It follows that  $h \geq \sqrt{\varepsilon}$ , whereas  $\varepsilon$  is the rounding error. The above shown equations are the approximation of the partial derivatives with respect to  $x$  only. To obtain partial derivatives with respect to  $y$ , the variable  $x$  needs to be substituted by  $y$ . For beam derivatives, the variable  $y$  needs to be set to zero.

## Appendix A5

### Spatial Derivatives of General Four-Wave Equation

The right-hand side beam displacement is given by:

$$u_+(x, t) = (A_+ e^{-kx} + B_+ e^{-jkx} + B_- e^{jkx} + A_- e^{kx}) e^{j\omega t}. \quad (\text{A5.1})$$

The spatial derivatives can be found to be:

$$\frac{\partial u_+(x, t)}{\partial x} = (-kA_+ e^{-kx} - jkB_+ e^{-jkx} + jkB_- e^{jkx} + kA_- e^{kx}) e^{j\omega t}, \quad (\text{A5.2})$$

$$\frac{\partial^2 u_+(x, t)}{\partial x^2} = (k^2 A_+ e^{-kx} - k^2 B_+ e^{-jkx} - k^2 B_- e^{jkx} + k^2 A_- e^{kx}) e^{j\omega t}, \quad (\text{A5.3})$$

$$\frac{\partial^3 u_+(x, t)}{\partial x^3} = (-k^3 A_+ e^{-kx} + jk^3 B_+ e^{-jkx} - jk^3 B_- e^{jkx} + k^3 A_- e^{kx}) e^{j\omega t}. \quad (\text{A5.4})$$

The left-hand side beam displacement is given by:

$$u_-(x, t) = (C_- e^{kx} + D_- e^{jkx} + D_+ e^{-jkx} + C_+ e^{-kx}) e^{j\omega t}. \quad (\text{A5.5})$$

Its spatial derivatives can be found to be:

$$\frac{\partial u_-(x, t)}{\partial x} = (kC_- e^{kx} + jkD_- e^{jkx} - jkD_+ e^{-jkx} - kC_+ e^{-kx}) e^{j\omega t}, \quad (\text{A5.6})$$

$$\frac{\partial^2 u_-(x, t)}{\partial x^2} = (k^2 C_- e^{kx} - k^2 D_- e^{jkx} - k^2 D_+ e^{-jkx} + k^2 C_+ e^{-kx}) e^{j\omega t}, \quad (\text{A5.7})$$

$$\frac{\partial^3 u_-(x, t)}{\partial x^3} = (k^3 C_- e^{kx} - jk^3 D_- e^{jkx} + jk^3 D_+ e^{-jkx} - k^3 C_+ e^{-kx}) e^{j\omega t}. \quad (\text{A5.8})$$

A complete wave field of a beam is given as:

$$u(x,t) = \left( A_+ e^{-kx} + B_+ e^{-jkx} + B_- e^{jkx} + A_- e^{kx} + C_- e^{kx} + D_- e^{jkx} + D_+ e^{-jkx} + C_+ e^{-kx} \right) e^{j\omega t}, \quad (\text{A5.9})$$

and its spatial derivatives are:

$$\frac{\partial u(x,t)}{\partial x} = \left( -kA_+ e^{-kx} - jkB_+ e^{-jkx} + jkB_- e^{jkx} + kA_- e^{kx} + kC_- e^{kx} + jkD_- e^{jkx} - jkD_+ e^{-jkx} - kC_+ e^{-kx} \right) e^{j\omega t}, \quad (\text{A5.10})$$

$$\frac{\partial^2 u(x,t)}{\partial x^2} = \left( k^2 A_+ e^{-kx} - k^2 B_+ e^{-jkx} - k^2 B_- e^{jkx} + k^2 A_- e^{kx} + k^2 C_- e^{kx} - k^2 D_- e^{jkx} - k^2 D_+ e^{-jkx} + k^2 C_+ e^{-kx} \right) e^{j\omega t}, \quad (\text{A5.11})$$

$$\frac{\partial^3 u(x,t)}{\partial x^3} = \left( -k^3 A_+ e^{-kx} + jk^3 B_+ e^{-jkx} - jk^3 B_- e^{jkx} + k^3 A_- e^{kx} + k^3 C_- e^{kx} - jk^3 D_- e^{jkx} + jk^3 D_+ e^{-jkx} - k^3 C_+ e^{-kx} \right) e^{j\omega t}. \quad (\text{A5.12})$$

## Appendix A6

### Four-Wave Vibrational Energy Flow Equation

By substituting equation (5.1) into equation (3.33), under consideration of the derivatives given in Appendix A5 and omitting the temporal term  $e^{j\omega t}$ , one may obtain the complex, time-averaged shear force energy transmission as:

$$(P_{x_s})_{4W} = \frac{EI k^3 \omega}{2} \left[ \begin{aligned} & (B_+ B_+^* - B_- B_-^* + B_+ B_-^* e^{-jk(2x-L)} - B_- B_+^* e^{jk(2x-L)} + \\ & j(e^{-kL}(A_+ A_-^* - A_- A_+^*) + (A_+ A_+^* e^{-2kx} - A_- A_-^* e^{2k(x-L)}))) + \\ & e^{-kx} \left( \begin{aligned} & (e^{-jkx} B_+ A_+^* + j e^{-jk(x-L)} A_+ B_-^* - \\ & e^{jk(x-L)} B_- A_+^* + j e^{jkx} A_+ B_+^*) \end{aligned} \right) + \\ & e^{k(x-L)} \left( \begin{aligned} & (e^{-jkx} B_+ A_-^* - j e^{-jk(x-L)} A_- B_-^* - \\ & e^{jk(x-L)} B_- A_-^* - j e^{jkx} A_- B_+^*) \end{aligned} \right) \end{aligned} \right]. \quad (A6.1)$$

Analogously, the complex, time-averaged bending moment energy flow can be found as:

$$(P_{x_b})_{4W} = \frac{EI k^3 \omega}{2} \left[ \begin{aligned} & (B_+ B_+^* - B_- B_-^* - B_+ B_-^* e^{-jk(2x-L)} + B_- B_+^* e^{jk(2x-L)} + \\ & j(e^{-kL}(A_+ A_-^* - A_- A_+^*) + (A_- A_-^* e^{2k(x-L)} - A_+ A_+^* e^{-2kx}))) + \\ & e^{-kx} \left( \begin{aligned} & (j e^{-jkx} B_+ A_+^* + e^{-jk(x-L)} A_+ B_-^* + \\ & j e^{jk(x-L)} B_- A_+^* - e^{jkx} A_+ B_+^*) \end{aligned} \right) - \\ & e^{k(x-L)} \left( \begin{aligned} & (j e^{-jkx} B_+ A_-^* - e^{-jk(x-L)} A_- B_-^* + \\ & j e^{jk(x-L)} B_- A_-^* + e^{jkx} A_- B_+^*) \end{aligned} \right) \end{aligned} \right]. \quad (A6.2)$$

The total, complex, time-averaged net energy, flowing through a rectangular beam section, is simply the sum of equation (A6.1) and equation (A6.2), i.e.

$$(P_x)_{4W} = (P_{x_s})_{4W} + (P_{x_b})_{4W} \text{ and, thus:}$$

$$(P_x)_{4W} = EIk^3\omega \left[ \begin{aligned} & B_+B_+^* - B_-B_-^* + je^{-kL}(A_+A_-^* - A_-A_+^*) + \\ & \left( \frac{1+j}{2} \right) \left( e^{-kx} (e^{-jkx} B_+A_+^* + e^{-jk(x-L)} A_+B_-^*) - \right. \\ & \left. e^{k(x-L)} (e^{jk(x-L)} B_-A_-^* + e^{jkx} A_-B_+^*) \right) - \\ & \left( \frac{1-j}{2} \right) \left( e^{-kx} (e^{jkx} A_+B_+^* + e^{jk(x-L)} B_-A_+^*) - \right. \\ & \left. e^{k(x-L)} (e^{-jk(x-L)} A_-B_-^* + e^{-jkx} B_+A_-^*) \right) \end{aligned} \right]. \quad (\text{A6.3})$$

Equation (A6.3) displays the total, complex net energy flow within a beam. The real part of (A6.3) is the active energy transmission. The imaginary part of equation (A6.3) is reactive VEF. Equation (A6.3) does not reveal real and active VEF directly and, thus, will be simplified further. If one takes the following relations into account:

$$\Re\{AB^*\} = \Re\{A^*B\}, \quad (\text{A6.4})$$

$$\Im\{AB^*\} = -\Im\{A^*B\}, \quad (\text{A6.5})$$

$$AB^* + A^*B = 2\Re\{AB^*\}, \quad (\text{A6.6})$$

$$AB^* - A^*B = 2j\Im\{AB^*\}, \quad (\text{A6.7})$$

where  $A$  and  $B$  are arbitrary complex numbers, the simplified time-averaged active energy flow within a beam can be written as:

$$(P_x)_{4W} = EIk^3\omega (B_+B_+^* - B_-B_-^* - 2e^{-kL}\Im\{A_+A_-^*\}). \quad (\text{A6.8})$$



The simplified time-averaged reactive VEF of equation (A6.3) can be found to be:

$$\begin{aligned}
 (P_{x_r})_{4W} = jEI k^3 \omega & \left( \begin{aligned} & e^{-kx} \begin{pmatrix} \cos(k(x-L)) \Im \{A_+ B_-^*\} + \\ \cos(kx) \Im \{B_+ A_+^*\} - \\ \sin(k(x-L)) \Re \{A_+ B_-^*\} - \\ \sin(kx) \Re \{B_+ A_+^*\} \end{pmatrix} - \\ & e^{k(x-L)} \begin{pmatrix} \cos(kx) \Im \{A_- B_+^*\} + \\ \cos(k(x-L)) \Im \{B_- A_-^*\} + \\ \sin(kx) \Re \{A_- B_+^*\} + \\ \sin(k(x-L)) \Re \{B_- A_-^*\} \end{pmatrix} + \\ & e^{-kx} \begin{pmatrix} \cos(k(x-L)) \Re \{A_+ B_-^*\} + \\ \cos(kx) \Re \{B_+ A_+^*\} + \\ \sin(k(x-L)) \Im \{A_+ B_-^*\} + \\ \sin(kx) \Im \{B_+ A_+^*\} \end{pmatrix} - \\ & e^{k(x-L)} \begin{pmatrix} \cos(kx) \Re \{A_- B_+^*\} + \\ \cos(k(x-L)) \Re \{B_- A_-^*\} - \\ \sin(kx) \Im \{A_- B_+^*\} - \\ \sin(k(x-L)) \Im \{B_- A_-^*\} \end{pmatrix} \end{aligned} \right). \quad (A6.9)
 \end{aligned}$$

## Appendix A7

### Forced Vibration of an Infinite Beam due to Point Force Excitation

The transverse displacement of the infinite beam is given to either side as:

$$u_+(x, t)_\infty = (A_+ e^{-kx} + B_+ e^{-jkx}) e^{j\omega t} \text{ for } x \geq 0, \quad (\text{A7.1})$$

$$u_-(x, t)_\infty = (C_- e^{kx} + D_- e^{jkx}) e^{j\omega t} \text{ for } x \leq 0. \quad (\text{A7.2})$$

Substituting equations (A7.1) and (A7.2) into the appropriate spatial derivatives, as given in Appendix A5, the boundary conditions of an infinite beam at the excitation location are:

$$u_+(0)_{F_\infty} = u_-(0)_{F_\infty} \Rightarrow A_+ + B_- - C_- - D_- = 0, \quad (\text{A7.3})$$

$$\frac{\partial u_+(0)_{F_\infty}}{\partial x} = \frac{\partial u_-(0)_{F_\infty}}{\partial x} \Rightarrow -A_+ - jB_+ - C_- - jD_- = 0, \quad (\text{A7.4})$$

$$EI \frac{\partial^2 u_+(0)_{F_\infty}}{\partial x^2} = EI \frac{\partial^2 u_-(0)_{F_\infty}}{\partial x^2} \Rightarrow A_+ - B_+ - C_- + D_- = 0, \quad (\text{A7.5})$$

$$\frac{\partial^3 u_+(0)_{F_\infty}}{\partial x^3} - \frac{\partial^3 u_-(0)_{F_\infty}}{\partial x^3} = \frac{F_0}{EI} \Rightarrow -A_+ + jB_+ - C_- + jD_- = \frac{F_0}{EI k^3}. \quad (\text{A7.6})$$

Note, here the sign conventions of Figure 5.2 are employed in combination with the excitation force direction and wave components, as shown in Figure 5.3.

From equations (A7.3) to (A7.6) a matrix system according to  $[C]\{A\} = \{F\}$  can be constructed as:

$$\begin{bmatrix} 1 & 1 & -1 & -1 \\ -1 & -j & -1 & -j \\ 1 & -1 & -1 & 1 \\ -1 & j & -1 & j \end{bmatrix} \begin{bmatrix} A_+ \\ B_+ \\ C_- \\ D_- \end{bmatrix} = \begin{bmatrix} 0 \\ 0 \\ 0 \\ \frac{F_0}{EI k^3} \end{bmatrix}. \quad (\text{A7.7})$$

Here,  $[C]$  is the  $4 \times 4$  wave amplitude coefficient matrix,  $\{A\}$  is the  $4 \times 1$  wave amplitude vector, and  $\{F\}$  is the load vector. Solving this simple matrix system to obtain the desired wave amplitudes, the inverse of the  $[C]$  matrix has to be determined. The equation system can be solved simply as  $\{A\} = [C]^{-1} \{F\}$  and, thus, the wave amplitudes are given by:

$$\begin{bmatrix} A_+ \\ B_+ \\ C_- \\ D_- \end{bmatrix} = \begin{bmatrix} -\frac{F_0}{4EI k^3} \\ -\frac{jF_0}{4EI k^3} \\ \frac{F_0}{4EI k^3} \\ -\frac{jF_0}{4EI k^3} \end{bmatrix}. \quad (\text{A7.8})$$

The transverse displacement in dependency upon the excitation force magnitude  $F_0$  can be found simply by substituting the wave amplitudes into equation (A7.1) and (A7.2), respectively, and thus:

$$u_+(x, t)_{F_0} = -\frac{F_0}{4EI k^3} (e^{-kx} + je^{-jkx}) e^{j\omega t} \text{ for } x \geq 0, \quad (\text{A7.9})$$

$$u_-(x, t)_{F_0} = -\frac{F_0}{4EI k^3} (e^{kx} + je^{jkx}) e^{j\omega t} \text{ for } x \leq 0. \quad (\text{A7.10})$$

## Appendix A8

### Forced Vibration of an Infinite Beam due to Moment Excitation

The general transverse displacement of the infinite beam is given by:

$$u_+(x, t)_\infty = (A_+ e^{-kx} + B_+ e^{-jkx}) e^{j\omega t} \text{ for } x \geq 0, \quad (\text{A7.1})$$

$$u_-(x, t)_\infty = (C_- e^{kx} + D_- e^{jkx}) e^{j\omega t} \text{ for } x \leq 0. \quad (\text{A7.2})$$

Applying the boundary conditions at the excitation location by substituting the general displacement equations (A7.1) and (A7.2) into the appropriate spatial derivative equations, as given in Appendix A5, one can write the boundary condition equations as:

$$u_+(0)_{M_\infty} = u_-(0)_{M_\infty} \Rightarrow A_+ + B_- - C_- - D_- = 0, \quad (\text{A8.1})$$

$$\frac{\partial u_+(0)_{M_\infty}}{\partial x} = \frac{\partial u_-(0)_{M_\infty}}{\partial x} \Rightarrow -A_+ - jB_+ - C_- - jD_- = 0, \quad (\text{A8.2})$$

$$\frac{\partial^2 u_+(0)_{M_\infty}}{\partial x^2} - \frac{\partial^2 u_-(0)_{F_\infty}}{\partial x^2} = \frac{M_0}{EI} \Rightarrow A_+ - B_+ - C_- + D_- = \frac{M_0}{EI k^2}, \quad (\text{A8.3})$$

$$EI \frac{\partial^3 u_+(0)_{M_\infty}}{\partial x^3} = EI \frac{\partial^3 u_-(0)_{M_\infty}}{\partial x^3} \Rightarrow -A_+ + jB_+ - C_- + jD_- = 0. \quad (\text{A8.4})$$

Also here, the defined sign conventions of Figure 5.2 are used in combination with the direction of the excitation moment and wave components, as shown in Figure 5.3.

The vibrational matrix equation is given as:

$$\begin{bmatrix} 1 & 1 & -1 & -1 \\ -1 & -j & -1 & -j \\ 1 & -1 & -1 & 1 \\ -1 & j & -1 & j \end{bmatrix} \begin{bmatrix} A_+ \\ B_+ \\ C_- \\ D_- \end{bmatrix} = \begin{bmatrix} 0 \\ 0 \\ \frac{M_0}{EI k^2} \\ 0 \end{bmatrix}. \quad (\text{A8.5})$$

By solving equation (A8.5), the wave amplitudes are found to be:

$$\begin{bmatrix} A_+ \\ B_+ \\ C_- \\ D_- \end{bmatrix} = \begin{bmatrix} \frac{M_0}{4EI k^2} \\ -\frac{M_0}{4EI k^2} \\ -\frac{M_0}{4EI k^2} \\ \frac{M_0}{4EI k^2} \end{bmatrix}. \quad (\text{A8.6})$$

Analogously, substituting equation (A8.6) into equation (A7.1) and (A7.2), respectively, one can find the transverse displacement of an infinite beam, loaded by a harmonically varying moment as:

$$u_+(x, t)_{M_\infty} = \frac{M_0}{4EI k^2} (e^{-kx} - e^{-jkx}) e^{j\omega t} \text{ for } x \geq 0, \quad (\text{A8.7})$$

$$u_-(x, t)_{M_\infty} = -\frac{M_0}{4EI k^2} (e^{kx} - e^{jkx}) e^{j\omega t} \text{ for } x \leq 0. \quad (\text{A8.8})$$

## Appendix A9

### Forced Vibration of a Simply Supported Beam due to Point Force Excitation

The beam displacement of a simply supported beam is composed of the infinite beam response and the reflection of the infinite wave travelling on the beam's ends. Hysteretic damping is included here, simply by employing a complex Young's modulus  $\underline{E} = E(1 + j\eta)$  and, thus, a complex wavenumber as:

$$\underline{k} \approx k \left( 1 - j \frac{\eta}{4} \right) = k(1 - j\bar{\eta}). \quad (\text{A9.1})$$

With equation (A9.1) the transverse finite beam displacement is given by:

$$u(x, t) = \left( u(x)_\infty + B_- e^{jk(x-L)} + A_- e^{k(x-L)} + D_+ e^{-jkx} + C_+ e^{-kx} \right) e^{j\omega t}. \quad (\text{A9.2})$$

It can be seen from equation (A7.8) that the respective right-hand side and left-hand side wave components are identical. It is more convenient to apply the infinite beam response in a finite beam analysis by a summation expression as:

$$u(x)_{F_\infty} = \sum_{n=1}^2 K_n e^{-k_n |x_0 - x|}. \quad (\text{A9.3})$$

Herein,  $\underline{k}_1 = \underline{k}$  and  $\underline{k}_2 = j\underline{k}$  and  $K_n$  is the wave amplitude of the nearfield for  $n = 1$  and of the farfield for  $n = 2$ . If one distinguishes between a right-hand side and left-hand side displacement of the excitation location, the infinite beam response can be written as:

$$u_\infty(x, t) = \left( A_+ e^{-\underline{k}(x-x_0)} + B_+ e^{-j\underline{k}(x-x_0)} \right) e^{j\omega t}, \text{ for } x \geq x_0, \quad (\text{A9.4})$$

$$u_{\infty}(x, t) = \left( C_- e^{-k(x_0 - x)} + D_- e^{jk(x_0 - x)} \right) e^{j\omega t}, \text{ for } x \leq x_0. \quad (\text{A9.5})$$

To derive boundary conditions, equations (A9.3) and (A9.4) are used. To plot the beam's response, equation (A9.2) is used instead. To find the eight unknown wave coefficients, eight boundary condition equations are required. Four of them are related to the conditions at the excitation location. These are identical to the boundary equations given by equations (A7.3) to (A7.6) as:

$$u_{\infty}(x_0)_{x > x_0} = u_{\infty}(x_0)_{x < x_0} \Rightarrow A_+ + B_- - C_- - D_- = 0, \quad (\text{A9.6})$$

$$\frac{\partial u_{\infty}(x_0)_{x > x_0}}{\partial x} = \frac{\partial u_{\infty}(x_0)_{x < x_0}}{\partial x} \Rightarrow -A_+ - jB_+ - C_- - jD_- = 0, \quad (\text{A9.7})$$

$$\underline{EI} \frac{\partial^2 u(x_0)_{x > x_0}}{\partial x^2} = \underline{EI} \frac{\partial^2 u(x_0)_{x < x_0}}{\partial x^2} \Rightarrow A_+ - B_+ - C_- + D_- = 0, \quad (\text{A9.8})$$

$$\left( \frac{\partial^3 u_{\infty}(x_0)_{x > x_0}}{\partial x^3} - \frac{\partial^3 u_{\infty}(x_0)_{x < x_0}}{\partial x^3} \right) = \frac{F_0}{\underline{EI}} \Rightarrow -A_+ + jB_+ - C_- + jD_- = \frac{F_0}{\underline{EI}k^3}. \quad (\text{A9.9})$$

The remaining boundary conditions can be found at the location  $x = 0$  and  $x = L$  of the beam, simply by assuming zero transverse displacement and zero bending moment there as:

$$u(0)_{ss} = 0 \Rightarrow \left( B_- e^{-jkL} + A_- e^{-kL} + C_- e^{-kx_0} + D_- e^{-jkx_0} + D_+ + C_+ \right) = 0, \quad (\text{A9.10})$$

$$\underline{EI} \frac{\partial^2 u(0)_{ss}}{\partial x^2} = 0 \Rightarrow \left( -B_- e^{-jkL} + A_- e^{-kL} + C_- e^{-kx_0} - D_- e^{-jkx_0} - D_+ + C_+ \right) = 0, \quad (\text{A9.11})$$

$$u(L)_{ss} = 0 \Rightarrow \begin{pmatrix} A_+ e^{-k(L-x_0)} + B_+ e^{-jk(L-x_0)} + \\ B_- + A_- + D_+ e^{-jkL} + C_+ e^{-kL} \end{pmatrix} = 0, \quad (A9.12)$$

$$\underline{EI} \frac{\partial^2 u(L)_{ss}}{\partial x^2} = 0 \Rightarrow \begin{pmatrix} A_+ e^{-k(L-x_0)} - B_+ e^{-jk(L-x_0)} - \\ B_- + A_- - D_+ e^{-jkL} + C_+ e^{-kL} \end{pmatrix} = 0. \quad (A9.13)$$

As shown in Appendix A7 and Appendix A8 a matrix system  $[C]\{A\} = \{F\}$  can be formed from equations (A9.6) to (A9.13), whereas the coefficient matrix  $[C]$  is given as:

$$[C] = \begin{bmatrix} 1 & 1 & 0 & 0 & -1 & -1 & 0 & 0 \\ -1 & -j & 0 & 0 & -1 & -j & 0 & 0 \\ 1 & -1 & 0 & 0 & -1 & 1 & 0 & 0 \\ -1 & j & 0 & 0 & -1 & j & 0 & 0 \\ 0 & 0 & e^{-jkL} & e^{-kL} & e^{-kx_0} & e^{-jkx_0} & 1 & 1 \\ 0 & 0 & -e^{-jkL} & e^{-kL} & e^{-kx_0} & -e^{-jkx_0} & -1 & 1 \\ e^{-k(L-x_0)} & e^{-jk(L-x_0)} & 1 & 1 & 0 & 0 & e^{-jkL} & e^{-kL} \\ e^{-k(L-x_0)} & -e^{-jk(L-x_0)} & -1 & 1 & 0 & 0 & -e^{-jkL} & e^{kL} \end{bmatrix}. \quad (A9.14)$$

The force vector is given by:

$$\{F\} = \left\{ 0 \quad 0 \quad 0 \quad \frac{F_0}{\underline{EI}k^3} \quad 0 \quad 0 \quad 0 \quad 0 \right\}^T. \quad (A9.15)$$

As demonstrated in Appendix A7 and Appendix A8, the inverse of the  $[C]$  matrix must be determined and the equation system can be solved as  $\{A\} = [C]^{-1} \{F\}$ .



With this procedure, one may find the exponential wave amplitudes as:

$$\begin{bmatrix} A_+ \\ B_+ \\ B_- \\ A_- \\ C_- \\ D_- \\ D_+ \\ C_+ \end{bmatrix} = \frac{F_0}{4EI\bar{k}^3} \begin{bmatrix} -1 \\ -j \\ \frac{j(e^{-j\bar{k}(L+x_0)} - e^{-j\bar{k}(L-x_0)})}{(e^{-2j\bar{k}L} - 1)} \\ \frac{(e^{-\bar{k}(L+x_0)} - e^{-\bar{k}(L-x_0)})}{(e^{-2\bar{k}L} - 1)} \\ -1 \\ -j \\ \frac{j(e^{-j\bar{k}(2L-x_0)} - e^{-j\bar{k}x_0})}{(e^{-2j\bar{k}L} - 1)} \\ \frac{(e^{-\bar{k}(2L-x_0)} - e^{-\bar{k}x_0})}{(e^{-2\bar{k}L} - 1)} \end{bmatrix} \quad (\text{A9.16})$$

Equation (A9.16) may be expressed by sinusoidal and hyperbolic functions as:

$$\begin{bmatrix} A_+ \\ B_+ \\ B_- \\ A_- \\ C_- \\ D_- \\ D_+ \\ C_+ \end{bmatrix} = \frac{F_0}{4EI\bar{k}^3} \begin{bmatrix} -1 \\ -j \\ \frac{j(\cos(\bar{k}(L-x_0)) - \cos(\bar{k}(L+x_0)))}{(1 - \cos(2\bar{k}L))} \\ \frac{(\cosh(\bar{k}(L-x_0)) - \cosh(\bar{k}(L+x_0)))}{(1 - \cosh(2\bar{k}L))} \\ -1 \\ -j \\ \frac{j(\cos(\bar{k}x_0) - \cos(\bar{k}(2L-x_0)))}{(1 - \cos(2\bar{k}L))} \\ \frac{(\cosh(\bar{k}x_0) - \cosh(\bar{k}(2L-x_0)))}{(1 - \cosh(2\bar{k}L))} \end{bmatrix} \quad (\text{A9.17})$$

If one neglects material damping by setting the loss factor equal to zero ( $\bar{\eta} = 0$ ), expression (A9.17) can be reduced to:

$$\begin{bmatrix} A_+ \\ B_+ \\ B_- \\ A_- \\ C_- \\ D_- \\ D_+ \\ C_+ \end{bmatrix} = \frac{F_0}{4EI k^3} \begin{bmatrix} -1 \\ -j \\ j \frac{\sin(kx_0)}{\sin(kL)} \\ \frac{\sinh(kx_0)}{\sinh(kL)} \\ -1 \\ -j \\ j \frac{\sin(k(L-x_0))}{\sin(kL)} \\ \frac{\sinh(k(L-x_0))}{\sinh(kL)} \end{bmatrix}. \quad (\text{A9.18})$$

Unfortunately, if one includes hysteretic damping, equation (A9.17) cannot be simplified further. Substituting equation (A9.16) into equation (A9.2) and using equation (A9.3), the exponential transverse displacement of a point force excited simply supported beam can be written as:

$$u(x, t)_{F_s} = -\frac{F_0 e^{j\omega t}}{4EI k^3} \begin{bmatrix} e^{-k|x_0-x|} + j e^{-j k |x_0-x|} - \\ \frac{j(e^{-jk(L+x_0)} - e^{-jk(L-x_0)})}{(e^{-2jkL} - 1)} e^{jk(x-L)} - \\ \frac{(e^{-k(L+x_0)} - e^{-k(L-x_0)})}{(e^{-2kL} - 1)} e^{k(x-L)} - \\ \frac{j(e^{-jk(2L-x_0)} - e^{-jkx_0})}{(e^{-2jkL} - 1)} e^{-jkx} - \\ \frac{(e^{-k(2L-x_0)} - e^{-kx_0})}{(e^{-2kL} - 1)} e^{-kx} \end{bmatrix}. \quad (\text{A9.19})$$

## Appendix A10

### Forced Vibration of a Simply Supported Beam due to Moment Excitation

The derivation of the transverse displacement of a simply supported beam excited by a moment is similar to the procedure demonstrated in Appendix A9. The general transverse displacement of a finite beam excited by a moment is given by:

$$u(x, t) = \left( u(x)_\infty + B_- e^{jk(x-L)} + A_- e^{\underline{k}(x-L)} + D_+ e^{-j\bar{k}x} + C_+ e^{-\underline{k}x} \right) e^{j\omega t}. \quad (\text{A9.2})$$

The infinite beam response due to an applied moment, as shown in Appendix A8, may be written in the following form:

$$u(x)_{M_\infty} = \sum_{n=1}^2 (-1)^{n-1} \text{sig}(x - x_0) F_n e^{-\underline{k}_n |x_0 - x|}. \quad (\text{A10.1})$$

Herein,  $\text{sig}(x - x_0)$  is a function similar to the well known signum function,  $\text{sgn}(x)$ . However, in this work  $\text{sig}(x - x_0)$  is defined as:

$$\text{sig}(x - x_0) = \begin{cases} 1 & \text{for } x \geq x_0 \\ -1 & \text{for } x \leq x_0 \end{cases}. \quad (\text{A10.2})$$

In equation (A10.1)  $F_n$  is the nearfield wave amplitude for  $n = 1$  and the farfield amplitude for  $n = 2$ . Furthermore,  $\underline{k}_1 = \underline{k}$  and  $\underline{k}_2 = j\bar{k}$ . The sig function is required because the respective left-hand side wave amplitudes and right-hand side wave amplitudes are identical in magnitude but different in sign. The infinite beam response in dependency upon a positive and negative spatial position is given by:

$$u_\infty(x, t) = \left( A_+ e^{-\underline{k}(x-x_0)} + B_+ e^{-j\bar{k}(x-x_0)} \right) e^{j\omega t}, \text{ for } x \geq x_0, \quad (\text{A9.4})$$

$$u_{\infty}(x, t) = \left( C_- e^{-k(x_0 - x)} + D_- e^{jk(x_0 - x)} \right) e^{j\omega t}, \text{ for } x \leq x_0. \quad (\text{A9.5})$$

The four boundary conditions at the excitation location can be written as:

$$u_{\infty}(x_0)_{x > x_0} = u_{\infty}(x_0)_{x < x_0} \Rightarrow A_+ + B_- - C_- - D_- = 0, \quad (\text{A9.6})$$

$$\frac{\partial u_{\infty}(x_0)_{x > x_0}}{\partial x} = \frac{\partial u_{\infty}(x_0)_{x < x_0}}{\partial x} \Rightarrow -A_+ - jB_+ - C_- - jD_- = 0, \quad (\text{A9.7})$$

$$\frac{\partial^2 u_{\infty}(x_0)_{x > x_0}}{\partial x^2} - \frac{\partial^2 u_{\infty}(x_0)_{x < x_0}}{\partial x^2} = \frac{M_0}{EI} \Rightarrow A_+ - B_+ - C_- + D_- = \frac{M_0}{EI k^2}, \quad (\text{A10.3})$$

$$\frac{EI}{\partial x^3} \frac{\partial^3 u_{\infty}(x_0)_{x > x_0}}{\partial x^3} = \frac{EI}{\partial x^3} \frac{\partial^3 u_{\infty}(x_0)_{x < x_0}}{\partial x^3} \Rightarrow -A_+ + jB_+ - C_- + jD_- = 0. \quad (\text{A10.4})$$

The four boundary conditions at  $x = 0$  and,  $x = L$  are identical to the point force excited case and are given by:

$$u(0)_{ss} = 0 \Rightarrow \begin{pmatrix} B_- e^{-jkL} + A_- e^{-kL} + \\ C_- e^{-kx_0} + D_- e^{-jkx_0} + D_+ + C_+ \end{pmatrix} = 0, \quad (\text{A9.10})$$

$$\frac{EI}{\partial x^2} \frac{\partial^2 u(0)_{ss}}{\partial x^2} = 0 \Rightarrow \begin{pmatrix} -B_- e^{-jkL} + A_- e^{-kL} + \\ C_- e^{-kx_0} - D_- e^{-jkx_0} - D_+ + C_+ \end{pmatrix} = 0, \quad (\text{A9.11})$$

$$u(L)_{ss} = 0 \Rightarrow \begin{pmatrix} A_+ e^{-k(L-x_0)} + B_+ e^{-jk(L-x_0)} + \\ B_- + A_- + D_+ e^{-jkL} + C_+ e^{-kL} \end{pmatrix} = 0, \quad (\text{A9.12})$$

$$\frac{EI}{\partial x^2} \frac{\partial^2 u(L)_{ss}}{\partial x^2} = 0 \Rightarrow \begin{pmatrix} A_+ e^{-k(L-x_0)} - B_+ e^{-jk(L-x_0)} - \\ B_- + A_- - D_+ e^{-jkL} + C_+ e^{-kL} \end{pmatrix} = 0. \quad (\text{A9.13})$$

The above given boundary equations may be combined into a matrix system, i.e.  $[C]\{A\} = \{M\}$ . Thus, the coefficient matrix  $[C]$  is found to be:

$$[C] = \begin{bmatrix} 1 & 1 & 0 & 0 & -1 & -1 & 0 & 0 \\ -1 & -j & 0 & 0 & -1 & -j & 0 & 0 \\ 1 & -1 & 0 & 0 & -1 & 1 & 0 & 0 \\ -1 & j & 0 & 0 & -1 & j & 0 & 0 \\ 0 & 0 & e^{-jkL} & e^{-kL} & e^{-kx_0} & e^{-jkx_0} & 1 & 1 \\ 0 & 0 & -e^{-jkL} & e^{-kL} & e^{-kx_0} & -e^{-jkx_0} & -1 & 1 \\ e^{-k(L-x_0)} & e^{-jk(L-x_0)} & 1 & 1 & 0 & 0 & e^{-jkL} & e^{-kL} \\ e^{-k(L-x_0)} & -e^{-jk(L-x_0)} & -1 & 1 & 0 & 0 & -e^{-jkL} & e^{kL} \end{bmatrix}. \quad (A10.5)$$

The moment vector is given as:

$$\{M\} = \left\{ 0 \quad 0 \quad \frac{M_0}{EI k^2} \quad 0 \quad 0 \quad 0 \quad 0 \quad 0 \right\}^T. \quad (A10.6)$$

By solving  $\{A\} = [C]^{-1} \{M\}$ , the wave amplitudes are given by:

$$\begin{bmatrix} A_+ \\ B_+ \\ B_- \\ A_- \\ C_- \\ D_- \\ D_+ \\ C_+ \end{bmatrix} = \frac{M_0}{4EI k^2} \begin{bmatrix} 1 \\ -1 \\ \frac{(e^{-jk(L+x_0)} + e^{-jk(L-x_0)})}{(e^{-2jkL} - 1)} \\ \frac{(e^{-k(L+x_0)} + e^{-k(L-x_0)})}{(e^{-2kL} - 1)} \\ -1 \\ 1 \\ \frac{(e^{-jk(2L-x_0)} + e^{-jkx_0})}{(e^{-2jkL} - 1)} \\ -\frac{(e^{-k(2L-x_0)} + e^{-kx_0})}{(e^{-2kL} - 1)} \end{bmatrix}. \quad (A10.7)$$

Expression (A10.7) can be written in sinusoidal and hyperbolic terms as:

$$\begin{bmatrix} A_+ \\ B_+ \\ B_- \\ A_- \\ C_- \\ D_- \\ D_+ \\ C_+ \end{bmatrix} = \frac{M_0}{4EI\bar{k}^2} \begin{bmatrix} 1 \\ -1 \\ \frac{j(\sin(\bar{k}(L-x_0)) + \sin(\bar{k}(L+x_0)))}{(1 - \cos(2\bar{k}L))} \\ \frac{(\sinh(\bar{k}(L-x_0)) + \sinh(\bar{k}(L+x_0)))}{(1 - \cosh(2\bar{k}L))} \\ -1 \\ 1 \\ \frac{j(\sin(\bar{k}x_0) + \sin(\bar{k}(2L-x_0)))}{(1 - \cos(2\bar{k}L))} \\ \frac{(\sinh(\bar{k}x_0) + \sinh(\bar{k}(2L-x_0)))}{(1 - \cosh(2\bar{k}L))} \end{bmatrix} \quad (\text{A10.8})$$

If no material damping is considered ( $\bar{\eta} = 0$ ) equation (A10.8) can be reduced to:

$$\begin{bmatrix} A_+ \\ B_+ \\ B_- \\ A_- \\ C_- \\ D_- \\ D_+ \\ C_+ \end{bmatrix} = \frac{M_0}{4EI\bar{k}^2} \begin{bmatrix} 1 \\ -1 \\ -j \frac{\cos(\bar{k}x_0)}{\sin(\bar{k}L)} \\ -\frac{\cosh(\bar{k}x_0)}{\sinh(\bar{k}L)} \\ -1 \\ 1 \\ j \frac{\cos(\bar{k}(L-x_0))}{\sin(\bar{k}L)} \\ \frac{\cosh(\bar{k}(L-x_0))}{\sinh(\bar{k}L)} \end{bmatrix} \quad (\text{A10.9})$$

By substituting the wave amplitudes of equation (A10.7) into equation (A9.2) and taking equation (A10.1) into account, one can write the transverse beam response due to an excitation moment as:

$$u(x, t)_{M_s} = \frac{M_0 e^{j\omega t}}{4EI k^2} \left[ \begin{aligned} & \left( \text{sig}(x_0 - x) \left( e^{-k|x_0 - x|} - e^{-jk|x_0 - x|} \right) - \right. \\ & \frac{\left( e^{-jk(L+x_0)} + e^{-jk(L-x_0)} \right)}{\left( e^{-2jkL} - 1 \right)} e^{jk(x-L)} + \\ & \frac{\left( e^{-jk(2L-x_0)} + e^{-jkx_0} \right)}{\left( e^{-2jkL} - 1 \right)} e^{-jkx} + \\ & \frac{\left( e^{-k(L+x_0)} + e^{-k(L-x_0)} \right)}{\left( e^{-2kL} - 1 \right)} e^{k(x-L)} - \\ & \left. \frac{\left( e^{-k(2L-x_0)} + e^{-kx_0} \right)}{\left( e^{-2kL} - 1 \right)} e^{-kx} \right] \quad (A10.10) \end{aligned} \right.$$

## Appendix A11

### Force Point Mobility of a Simply Supported Beam

Point mobility at the excitation location  $x_0$  due to a harmonic point force excitation is defined as:

$$Y(\omega)_F = \frac{\partial u(x_0, t)_F}{\partial t F_0 e^{j\omega t}}. \quad (\text{A11.1})$$

The transverse velocity response at the excitation location is simply given by:

$$\frac{\partial u(x, t)_F}{\partial t} = j\omega u(x, t)_F. \quad (\text{A11.2})$$

Using relation (A11.2) to obtain the temporal derivative of equation (A9.19) and substituting this expression in equation (A11.1), the exponential form of the force point mobility is given as:

$$Y(\omega)_{F_u} = \frac{\omega}{4EI\bar{k}^3} \left( 1 - j - \left( \frac{2e^{-2j\bar{k}L} - e^{-2j\bar{k}(L-x_0)} - e^{-2j\bar{k}\bar{x}_0}}{e^{-2j\bar{k}L} - 1} \right) + j \left( \frac{2e^{-2\bar{k}L} - e^{-2\bar{k}(L-x_0)} - e^{-2\bar{k}\bar{x}_0}}{e^{-2\bar{k}L} - 1} \right) \right). \quad (\text{A11.3})$$

Equation (A11.3) can be simplified further. If the exponential travelling and exponential decaying fractions of equation (A11.3) are extended complex conjugate and the following two well known exponential identities are taken into account:

$$e^{\pm jx} = \cos(x) \pm j \sin(x), \quad (\text{A11.4})$$

$$e^{\pm x} = \cosh(x) \pm \sinh(x), \quad (\text{A11.5})$$



one can rewrite equation (A11.3) by using sinusoidal and hyperbolic functions as:

$$Y(\omega)_{F_{ss}} = \frac{j\omega}{4EI\bar{k}^3} \left( \left( \frac{\sin(2\bar{k}x_0) + \sin(2\bar{k}(L - x_0)) - \sin(2\bar{k}L)}{1 - \cos(2\bar{k}L)} \right) - \left( \frac{\sinh(2\bar{k}x_0) + \sinh(2\bar{k}(L - x_0)) - \sinh(2\bar{k}L)}{1 - \cosh(2\bar{k}L)} \right) \right). \quad (\text{A11.6})$$

If one neglects internal damping within the beam ( $\bar{\eta} = 0$ ), equation (A11.6) can be reduced to:

$$Y(\omega)_{F_{ss}} = \frac{j\omega}{2EI\bar{k}^3} \left( \left( \frac{\sin(kx_0) \sin(k(L - x_0))}{\sin(kL)} \right) - \left( \frac{\sinh(kx_0) \sinh(k(L - x_0))}{\sinh(kL)} \right) \right). \quad (\text{A11.7})$$

## Appendix A12

### Moment Point Mobility of a Simply Supported Beam

Moment point mobility at excitation location  $x_0$  is defined as:

$$Y(\omega)_M = \frac{\partial^2 u(x_0, t)_M}{\partial x \partial t M_0 e^{j\omega t}}. \quad (\text{A12.1})$$

The rotational velocity response at the excitation location can be found by substituting  $x = x_0$  into the first temporal and first spatial derivative of equation (A10.10). Note, the signum function is omitted, since one side of the infinite waves at the excitation location is used only. Substituting this expression in equation (A12.1), the exponential form of the moment point mobility is:

$$Y(\omega)_{M_{ss}} = \frac{\omega}{4EI\bar{k}} \left( -1 - j + \left( \frac{2e^{-2j\bar{k}L} + e^{-2j\bar{k}(L-x_0)} + e^{-2j\bar{k}x_0}}{e^{-2j\bar{k}L} - 1} \right) + j \left( \frac{2e^{-2\bar{k}L} + e^{-2\bar{k}(L-x_0)} + e^{-2\bar{k}x_0}}{e^{-2\bar{k}L} - 1} \right) \right). \quad (\text{A12.2})$$

Analogously, to the procedure as described in the previous appendix, equation (A12.2) is presented in terms of sinusoidal and hyperbolic functions. By applying relations (A11.4) and (A11.5), one can write equation (A12.2) as:

$$Y(\omega)_{M_{ss}} = \frac{j\omega}{4EI\bar{k}} \left( \left( \frac{\sin(2\bar{k}x_0) + \sin(2\bar{k}(L-x_0)) + \sin(2\bar{k}L)}{1 - \cos(2\bar{k}L)} \right) + \left( \frac{\sinh(2\bar{k}x_0) + \sinh(2\bar{k}(L-x_0)) + \sinh(2\bar{k}L)}{1 - \cosh(2\bar{k}L)} \right) \right). \quad (\text{A12.3})$$

If one assumes that  $\bar{\eta} = 0$ , then equation (A12.3) simplifies to:

$$Y(\omega)_{M_{**}} = \frac{j\omega}{2EI k} \left( \left( \frac{\cos(kx_0) \cos(k(L - x_0))}{\sin(kL)} \right) - \left( \frac{\cosh(kx_0) \cosh(k(L - x_0))}{\sinh(kL)} \right) \right). \quad (\text{A12.4})$$

## Appendix A13

### Four-Wave Vibrational Energy Flow Equation Including Damping

Within the derived four-wave energy flow expressions, given in Appendix A6, damping was neglected. However, when dealing with finite structures, damping needs to be included. Using the complex wavenumber, as given in (A9.1), the spatially damped general beam displacement is given by:

$$u(x, t) = (A_+ e^{-kx} + B_+ e^{-jkx} + B_- e^{jk\tilde{x}} + A_- e^{k\tilde{x}}) e^{j\omega t}. \quad (\text{A13.1})$$

Here, the simplification  $\tilde{x} = (x - L)$  is used. If one substitutes equation (A13.1) into equation (3.33) under consideration of the derivatives given in Appendix A5 and omits the temporal term  $e^{j\omega t}$ , one may obtain the hysteretically damped, complex and time-averaged shear force energy flow as:

$$(\underline{P}_{x_s})_{4W} = \frac{EI k^3 (1 - j\bar{\eta})^3 \omega}{2} \left[ \begin{aligned} & B_+ B_+^* e^{-2kx\bar{\eta}} - B_- B_-^* e^{2k\tilde{x}\bar{\eta}} + \\ & B_+ B_-^* e^{-k\bar{\eta}(x-\tilde{x})} e^{-jk(x+\tilde{x})} - B_- B_+^* e^{-k\bar{\eta}(x-\tilde{x})} e^{jk(x+\tilde{x})} + \\ & j e^{-k(x-\tilde{x})} (A_+ A_-^* e^{jkx\bar{\eta}} e^{jk\tilde{x}\bar{\eta}} - A_- A_+^* e^{-jkx\bar{\eta}} e^{jk\tilde{x}\bar{\eta}}) + \\ & j (A_+ A_+^* e^{-2kx} - A_- A_-^* e^{2k\tilde{x}}) + \\ & e^{-kx} \left[ \begin{aligned} & B_+ A_+^* e^{-jkx} e^{-kx\bar{\eta}} e^{-jkx\bar{\eta}} + \\ & j A_+ B_-^* e^{-jk\tilde{x}} e^{k\tilde{x}\bar{\eta}} e^{jkx\bar{\eta}} - \\ & B_- A_+^* e^{jk\tilde{x}} e^{k\tilde{x}\bar{\eta}} e^{-jkx\bar{\eta}} + \\ & j A_+ B_+^* e^{jkx} e^{-kx\bar{\eta}} e^{jkx\bar{\eta}} \end{aligned} \right] + \\ & e^{k\tilde{x}} \left[ \begin{aligned} & B_+ A_-^* e^{-jkx} e^{-kx\bar{\eta}} e^{jk\tilde{x}\bar{\eta}} - \\ & j A_- B_-^* e^{-jk\tilde{x}} e^{k\tilde{x}\bar{\eta}} e^{-jk\tilde{x}\bar{\eta}} - \\ & B_- A_-^* e^{jk\tilde{x}} e^{k\tilde{x}\bar{\eta}} e^{jk\tilde{x}\bar{\eta}} - \\ & j A_- B_+^* e^{jkx} e^{-kx\bar{\eta}} e^{-jk\tilde{x}\bar{\eta}} \end{aligned} \right] \end{aligned} \right]. \quad (\text{A13.2})$$

Analogously, the hysteretically damped, complex, time-averaged bending moment energy flow is given as:

$$\begin{aligned}
 (\underline{P}_{x_B})_{4W} = & \frac{EI k^3 (1 - j\bar{\eta})^2 \omega}{2(1 + j\bar{\eta})^{-1}} \left[ \begin{aligned} & B_+ B_+^* e^{-2kx\bar{\eta}} - B_- B_-^* e^{2k\bar{x}\bar{\eta}} - \\ & B_+ B_-^* e^{-k\bar{\eta}(x-\bar{x})} e^{-jk(x+\bar{x})} + B_- B_+^* e^{-k\bar{\eta}(x-\bar{x})} e^{jk(x+\bar{x})} + \\ & j e^{-k(x-\bar{x})} (A_+ A_-^* e^{jkx\bar{\eta}} e^{jk\bar{x}\bar{\eta}} - A_- A_+^* e^{-jkx\bar{\eta}} e^{jk\bar{x}\bar{\eta}}) + \\ & j (A_- A_-^* e^{2k\bar{x}} - A_+ A_+^* e^{-2kx}) + \\ & e^{-kx} \left[ \begin{aligned} & j B_+ A_+^* e^{-jkx} e^{-kx\bar{\eta}} e^{-jkx\bar{\eta}} + \\ & A_+ B_-^* e^{-jk\bar{x}} e^{k\bar{x}\bar{\eta}} e^{jkx\bar{\eta}} + \\ & j B_- A_+^* e^{jk\bar{x}} e^{k\bar{x}\bar{\eta}} e^{-jkx\bar{\eta}} - \\ & A_+ B_+^* e^{jkx} e^{-kx\bar{\eta}} e^{jkx\bar{\eta}} \end{aligned} \right] - \\ & e^{k\bar{x}} \left[ \begin{aligned} & j B_+ A_-^* e^{-jkx} e^{-kx\bar{\eta}} e^{jk\bar{x}\bar{\eta}} - \\ & A_- B_-^* e^{-jk\bar{x}} e^{k\bar{x}\bar{\eta}} e^{-jk\bar{x}\bar{\eta}} + \\ & j B_- A_-^* e^{jk\bar{x}} e^{k\bar{x}\bar{\eta}} e^{jk\bar{x}\bar{\eta}} + \\ & A_- B_+^* e^{jkx} e^{-kx\bar{\eta}} e^{-jk\bar{x}\bar{\eta}} \end{aligned} \right] \end{aligned} \right] \quad (A13.3)
 \end{aligned}$$

Under use of relations (A6.4) to (A6.7) and the following simplifications:

$$D_{B_+ A_+}^\pm = \Re\{B_+ A_+^*\} \pm \Im\{B_+ A_+^*\}, \quad (A13.4)$$

$$D_{A_+ B_-}^\pm = \Re\{A_+ B_-^*\} \pm \Im\{A_+ B_-^*\}, \quad (A13.5)$$

$$D_{B_+ A_-}^\pm = \Re\{B_+ A_-^*\} \pm \Im\{B_+ A_-^*\}, \quad (A13.6)$$

$$D_{A_- B_-}^\pm = \Re\{A_- B_-^*\} \pm \Im\{A_- B_-^*\}, \quad (A13.7)$$

the total, complex, time-averaged energy transmission, i.e.  $(\underline{P}_x)_{4W} = (\underline{P}_{x_S})_{4W} + (\underline{P}_{x_B})_{4W}$  of four waves present and including hysteretic damping may be written as:

$$(\underline{P}_x)_{4W} = C_{4W} \left[ \begin{aligned} & (1 + j\bar{\eta})(B_+ B_+^* e^{-2kx\bar{\eta}} - B_- B_-^* e^{2k\tilde{x}\bar{\eta}}) + \\ & 2(\bar{\eta} + j\bar{\eta}^2) e^{-k\bar{\eta}(x-\tilde{x})} \left[ \frac{\cos(k(x+\tilde{x})) \Im\{B_+ B_-^*\} - \sin(k(x+\tilde{x})) \Re\{B_+ B_-^*\}}{\sin(kx\bar{\eta}) \Re\{A_+ A_-^*\}} \right] - \\ & 2(1 + j\bar{\eta}) e^{-k(x-\tilde{x})} \cos(k\tilde{x}\bar{\eta}) \left[ \frac{\cos(kx\bar{\eta}) \Im\{A_+ A_-^*\} + \sin(kx\bar{\eta}) \Re\{A_+ A_-^*\}}{\sin(kx\bar{\eta}) \Re\{A_+ A_-^*\}} \right] + \\ & 2(\bar{\eta} - j) e^{-k(x-\tilde{x})} \sin(k\tilde{x}\bar{\eta}) \left[ \frac{\cos(kx\bar{\eta}) \Im\{A_+ A_-^*\} + \sin(kx\bar{\eta}) \Re\{A_+ A_-^*\}}{\sin(kx\bar{\eta}) \Re\{A_+ A_-^*\}} \right] + \\ & (\bar{\eta} + j\bar{\eta}^2)(A_+ A_+^* e^{-2kx} - A_- A_-^* e^{2k\tilde{x}}) + \\ & (\bar{\eta} - j) e^{-kx} \left[ \begin{aligned} & e^{-kx\bar{\eta}} (\bar{\eta} - 1) \left[ \frac{D_{B_+ A_+}^+ \cos(kx(1+\bar{\eta})) - D_{B_+ A_+}^- \sin(kx(1+\bar{\eta}))}{D_{A_+ B_-}^- \sin(k(\tilde{x} - x\bar{\eta})) - D_{A_+ B_-}^+ \cos(k(\tilde{x} - x\bar{\eta}))} \right] + \\ & e^{k\tilde{x}\bar{\eta}} (\bar{\eta} + 1) \left[ \frac{D_{A_+ B_-}^- \sin(k(\tilde{x} - x\bar{\eta})) - D_{A_+ B_-}^+ \cos(k(\tilde{x} - x\bar{\eta}))}{D_{B_+ A_+}^+ \cos(k(x - \tilde{x}\bar{\eta})) + D_{B_+ A_+}^- \sin(k(x - \tilde{x}\bar{\eta}))} \right] - \\ & e^{-kx\bar{\eta}} (\bar{\eta} + 1) \left[ \frac{D_{B_+ A_+}^- \cos(k(x - \tilde{x}\bar{\eta})) + D_{B_+ A_+}^+ \sin(k(x - \tilde{x}\bar{\eta}))}{D_{A_+ B_-}^- \cos(k\tilde{x}(1+\bar{\eta})) + D_{A_+ B_-}^+ \sin(k\tilde{x}(1+\bar{\eta}))} \right] - \\ & e^{k\tilde{x}\bar{\eta}} (\bar{\eta} - 1) \left[ \frac{D_{A_+ B_-}^- \cos(k\tilde{x}(1+\bar{\eta})) + D_{A_+ B_-}^+ \sin(k\tilde{x}(1+\bar{\eta}))}{D_{B_+ A_+}^+ \cos(kx(1+\bar{\eta})) - D_{B_+ A_+}^- \sin(kx(1+\bar{\eta}))} \right] \end{aligned} \right] \end{aligned} \right]. \quad (\text{A13.8})$$

Herein,  $C_{4W}$  is given by:

$$C_{4W} = \frac{EIk^3\omega(1-j\bar{\eta})^3}{1+\bar{\eta}^2}. \quad (\text{A13.9})$$

## Appendix A14

### Coupled Transmitted Vibrational Energy

The general finite beam displacement is given by the summation of infinite waves beam response  $u(x)_\infty$  and reflection waves beam response  $u(x)_r$ , as:

$$u(x, t) = (u(x)_\infty + u(x)_r) e^{j\omega t}. \quad (\text{A14.1})$$

The infinite beam displacement is given as:

$$u(x)_\infty = C_1 e^{-\underline{k}\bar{x}} + C_2 e^{-j\underline{k}\bar{x}}. \quad (\text{A14.2})$$

Herein, the simplification  $\bar{x} = |x_0 - x|$  is used. Further,  $C_1$  and  $C_2$  are defined as the nearfield and farfield wave amplitudes. The complex wavenumber is denoted as  $\underline{k}$ . The reflection waves beam displacement  $u(x)_r$  is given as:

$$u(x)_r = D_+ e^{-j\underline{k}\tilde{x}} + C_+ e^{-\underline{k}\tilde{x}} + B_- e^{j\underline{k}\tilde{x}} + A_- e^{\underline{k}\tilde{x}}. \quad (\text{A14.3})$$

Here,  $\tilde{x} = (x - L)$  is used. It is apparent from equation (A14.2) that the derivatives of the infinite waves beam response due to the absolute argument of the exponential function follow the rule:

$$\left( \frac{\partial^n u(x, t)_\infty}{\partial x^n} \right)_{x < x_0} = - \left( \frac{\partial^n u(x, t)_\infty}{\partial x^n} \right)_{x > x_0}, \quad n = 1, 3, 5, \dots, \quad (\text{A14.4})$$

$$\left( \frac{\partial^n u(x, t)_\infty}{\partial x^n} \right)_{x < x_0} = \left( \frac{\partial^n u(x, t)_\infty}{\partial x^n} \right)_{x > x_0}, \quad n = 2, 4, 6, \dots, \quad (\text{A14.5})$$

where  $n$  is the  $n^{\text{th}}$  order of the respective spatial derivative. This means that odd-numbered derivatives of the infinite waves beam response are equal in

magnitude, but different in sign in dependency upon the location to the left or the right of the excitation location  $x_0$ . Thus, the sig function, as defined in (A10.2), is employed for odd-numbered functions as:

$$\frac{\partial^n u(x, t)_\infty}{\partial x^n} = \text{sig}(\hat{x}) \left( \frac{\partial^n u(x, t)_\infty}{\partial x^n} \right)_{x > x_0}, \quad n = 1, 3, 5, \dots \quad (\text{A14.6})$$

Herein, the simplification  $\hat{x} = x - x_0$  is employed. From equations (5.45) and (5.46), two coupled vibrational energy flow terms can be identified. One term arises due to the complex product of internal shear force and bending moment of the reflection waves and the appropriate infinite wave velocity components. This term can be written as:

$$(P_x)_{r, \infty} = \frac{EI}{2} \left( \frac{\partial^3 u(x, t)_r}{\partial x^3} \left( \frac{\partial u(x, t)_\infty}{\partial t} \right)^* + \frac{\partial^2 u(x, t)_r}{\partial x^2} \left( \frac{\partial^2 u(x, t)_\infty}{\partial x \partial t} \right)^* \right). \quad (\text{A14.7})$$

Vice versa, from (5.45) and (5.46), the coupled VEF term due to the complex product of internal shear force and bending moment of the infinite waves and the appropriate reflection waves velocity components can be found to be:

$$(P_x)_{\infty, r} = \frac{EI}{2} \left( \frac{\partial^3 u(x, t)_\infty}{\partial x^3} \left( \frac{\partial u(x, t)_r}{\partial t} \right)^* + \frac{\partial^2 u(x, t)_\infty}{\partial x^2} \left( \frac{\partial^2 u(x, t)_r}{\partial x \partial t} \right)^* \right). \quad (\text{A14.8})$$

If one substitutes equations (A14.2) and (14.3) into the shear force term of A(14.7), one can find time-averaged vibrational shear force energy flow as:

$$(P_{x_s})_{r, \infty} = \frac{EI k_s \omega}{2} \left[ C_1^* \left( D_+ e^{-k(\bar{x} + j\bar{x})} e^{-k\bar{\eta}(x + j\bar{x})} - B_- e^{-k(\bar{x} - j\bar{x})} e^{k\bar{\eta}(\bar{x} - j\bar{x})} + j(C_+ e^{-k(\bar{x} + x)} e^{-jk\bar{\eta}(\bar{x} - x)} - A_- e^{-k(\bar{x} - \bar{x})} e^{-jk\bar{\eta}(\bar{x} + \bar{x})}) \right) + C_2^* \left( D_+ e^{jk(\bar{x} - x)} e^{-k\bar{\eta}(\bar{x} + x)} - B_- e^{jk(\bar{x} + \bar{x})} e^{-k\bar{\eta}(\bar{x} - \bar{x})} + j(C_+ e^{-k(x - j\bar{x})} e^{-k\bar{\eta}(\bar{x} - j\bar{x})} - A_- e^{k(\bar{x} + j\bar{x})} e^{-k\bar{\eta}(\bar{x} + j\bar{x})}) \right) \right]. \quad (\text{A14.9})$$



In case of  $\bar{\eta} = 0$ , equation (A14.9) reduces to:

$$(P_{x_s})_{r,\infty} = \frac{EI k^3 \omega}{2} \left[ C_1^* \begin{pmatrix} D_+ e^{-k(\bar{x}+j\bar{x})} - B_- e^{-k(\bar{x}-j\bar{x})} + \\ j(C_+ e^{-k(\bar{x}+x)} - A_- e^{-k(\bar{x}-\bar{x})}) \end{pmatrix} + C_2^* \begin{pmatrix} D_+ e^{jk(\bar{x}-x)} - B_- e^{jk(\bar{x}+\bar{x})} + \\ j(C_+ e^{-k(x-j\bar{x})} - A_- e^{k(\bar{x}+j\bar{x})}) \end{pmatrix} \right]. \quad (\text{A14.10})$$

Analogously, the bending moment VEF can be written as:

$$(P_{x_B})_{r,\infty} = \frac{EI k^3 \omega \text{sig}(\hat{x}) Q}{2} \left[ jC_1^* \begin{pmatrix} D_+ e^{-k(\bar{x}+j\bar{x})} e^{-k\bar{\eta}(x+j\bar{x})} + \\ B_- e^{-k(\bar{x}-j\bar{x})} e^{k\bar{\eta}(\bar{x}-j\bar{x})} - \\ C_+ e^{-k(\bar{x}+x)} e^{-jk\bar{\eta}(\bar{x}-x)} - \\ A_- e^{-k(\bar{x}-\bar{x})} e^{-jk\bar{\eta}(\bar{x}+\bar{x})} \end{pmatrix} + C_2^* \begin{pmatrix} D_+ e^{jk(\bar{x}-x)} e^{-k\bar{\eta}(\bar{x}+x)} + \\ B_- e^{jk(\bar{x}+\bar{x})} e^{-k\bar{\eta}(\bar{x}-\bar{x})} - \\ C_+ e^{-k(x-j\bar{x})} e^{-k\bar{\eta}(\bar{x}-j\bar{x})} - \\ A_- e^{k(\bar{x}+j\bar{x})} e^{-k\bar{\eta}(\bar{x}+j\bar{x})} \end{pmatrix} \right]. \quad (\text{A14.11})$$

Herein,  $Q = (1 + j\bar{\eta}) / (1 - j\bar{\eta})$  is regarded. In the undamped case of  $\bar{\eta} = 0$ , equation (14.11) can be simplified as:

$$(P_{x_B})_{r,\infty} = \frac{EI k^3 \omega \text{sig}(\hat{x})}{2} \left[ jC_1^* \begin{pmatrix} D_+ e^{-k(\bar{x}+j\bar{x})} + B_- e^{-k(\bar{x}-j\bar{x})} - \\ C_+ e^{-k(\bar{x}+x)} - A_- e^{-k(\bar{x}-\bar{x})} \end{pmatrix} + C_2^* \begin{pmatrix} D_+ e^{jk(\bar{x}-x)} + B_- e^{jk(\bar{x}+\bar{x})} - \\ C_+ e^{-k(x-j\bar{x})} - A_- e^{k(\bar{x}+j\bar{x})} \end{pmatrix} \right]. \quad (\text{A14.12})$$

The summation of shear force and bending moment energy flow gives:

$$(P_x)_{r,\infty} = \frac{EI k^3 \omega}{2} \left[ C_1^* \begin{pmatrix} (1 + j \operatorname{sig}(\hat{x})Q) D_+ e^{-k(\bar{x}+jx)} e^{-k\bar{\eta}(x+j\bar{x})} + \\ (j \operatorname{sig}(\hat{x})Q - 1) B_- e^{-k(\bar{x}-j\bar{x})} e^{k\bar{\eta}(\bar{x}-j\bar{x})} + \\ j(1 - \operatorname{sig}(\hat{x})Q) C_+ e^{-k(\bar{x}+x)} e^{-jk\bar{\eta}(\bar{x}-x)} - \\ j(1 + \operatorname{sig}(\hat{x})Q) A_- e^{-k(\bar{x}-\bar{x})} e^{-jk\bar{\eta}(\bar{x}+\bar{x})} \end{pmatrix} + C_2^* \begin{pmatrix} (1 + \operatorname{sig}(\hat{x})Q) D_+ e^{jk(\bar{x}-x)} e^{-k\bar{\eta}(\bar{x}+x)} + \\ (\operatorname{sig}(\hat{x})Q - 1) B_- e^{jk(\bar{x}+\bar{x})} e^{-k\bar{\eta}(\bar{x}-\bar{x})} + \\ (j - \operatorname{sig}(\hat{x})Q) C_+ e^{-k(x-j\bar{x})} e^{-k\bar{\eta}(\bar{x}-jx)} - \\ (\operatorname{sig}(\hat{x})Q + j) A_- e^{k(\bar{x}+j\bar{x})} e^{-k\bar{\eta}(\bar{x}+j\bar{x})} \end{pmatrix} \right]. \quad (\text{A14.13})$$

In case of  $\bar{\eta} = 0$ , equation (14.13) reduces to:

$$(P_x)_{r,\infty} = \frac{EI k^3 \omega}{2} \left[ C_1^* \begin{pmatrix} (1 + j \operatorname{sig}(\hat{x})) D_+ e^{-k(\bar{x}+jx)} + \\ (j \operatorname{sig}(\hat{x}) - 1) B_- e^{-k(\bar{x}-j\bar{x})} + \\ j(1 - \operatorname{sig}(\hat{x})) C_+ e^{-k(\bar{x}+x)} - \\ j(1 + \operatorname{sig}(\hat{x})) A_- e^{-k(\bar{x}-\bar{x})} \end{pmatrix} + C_2^* \begin{pmatrix} (1 + \operatorname{sig}(\hat{x})) D_+ e^{jk(\bar{x}-x)} + \\ (\operatorname{sig}(\hat{x}) - 1) B_- e^{jk(\bar{x}+\bar{x})} + \\ (j - \operatorname{sig}(\hat{x})) C_+ e^{-k(x-j\bar{x})} - \\ (\operatorname{sig}(\hat{x}) + j) A_- e^{k(\bar{x}+j\bar{x})} \end{pmatrix} \right]. \quad (\text{A14.14})$$

The second type of coupled transmitted vibrational energy due to the internal shear force and bending moment of the infinite waves and the appropriate reflection waves velocity components can be found by substituting equations (A14.2) and (A14.3) into equation (A14.8). By taking out the shear force component, one may find the time-averaged shear force VEF as:

$$(\underline{P}_{x_s})_{\infty,r} = \frac{EI k^3 \omega \text{sig}(\hat{x})}{2} \left[ \begin{array}{l} jC_1 \left( \begin{array}{l} D_+^* e^{-k(\bar{x}-j\bar{x})} e^{-k\bar{\eta}(x-j\bar{x})} + \\ B_-^* e^{-k(\bar{x}+j\bar{x})} e^{k\bar{\eta}(\bar{x}+j\bar{x})} + \\ C_+^* e^{-k(\bar{x}+x)} e^{jk\bar{\eta}(\bar{x}-x)} + \\ A_-^* e^{-k(\bar{x}-\bar{x})} e^{jk\bar{\eta}(\bar{x}+\bar{x})} \end{array} \right) + \\ C_2 \left( \begin{array}{l} D_+^* e^{-jk(\bar{x}-x)} e^{-k\bar{\eta}(\bar{x}+x)} + \\ B_-^* e^{-jk(\bar{x}+\bar{x})} e^{-k\bar{\eta}(\bar{x}-\bar{x})} + \\ C_+^* e^{-k(x+j\bar{x})} e^{-k\bar{\eta}(\bar{x}+j\bar{x})} + \\ A_-^* e^{k(\bar{x}-j\bar{x})} e^{-k\bar{\eta}(\bar{x}-j\bar{x})} \end{array} \right) \end{array} \right]. \quad (\text{A14.15})$$

For  $\bar{\eta} = 0$ , equation (A14.15) simplifies to:

$$(\underline{P}_{x_s})_{\infty,r} = \frac{EI k^3 \omega \text{sig}(\hat{x})}{2} \left[ \begin{array}{l} jC_1 \left( \begin{array}{l} D_+^* e^{-k(\bar{x}-j\bar{x})} + B_-^* e^{-k(\bar{x}+j\bar{x})} + \\ C_+^* e^{-k(\bar{x}+x)} + A_-^* e^{-k(\bar{x}-\bar{x})} \end{array} \right) + \\ C_2 \left( \begin{array}{l} D_+^* e^{-jk(\bar{x}-x)} + B_-^* e^{-jk(\bar{x}+\bar{x})} + \\ C_+^* e^{-k(x+j\bar{x})} + A_-^* e^{k(\bar{x}-j\bar{x})} \end{array} \right) \end{array} \right]. \quad (\text{A14.16})$$

The bending moment VEF term can be found to be:

$$(\underline{P}_{x_B})_{\infty,r} = \frac{EI k^3 \omega Q}{2} \left[ \begin{array}{l} C_2 \left( \begin{array}{l} D_+^* e^{-jk(\bar{x}-x)} e^{-k\bar{\eta}(\bar{x}+x)} - B_-^* e^{-jk(\bar{x}+\bar{x})} e^{-k\bar{\eta}(\bar{x}-\bar{x})} + \\ j \left( C_+^* e^{-k(c+j\bar{x})} e^{-k\bar{\eta}(\bar{x}+j\bar{x})} - A_-^* e^{k(\bar{x}-j\bar{x})} e^{-k\bar{\eta}(\bar{x}-j\bar{x})} \right) \end{array} \right) - \\ C_1 \left( \begin{array}{l} D_+^* e^{-k(\bar{x}-j\bar{x})} e^{-k\bar{\eta}(x-j\bar{x})} - B_-^* e^{-k(\bar{x}+j\bar{x})} e^{k\bar{\eta}(\bar{x}+j\bar{x})} - \\ j \left( C_+^* e^{-k(\bar{x}+x)} e^{jk\bar{\eta}(\bar{x}-x)} - A_-^* e^{-k(\bar{x}-\bar{x})} e^{jk\bar{\eta}(\bar{x}+\bar{x})} \right) \end{array} \right) \end{array} \right]. \quad (\text{A14.17})$$

In case of  $\bar{\eta} = 0$ , equation (A14.17) reduces to:

$$(\underline{P}_{x_B})_{\infty,r} = \frac{EI k^3 \omega Q}{2} \left[ \begin{array}{l} C_2 \left( \begin{array}{l} D_+^* e^{-jk(\bar{x}-x)} - B_-^* e^{-jk(\bar{x}+\bar{x})} + \\ j \left( C_+^* e^{-k(c+j\bar{x})} - A_-^* e^{k(\bar{x}-j\bar{x})} \right) \end{array} \right) - \\ C_1 \left( \begin{array}{l} D_+^* e^{-k(\bar{x}-j\bar{x})} - B_-^* e^{-k(\bar{x}+j\bar{x})} - \\ j \left( C_+^* e^{-k(\bar{x}+x)} - A_-^* e^{-k(\bar{x}-\bar{x})} \right) \end{array} \right) \end{array} \right]. \quad (\text{A14.18})$$

The coupled transmitted energy due to the internal infinite waves shear force and bending moment and the appropriate reflection waves velocity components can be found to be:

$$(\underline{P}_x)_{\infty,r} = \frac{EI k^3 \omega}{2} \left[ C_1 \begin{pmatrix} (j \sin(\hat{x}) - Q) D_+^* e^{-k(\bar{x}-j\bar{x})} e^{-k\bar{\eta}(x-j\bar{x})} + \\ (j \sin(\hat{x}) + Q) B_-^* e^{-k(\bar{x}+j\bar{x})} e^{k\bar{\eta}(\bar{x}+j\bar{x})} + \\ j(\sin(\hat{x}) - Q) C_+^* e^{-k(\bar{x}+x)} e^{jk\bar{\eta}(\bar{x}-x)} + \\ j(\sin(\hat{x}) + Q) A_-^* e^{-k(\bar{x}-\bar{x})} e^{jk\bar{\eta}(\bar{x}+\bar{x})} \end{pmatrix} + C_2 \begin{pmatrix} (\sin(\hat{x}) + Q) D_+^* e^{-jk(\bar{x}-x)} e^{-k\bar{\eta}(\bar{x}+x)} + \\ (\sin(\hat{x}) - Q) B_-^* e^{-jk(\bar{x}+\bar{x})} e^{-k\bar{\eta}(\bar{x}-\bar{x})} + \\ (\sin(\hat{x}) + jQ) C_+^* e^{-k(x+j\bar{x})} e^{-k\bar{\eta}(\bar{x}+j\bar{x})} + \\ (\sin(\hat{x}) - jQ) A_-^* e^{k(\bar{x}-j\bar{x})} e^{-k\bar{\eta}(\bar{x}-j\bar{x})} \end{pmatrix} \right]. \quad (A14.19)$$

Equation (A14.19) reduces for  $\bar{\eta} = 0$  to:

$$(P_x)_{\infty,r} = \frac{EI k^3 \omega}{2} \left[ C_1 \begin{pmatrix} (j \sin(\hat{x}) - 1) D_+^* e^{-k(\bar{x}-j\bar{x})} + \\ (j \sin(\hat{x}) + 1) B_-^* e^{-k(\bar{x}+j\bar{x})} + \\ j(\sin(\hat{x}) - 1) C_+^* e^{-k(\bar{x}+x)} + \\ j(\sin(\hat{x}) + 1) A_-^* e^{-k(\bar{x}-\bar{x})} \end{pmatrix} + C_2 \begin{pmatrix} (\sin(\hat{x}) + 1) D_+^* e^{-jk(\bar{x}-x)} + \\ (\sin(\hat{x}) - 1) B_-^* e^{-jk(\bar{x}+\bar{x})} + \\ (\sin(\hat{x}) + j) C_+^* e^{-k(x+j\bar{x})} + \\ (\sin(\hat{x}) - j) A_-^* e^{k(\bar{x}-j\bar{x})} \end{pmatrix} \right]. \quad (A14.20)$$

The total coupled transmitted energy due to coupling of infinite waves and reflection waves is given by the sum of both energy flow term as:

$$(P_x)_c = (P_x)_{r,\infty} + (P_x)_{\infty,r}. \quad (A14.21)$$

Substituting equations (A14.13) and (A14.19) into (A14.21), one may obtain:

$$(P_x)_c = \frac{EI k^3 \omega}{1 + \bar{\eta}^2} \left[ \begin{aligned} & (1 + j\bar{\eta}) e^{-k\bar{\eta}(\bar{x}+x)} \left[ \begin{aligned} & \left( \text{sig}(\hat{x}) + 1 \right) \begin{pmatrix} \cos(k(x - \bar{x})) \Re \{C_2^* D_+\} + \\ \sin(k(x - \bar{x})) \Im \{C_2^* D_+\} \end{pmatrix} - \\ & \bar{\eta} (\text{sig}(\hat{x}) - 1) \begin{pmatrix} \cos(k(x - \bar{x})) \Im \{C_2^* D_+\} - \\ \sin(k(x - \bar{x})) \Re \{C_2^* D_+\} \end{pmatrix} \end{aligned} \right] + \\ & (1 + j\bar{\eta}) e^{-k\bar{\eta}(\bar{x}-\hat{x})} \left[ \begin{aligned} & \left( \text{sig}(\hat{x}) - 1 \right) \begin{pmatrix} \cos(k(\bar{x} + \hat{x})) \Re \{C_2^* B_-\} - \\ \sin(k(\bar{x} + \hat{x})) \Im \{C_2^* B_-\} \end{pmatrix} - \\ & \bar{\eta} (\text{sig}(\hat{x}) + 1) \begin{pmatrix} \cos(k(\bar{x} + \hat{x})) \Im \{C_2^* B_-\} + \\ \sin(k(\bar{x} + \hat{x})) \Re \{C_2^* B_-\} \end{pmatrix} \end{aligned} \right] + \\ & (1 + j\bar{\eta}) e^{-k(x-\hat{x})} \left[ \begin{aligned} & \bar{\eta} (\text{sig}(\hat{x}) - 1) \begin{pmatrix} \cos(k\bar{\eta}(\bar{x} + \hat{x})) \Re \{C_1^* A_-\} + \\ \sin(k\bar{\eta}(\bar{x} + \hat{x})) \Im \{C_1^* A_-\} \end{pmatrix} + \\ & (\text{sig}(\hat{x}) + 1) \begin{pmatrix} \cos(k\bar{\eta}(\bar{x} + \hat{x})) \Im \{C_1^* A_-\} - \\ \sin(k\bar{\eta}(\bar{x} + \hat{x})) \Re \{C_1^* A_-\} \end{pmatrix} \end{aligned} \right] + \\ & (1 + j\bar{\eta}) e^{-k(x+\bar{x})} \left[ \begin{aligned} & \bar{\eta} (\text{sig}(\hat{x}) + 1) \begin{pmatrix} \cos(k\bar{\eta}(x - \bar{x})) \Re \{C_1^* C_+\} - \\ \sin(k\bar{\eta}(x - \bar{x})) \Im \{C_1^* C_+\} \end{pmatrix} - \\ & (1 - \text{sig}(\hat{x})) \begin{pmatrix} \cos(k\bar{\eta}(x - \bar{x})) \Im \{C_1^* C_+\} + \\ \sin(k\bar{\eta}(x - \bar{x})) \Re \{C_1^* C_+\} \end{pmatrix} \end{aligned} \right] + \\ & (\bar{\eta} - j) e^{-k(\bar{x}+x\bar{\eta})} \left[ \begin{aligned} & (\bar{\eta} - \text{sig}(\hat{x})) \begin{pmatrix} \cos(k(x + \bar{x}\bar{\eta})) \Re \{C_1^* D_+\} + \\ \sin(k(x + \bar{x}\bar{\eta})) \Im \{C_1^* D_+\} \end{pmatrix} - \\ & (1 - \text{sig}(\hat{x})\bar{\eta}) \begin{pmatrix} \cos(k(x + \bar{x}\bar{\eta})) \Im \{C_1^* D_+\} - \\ \sin(k(x + \bar{x}\bar{\eta})) \Re \{C_1^* D_+\} \end{pmatrix} \end{aligned} \right] - \\ & (\bar{\eta} - j) e^{-k(\bar{x}-\hat{x}\bar{\eta})} \left[ \begin{aligned} & (\text{sig}(\hat{x}) + \bar{\eta}) \begin{pmatrix} \cos(k(\hat{x} - \bar{x}\bar{\eta})) \Re \{C_1^* B_-\} - \\ \sin(k(\hat{x} - \bar{x}\bar{\eta})) \Im \{C_1^* B_-\} \end{pmatrix} - \\ & (\text{sig}(\hat{x})\bar{\eta} + 1) \begin{pmatrix} \cos(k(\hat{x} - \bar{x}\bar{\eta})) \Im \{C_1^* B_-\} + \\ \sin(k(\hat{x} - \bar{x}\bar{\eta})) \Re \{C_1^* B_-\} \end{pmatrix} \end{aligned} \right] + \\ & (\bar{\eta} - j) e^{-k(x+\bar{x}\bar{\eta})} \left[ \begin{aligned} & (\text{sig}(\hat{x})\bar{\eta} - 1) \begin{pmatrix} \cos(k(\bar{x} + x\bar{\eta})) \Re \{C_2^* C_+\} - \\ \sin(k(\bar{x} + x\bar{\eta})) \Im \{C_2^* C_+\} \end{pmatrix} - \\ & (\bar{\eta} - \text{sig}(\hat{x})) \begin{pmatrix} \cos(k(\bar{x} + x\bar{\eta})) \Im \{C_2^* C_+\} + \\ \sin(k(\bar{x} + x\bar{\eta})) \Re \{C_2^* C_+\} \end{pmatrix} \end{aligned} \right] + \\ & (\bar{\eta} - j) e^{k(\hat{x}-\bar{x}\bar{\eta})} \left[ \begin{aligned} & (\text{sig}(\hat{x})\bar{\eta} + 1) \begin{pmatrix} \cos(k(\bar{x} - \hat{x}\bar{\eta})) \Re \{C_2^* A_-\} - \\ \sin(k(\bar{x} - \hat{x}\bar{\eta})) \Im \{C_2^* A_-\} \end{pmatrix} + \\ & (\text{sig}(\hat{x}) + \bar{\eta}) \begin{pmatrix} \cos(k(\bar{x} - \hat{x}\bar{\eta})) \Im \{C_2^* A_-\} + \\ \sin(k(\bar{x} - \hat{x}\bar{\eta})) \Re \{C_2^* A_-\} \end{pmatrix} \end{aligned} \right] \end{aligned} \right] \quad (A14.22)$$

Usually, the real part (active VEF) and imaginary part (reactive VEF) of the complex, transmitted energy is presented. However, for the damped case the total energy transmission definition is very complicate and, thus, only the total, complex flow is presented. In the case of  $\bar{\eta} = 0$ , the real part (active energy flow) of equation (A14.22) can be written as:

$$(P_x)_{c_a} = EIk^3\omega \left( \begin{array}{l} (\text{sig}(\hat{x}) + 1) \left( \begin{array}{l} \Re \{C_2^* D_+\} \cos(k(x - \bar{x})) + \\ \Im \{C_2^* D_+\} \sin(k(x - \bar{x})) \end{array} \right) + \\ (\text{sig}(\hat{x}) - 1) \left( \begin{array}{l} \Re \{C_2^* B_-\} \cos(k(\tilde{x} + \bar{x})) - \\ \Im \{C_2^* B_-\} \sin(k(\tilde{x} + \bar{x})) \end{array} \right) + \\ e^{-k\tilde{x}} \left( \begin{array}{l} e^{k\tilde{x}} (1 + \text{sig}(\hat{x})) \Im \{C_1^* A_-\} - \\ e^{kx} (1 - \text{sig}(\hat{x})) \Im \{C_1^* C_+\} \end{array} \right) \end{array} \right). \quad (\text{A14.23})$$

Also, in the case of  $\bar{\eta} = 0$ , the reactive part of the total coupled VEF is given by:

$$(P_x)_{c_r} = jEIk^3\omega \left( \begin{array}{l} e^{-k\tilde{x}} \left( \begin{array}{l} \Re \{C_1^* D_+\} (\text{sig}(\hat{x}) \cos(kx) - \sin(kx)) + \\ \Im \{C_1^* D_+\} (\cos(kx) + \text{sig}(\hat{x}) \sin(kx)) + \\ \Re \{C_1^* B_-\} (\text{sig}(\hat{x}) \cos(k\tilde{x}) - \sin(k\tilde{x})) - \\ \Im \{C_1^* B_-\} (\cos(k\tilde{x}) + \text{sig}(\hat{x}) \sin(k\tilde{x})) \end{array} \right) + \\ e^{-kx} \left( \begin{array}{l} \Re \{C_2^* C_+\} (\cos(k\bar{x}) - \text{sig}(\hat{x}) \sin(k\bar{x})) - \\ \Im \{C_2^* C_+\} (\text{sig}(\hat{x}) \cos(k\bar{x}) + \sin(k\bar{x})) \end{array} \right) - \\ e^{k\tilde{x}} \left( \begin{array}{l} \Re \{C_2^* A_-\} (\cos(k\bar{x}) + \text{sig}(\hat{x}) \sin(k\bar{x})) + \\ \Im \{C_2^* A_-\} (\text{sig}(\hat{x}) \cos(k\bar{x}) - \sin(k\bar{x})) \end{array} \right) \end{array} \right). \quad (\text{A14.24})$$

## Appendix A15

### Transmitted Vibrational Energy in a Simply Supported Beam due to Point Force Excitation Excluding Structural Damping

Infinite wave energy flow in a simply supported point force excited beam can be found by substituting the complex, infinite wave amplitudes given in (A9.18) into the general 4-wave energy flow equation by setting  $A_-$  and  $B_-$  equal to zero. Thus, using (A9.18) and (A6.8), the active VEF is given by:

$$(P_{x_a})_{F_\infty} = \text{sig}(\hat{x}) \frac{F_0^2 \omega}{16EI k^3}. \quad (\text{A15.1})$$

The reactive VEF can be found from equations (A9.18) and (A6.9) as:

$$(P_{x_r})_{F_\infty} = \text{sig}(\hat{x}) \frac{jF_0^2 \omega e^{-k\bar{x}}}{16EI k^3} (\cos(k\bar{x}) + \sin(k\bar{x})). \quad (\text{A15.2})$$

The above shown expressions are identical to the infinite beam VEF equations given in section 5.3.3.1. However, to relate these definitions to a beam of finite length, the sig function is employed and  $x$  has been substituted by  $\bar{x} = |x_0 - x|$  to account for energy transport to either side of the beam.

If one substitutes the complex, reflection wave amplitudes  $A_-$ ,  $B_-$ ,  $C_+$  and  $D_+$ , as given in (A9.18), into equation (A6.8), where  $A_+ = C_+$  and  $B_+ = D_+$ , one may obtain the transmitted energy in a simply supported beam due to the reflection waves as:

$$(P_{x_a})_{F_r} = \frac{F_0^2 \omega}{16EI k^3} \left( \frac{\sin^2(k(L - x_0)) - \sin^2(kx_0)}{\sin^2(kL)} \right). \quad (\text{A15.3})$$

The reactive part from equations (A9.18) and (A6.9) is given by:

$$(P_{x_r})_{F_r} = C_{F_r} \begin{pmatrix} e^{-kx} \begin{pmatrix} \sin(k(L-x_0)) \sinh(k(L-x_0)) \begin{pmatrix} \cos(kx) + \\ \sin(kx) \end{pmatrix} - \\ \sin(kx_0) \sinh(k(L-x_0)) \begin{pmatrix} \cos(k(x-L)) + \\ \sin(k(x-L)) \end{pmatrix} \end{pmatrix} - \\ e^{k(x-L)} \begin{pmatrix} \sin(kx_0) \sinh(kx_0) \begin{pmatrix} \cos(k(x-L)) - \\ \sin(k(x-L)) \end{pmatrix} - \\ \sin(k(L-x_0)) \sinh(kx_0) \begin{pmatrix} \cos(kx) - \\ \sin(kx) \end{pmatrix} \end{pmatrix} \end{pmatrix}, \quad (\text{A15.4})$$

with the constant  $C_{F_r}$  being defined as:

$$C_{F_r} = \frac{jF_0^2 \omega}{16EI k^3 \sin(kL) \sinh(kL)}. \quad (\text{A15.5})$$

It can be seen that the undamped energy flow due to the reflection waves is divided by the function  $\sin(kL)$ , which is the characteristic equation of a simply supported beam. Thus, at resonant wavenumber  $k_n = n\pi/L$ , the undamped vibrational energy flow tends towards infinity, which is certainly not true for real structures.

The coupled transmitted energy of a simply supported beam can be found by substituting the complex wave amplitudes, as given by equation (A9.18), into equation (A14.23) and (A14.24), respectively, using the amplitude substitutions  $C_1 = A_+$  and  $C_2 = B_+$ . Thus:

$$(P_{x_s})_{F_s} = -\frac{F_0^2 \omega}{16EI k^3 \sin(kL)} \begin{pmatrix} (\text{sig}(\hat{x}) + 1) \sin(k(L-x_0)) \cos(k(x-\bar{x})) + \\ (\text{sig}(\hat{x}) - 1) \sin(kx_0) \cos(k(\bar{x} + \tilde{x})) \end{pmatrix}. \quad (\text{A15.6})$$



From equations (A9.18) and (A14.24), the reactive energy transmission due to wave coupling can be found to be:

$$(P_{x_r})_{F_e} = C_{F_e} \begin{pmatrix} e^{-k\bar{x}} \begin{pmatrix} \sin(k(L-x_0)) \sinh(kL) \begin{pmatrix} \cos(kx) + \\ \text{sig}(\hat{x}) \sin(kx) \end{pmatrix} - \\ \sin(kx_0) \sinh(kL) \begin{pmatrix} \cos(k\bar{x}) + \\ \text{sig}(\hat{x}) \sin(k\bar{x}) \end{pmatrix} \end{pmatrix} - \\ e^{-kx} \sin(kL) \sinh(k(L-x_0)) \begin{pmatrix} \text{sig}(\hat{x}) \cos(k\bar{x}) + \\ \sin(k\bar{x}) \end{pmatrix} - \\ e^{k\bar{x}} \sin(kL) \sinh(kx_0) \begin{pmatrix} \text{sig}(\hat{x}) \cos(k\bar{x}) - \\ \sin(k\bar{x}) \end{pmatrix} \end{pmatrix}. \quad (\text{A15.7})$$

Herein, the constant  $C_{F_e}$  is defined as:

$$C_{F_e} = -\frac{jF_0^2\omega}{16EI k^3 \sin(kL) \sinh(kL)}. \quad (\text{A15.8})$$

## Appendix A16

### Transmitted Vibrational Energy in a Simply Supported Beam due to Moment Excitation Excluding Structural Damping

Analogously to the procedure given in Appendix A15, the infinite wave energy flow in a simply supported moment excited beam can be found by substituting the complex, infinite wave amplitudes given in (A10.9) into the general 4-wave VEF equation by setting  $A_-$  and  $B_-$  equal to zero. Thus, using equations (A10.9) and (A6.8), the active moment induced VEF is given by:

$$(P_{x_a})_{M_\infty} = \text{sig}(\hat{x}) \frac{M_0^2 \omega}{16EI k}. \quad (\text{A16.1})$$

The reactive moment induced VEF can be written from equations (A10.9) and (A6.9) as:

$$(P_{x_r})_{M_\infty} = \text{sig}(\hat{x}) \frac{jM_0^2 \omega e^{-k\bar{x}}}{16EI k} (\sin(k\bar{x}) - \cos(k\bar{x})). \quad (\text{A16.2})$$

Also here, the above given definitions are identical to the transmitted moment energy given in section 5.3.3.2. Finite beam conditions have been accounted by using the sig function and by substituting  $x$  by  $\bar{x} = |x_0 - x|$ .

If one substitutes the complex, reflection wave amplitudes  $A_-$ ,  $B_-$ ,  $C_+$  and  $D_+$ , as given in equation (A10.9) into equation (A6.8) and accounts for  $A_+ = C_+$  and  $B_+ = D_+$ , one may obtain the transmitted reflection waves energy due to moment excitation in a simply supported beam as:

$$(P_{x_a})_{M_r} = \frac{M_0^2 \omega}{16EI k} \left( \frac{\cos^2(k(L - x_0)) - \cos^2(kx_0)}{\sin^2(kL)} \right). \quad (\text{A16.3})$$

The reactive VEF flow from equations (A10.9) and (A6.9) is given as:

$$(P_{x_r})_{M_r} = C_{M_r} \left[ \begin{array}{c} e^{-kx} \left[ \begin{array}{c} \cos(kx_0) \cosh(k(L-x_0)) \left( \frac{\cos(k(x-L))}{\sin(k(x-L))} + \right) \\ \cos(k(L-x_0)) \cosh(k(L-x_0)) \left( \frac{\cos(kx)}{\sin(kx)} - \right) \end{array} \right] + \\ e^{k(x-L)} \left[ \begin{array}{c} \cos(k(L-x_0)) \cosh(kx_0) \left( \frac{\cos(kx)}{\sin(kx)} - \right) \\ \cos(kx_0) \cosh(kx_0) \left( \frac{\cos(k(x-L))}{\sin(k(x-L))} - \right) \end{array} \right] + \end{array} \right] \quad (A16.4)$$

Here, the constant  $C_{M_r}$  is defined as:

$$C_{M_r} = \frac{jM_0^2 \omega}{16EI k \sin(kL) \sinh(kL)}. \quad (A16.5)$$

The coupled transmitted energy can be determined by substituting the wave amplitudes given in (A10.9) into equation (A14.23) and (A14.24), respectively and using the amplitude substitutions  $C_1 = \text{sig}(\hat{x})A_+$  and  $C_2 = \text{sig}(\hat{x})B_+$ . With the above given amplitude substitutions, the active reflected waves VEF can be written as:

$$(P_{x_a})_{M_e} = -\frac{M_0^2 \omega}{16EI k \sin(kL)} \left[ \begin{array}{c} (1 + \text{sig}(\hat{x})) \cos(k(L-x_0)) \sin(k(x-\bar{x})) + \\ (1 - \text{sig}(\hat{x})) \cos(kx_0) \sin(k(\bar{x} + \tilde{x})) \end{array} \right]. \quad (A16.6)$$

From equations (A10.9) and (A14.24), the reactive VEF due to wave coupling can be found to be:

$$(P_{x_r})_{M_c} = C_{M_c} \begin{pmatrix} e^{-k\bar{x}} \begin{pmatrix} \cos(k(L-x_0)) \sinh(kL) \begin{pmatrix} \text{sig}(\hat{x}) \cos(kx) + \\ \sin(kx) \end{pmatrix} + \\ \cos(kx_0) \sinh(kL) \begin{pmatrix} \text{sig}(\hat{x}) \cos(k\tilde{x}) + \\ \sin(k\tilde{x}) \end{pmatrix} \end{pmatrix} - \\ e^{-kx} \sin(kL) \cosh(k(L-x_0)) \begin{pmatrix} \text{sig}(\hat{x}) \cos(k\bar{x}) - \\ \sin(k\bar{x}) \end{pmatrix} - \\ e^{k\tilde{x}} \sin(kL) \cosh(kx_0) \begin{pmatrix} \text{sig}(\hat{x}) \cos(k\bar{x}) + \\ \sin(k\bar{x}) \end{pmatrix} \end{pmatrix}. \quad (\text{A16.7})$$

Here, the constant  $C_{M_c}$  is defined as:

$$C_{M_c} = \frac{jM_0^2\omega}{16EI k \sin(kL) \sinh(kL)}. \quad (\text{A16.8})$$

## Appendix A17

### Unconstrained Layer Damping of Beams

Attaching a damping layer to a beam shifts the neutral axis of bending away from the middle axis of the beam, as shown in Figure 5.13. It is well known that the bending stresses are zero at the neutral axis location. Thus, by taking moment of the products  $EA$  about the neutral axis, where the relation  $\int EzdA = 0$  holds true, one may obtain [1]:

$$\underline{E}_B A_B z_B - \underline{E}_D A_D z_D = 0. \quad (\text{A17.1})$$

Note, the subscript  $B$  denotes beam properties, the subscript  $D$  denotes damping layer properties and the under-bar denotes complex quantities. A uniform damping layer distribution is assumed over the beam length. In equation (A17.1)  $\underline{E}$  is the complex Young's modulus,  $A$  is the cross-sectional area and  $z$  is the distance of the respective middle line to the neutral fibre of the beam-damping layer structure. Herein, the complex Young's modulus of the beam and damping layer are given as:

$$\underline{E}_B = E_B (1 + j\eta_B), \quad (\text{A17.2})$$

$$\underline{E}_D = E_D (1 + j\eta_D). \quad (\text{A17.3})$$

Here,  $\eta$  is the respective linear hysteretic loss factor. Substituting equations (A17.2) and (A17.3) into equation (A17.1) and using the relationship  $z_{BD} = z_D + z_B$ , the distance  $z_B$  can be found to be (see Figure 5.13):

$$z_B = z_{BD} C_D \frac{C_B (1 + \eta_B \eta_D) + C_D (1 + \eta_D^2) + j C_B (\eta_D - \eta_B)}{(C_B + C_D)^2 + (C_B \eta_B + C_D \eta_D)^2}. \quad (\text{A17.4})$$

Herein, the abbreviation  $C_B$  and  $C_D$  are defined as:

$$C_B = E_B A_B, \quad (\text{A17.5})$$

$$C_D = E_D A_D. \quad (\text{A17.6})$$

The sum of the complex beam and bending layer stiffness, i.e.  $(\underline{EI})_{BD} = \underline{E}_B \underline{I}_B + \underline{E}_D \underline{I}_D$  can be written as:

$$(\underline{EI})_{BD} = (\underline{E}_B \underline{I}_B + \underline{E}_D \underline{I}_D) \left( 1 + j \left( \eta_B \left( 1 - \frac{\underline{E}_D \underline{I}_D}{\underline{E}_B \underline{I}_B + \underline{E}_D \underline{I}_D} \right) + \eta_D \left( 1 - \frac{\underline{E}_B \underline{I}_B}{\underline{E}_B \underline{I}_B + \underline{E}_D \underline{I}_D} \right) \right) \right). \quad (\text{A17.7})$$

In equation (A17.7) the complex second moment of inertia  $\underline{I} = \int z^2 dA$  of the respective structure is given by using the parallel axis theorem as:

$$\underline{I}_B = \frac{b_B t_B^3}{12} + A_B z_B^2, \quad (\text{A17.8})$$

$$\underline{I}_D = \frac{b_D t_D^3}{12} + A_D (z_{BD} - z_B)^2. \quad (\text{A17.9})$$

Note, the second moment of area is complex because the offset  $z_B$  is complex. However, for small values of  $(\eta_D - \eta_B)^2 \ll 1$ , it can be shown that  $\Re\{\underline{I}\} \gg \Im\{\underline{I}\}$  and, hence, the imaginary part of equations (A17.8) and (A17.9) can be ignored. Thus, the bending stiffness of the beam-damping layer structure is given by:

$$(\underline{EI})_{BD} = (EI)_{BD} (1 + j\eta_{BD}), \quad (\text{A17.10})$$

where the combined bending stiffness  $(EI)_{BD}$  is defined as:

$$(EI)_{BD} = (E_B I_B + E_D I_D). \quad (\text{A17.11})$$

The linear hysteretic loss factor of the beam-damping layer structure  $\eta_{BD}$  can be written from equation (A17.7) as:

$$\eta_{BD} = \eta_B \left( 1 - \frac{E_D I_D}{E_B I_B + E_D I_D} \right) + \eta_D \left( 1 - \frac{E_B I_B}{E_B I_B + E_D I_D} \right). \quad (\text{A17.12})$$

## Appendix A18

### Signal-To-Noise Ratio

A measured displacement signal may be seen as a superposition of pure displacement signal and pure noise signal. Assume that the uncontaminated spatial displacement signal varies sinusoidal with beam distance. In contrast, the noise signal is distributed randomly over the beam distance. Thus, an averaged quantity is needed, which contains information of both spatially varying deflections. Hence, the signal-to-noise ratio (SNR) for signals of finite length is defined in this work as the uncontaminated mean squared displacement signal and the mean squared noise signal. This is given by:

$$SNR = \frac{\frac{1}{b_x - a_x} \int_{a_x}^{b_x} |u(x)_S|^2 dx}{\frac{1}{b_x - a_x} \int_{a_x}^{b_x} |u(x)_N|^2 dx} \quad (A18.1)$$

Herein,  $u(x)_S$  is the displacement signal that is not contaminated by noise and  $u(x)_N$  is the randomly distributed noise signal. In practice, the spatial functions  $u(x)_S$  and  $u(x)_N$  are not easy accessible. However, its spectral components can be retrieved from the wavenumber spectrum of the superimposed signal. If one applies Parseval's theorem (energy theorem), which provides a useful relation between the average power of the spatial signal and the averaged power of the spectral signal, it can be shown that the squared spectral magnitude of the displacement signal and noise signal can be used instead to approximate the SNR as [142]:

$$SNR = \frac{\frac{1}{b_k - a_k} \int_{a_k}^{b_k} |U(k)_S|^2 dk}{\frac{1}{b_k - a_k} \int_{a_k}^{b_k} |U(k)_N|^2 dk} \quad (A18.2)$$



Herein,  $|U(k)_s|^2$  is the wavenumber power spectrum of the uncontaminated displacement signal and  $|U(k)_N|^2$  is the wavenumber power spectrum of the noise. Note, the factor in front of both integral expressions can be cancelled. However, it is kept to remind the reader of the mean squared value origin. The advantage of this method is that these spectral data are easily accessible from applying a fast Fourier transform (FFT) to the recorded data. Thus, for single frequency excitation the squared magnitude spectra,  $|U(k)_s|^2$  and  $|U(k)_N|^2$  can be extracted from the wavenumber domain by simple spectrum manipulation. To solve the integral expression for a complex, single-frequency signal, as shown in the numerator in equation (A18.1), the mean squared amplitude of the uncontaminated, complex displacement signal can be written as:

$$\frac{1}{b_x - a_x} \int_{a_x}^{b_x} |u(x)_s|^2 dx = \frac{1}{2\pi} \int_0^{2\pi} |A_s e^{-jk_0 x}|^2 dx = A_s^2. \quad (\text{A18.3})$$

Here,  $A_s$  is the peak amplitude of the complex beam displacement that can be obtained from the spectrum. Taking the above given uncontaminated displacement definition into account, equation (A18.1) can be rewritten as:

$$SNR = \frac{A_s^2}{\frac{1}{b_x - a_x} \int_{a_x}^{b_x} |u(x)_N|^2 dx}. \quad (\text{A18.4})$$

When integrating the noise in the wavenumber spectrum, as shown in the denominator of equation (A18.4), the mean squared noise amplitude can be found. By taking the square root of this value, the root-mean-squared (RMS) noise amplitude may be determined.

## Appendix A19

**Tables of Predicted Cut-Off Points and Relative Mean Square Error of Three Differently Damped Simply Supported Beam Structures Using Extracted ESPI Noise and Measured Force Magnitude**

$n$	6	8	9	11
$f_n$	838.3 Hz	1490.3 Hz	1886.1 Hz	2817.5 Hz
(% of $ B_+ _{real}$ [%])	2	3.4	8.8	6.8
$\Re(10 \cdot \log_{10}(\Pi))$	3.61	-2.84	8.58	5.15
(% of $ B_+ _{imag}$ [%])	3.6	3.4	6	6.8
$\Im(10 \cdot \log_{10}(\Pi))$	49.51	43.14	90.69	20.60

**Table A19.1** Optimum ideal filtered non-layer damped beam cut-off points and relative MSE using the VEFESPI method.

$n$	6	8	9	11
$f_n$	818.2 Hz	1454.5 Hz	1840.8 Hz	2749.9 Hz
(% of $ B_+ _{real}$ [%])	3.8	3	5.8	3.6
$\Re(10 \cdot \log_{10}(\Pi))$	1.75	-3.46	-4.66	-3.70
(% of $ B_+ _{imag}$ [%])	5	4	3.8	4
$\Im(10 \cdot \log_{10}(\Pi))$	73.61	41.98	61.15	26.26

**Table A19.2** Optimum ideal filtered single-layer damped beam cut-off points and relative MSE using the VEFESPI method.

$n$	6	8	9	11
$f_n$	799.9 Hz	1422 Hz	1799.7 Hz	2688.4 Hz
(% of $ B_+ $ ) <sub>real</sub> [%]	6.6	9.4	10	7.2
$\Re(10 \cdot \log_{10}(\Pi))$	-5.59	-5.45	11.87	5.94
(% of $ B_+ $ ) <sub>imag</sub> [%]	6.4	9.4	10	7.4
$\Im(10 \cdot \log_{10}(\Pi))$	64.28	37.76	48.18	23.37

**Table A19.3** Optimum ideal filtered double-layer damped beam cut-off points and relative MSE using the VEFESPI method.

$n$	6	8	9	11
$f_n$	838.3 Hz	1490.3 Hz	1886.1 Hz	2817.5 Hz
$(k_c)_{real}$ [rad/m]	$1.15 \cdot k_0$	$1.0 \cdot k_0$	$1.0 \cdot k_0$	$1.02 \cdot k_0$
$\Re(10 \cdot \log_{10}(\Pi))$	2.63	-6.91	3.74	3.98
$(k_c)_{imag}$ [rad/m]	$1.15 \cdot k_0$	$1.0 \cdot k_0$	$2.025 \cdot k_0$	$1.46 \cdot k_0$
$\Im(10 \cdot \log_{10}(\Pi))$	62.1	41.81	65.68	28.54

**Table A19.4** Optimum Butterworth filtered non-layer damped beam cut-off frequencies and relative MSE using the VEFESPI method.

$n$	6	8	9	11
$f_n$	818.2 Hz	1454.5 Hz	1840.8 Hz	2749.9 Hz
$(k_c)_{real}$ [rad/m]	$1.15 \cdot k_0$	$1.3 \cdot k_0$	$1.2 \cdot k_0$	$1.04 \cdot k_0$
$\Re(10 \cdot \log_{10}(\Pi))$	2.24	-3.90	2.75	-3.25
$(k_c)_{imag}$ [rad/m]	$2.05 \cdot k_0$	$2.0 \cdot k_0$	$1.275 \cdot k_0$	$1.02 \cdot k_0$
$\Im(10 \cdot \log_{10}(\Pi))$	52.57	48.01	62.26	35.14

**Table A19.5** Optimum Butterworth filtered single-layer damped beam cut-off frequencies and relative MSE using the VEFESPI method.

$n$	6	8	9	11
$f_n$	799.9 Hz	1422 Hz	1799.7 Hz	2688.4 Hz
$(k_c)_{real}$ [rad/m]	$1.45 \cdot k_0$	$1.033 \cdot k_0$	$1.0 \cdot k_0$	$1.02 \cdot k_0$
$\Re(10 \cdot \log_{10}(\Pi))$	-6.16	-8.04	3.84	-3.23
$(k_c)_{imag}$ [rad/m]	$1.0 \cdot k_0$	$1.0 \cdot k_0$	$1.0 \cdot k_0$	$1.3 \cdot k_0$
$\Im(10 \cdot \log_{10}(\Pi))$	77.24	36.70	51.92	27.21

**Table A19.6** Optimum Butterworth filtered double-layer damped beam cut-off frequencies and relative MSE using the VEFESPI method.

$n$	6	8	9	11
$f_n$	838.3 Hz	1490.3 Hz	1886.1 Hz	2817.5 Hz
(% of $ B_+ $ ) <sub>real</sub> [%]	3.6	7.0	8.8	4.2
$\Re(10 \cdot \log_{10}(\Pi))$	-38.90	-38.25	-38.62	-38.79
(% of $ B_+ $ ) <sub>imag</sub> [%]	4.2	7	8.8	10
$\Im(10 \cdot \log_{10}(\Pi))$	15.10	8.43	49.94	37.58

**Table A19.7** Optimum ideal filtered non-layer damped beam cut-off points and relative MSE using the IEDI method.

$n$	6	8	9	11
$f_n$	818.2 Hz	1454.5 Hz	1840.8 Hz	2749.9 Hz
(% of $ B_+ $ ) <sub>real</sub> [%]	6.6	5.2	6	4.4
$\Re(10 \cdot \log_{10}(\Pi))$	-39.81	-38.74	-38.90	-38.46
(% of $ B_+ $ ) <sub>imag</sub> [%]	6.6	5.2	6	4.4
$\Im(10 \cdot \log_{10}(\Pi))$	46.07	9.44	37.28	7.13

**Table A19.8** Optimum ideal filtered single-layer damped beam cut-off points and relative MSE using the IEDI method.

$n$	6	8	9	11
$f_n$	799.9 Hz	1422 Hz	1799.7 Hz	2688.4 Hz
(% of $ B_+ _{real}$ [%])	3.6	9.2	10	3.4
$\Re(10 \cdot \log_{10}(\Pi))$	-42.07	-31.43	-32.23	-31.61
(% of $ B_+ _{imag}$ [%])	8.8	8	7.2	5.6
$\Im(10 \cdot \log_{10}(\Pi))$	44.36	49.95	58.14	41.08

**Table A19.9** Optimum ideal filtered double-layer damped beam cut-off points and relative MSE using the IEDI method.

$n$	6	8	9	11
$f_n$	838.3 Hz	1490.3 Hz	1886.1 Hz	2817.5 Hz
$(k_c)_{real}$ [rad/m]	$1.3 \cdot k_0$	$1.233 \cdot k_0$	$1.175 \cdot k_0$	$1.22 \cdot k_0$
$\Re(10 \cdot \log_{10}(\Pi))$	-37.32	-34.13	-38.04	-42.05
$(k_c)_{imag}$ [rad/m]	$1.0 \cdot k_0$	$1.0 \cdot k_0$	$1.5 \cdot k_0$	$1.26 \cdot k_0$
$\Im(10 \cdot \log_{10}(\Pi))$	64.28	51.80	74.25	46.57

**Table A19.10** Optimum Butterworth filtered non-layer damped beam cut-off frequencies and relative MSE using the IEDI method.

$n$	6	8	9	11
$f_n$	818.2 Hz	1454.5 Hz	1840.8 Hz	2749.9 Hz
$(k_c)_{real}$ [rad/m]	$1.45 \cdot k_0$	$1.233 \cdot k_0$	$1.175 \cdot k_0$	$1.22 \cdot k_0$
$\Re(10 \cdot \log_{10}(\Pi))$	-36.00	-32.91	-33.80	-37.21
$(k_c)_{imag}$ [rad/m]	$1.75 \cdot k_0$	$1.033 \cdot k_0$	$1.2 \cdot k_0$	$1.02 \cdot k_0$
$\Im(10 \cdot \log_{10}(\Pi))$	69.28	59.29	71.66	46.37

**Table A19.11** Optimum Butterworth filtered single-layer damped beam cut-off frequencies and relative MSE using the IEDI method.

$n$	6	8	9	11
$f_n$	799.9 Hz	1422 Hz	1799.7 Hz	2688.4 Hz
$(k_c)_{real}$ [rad/m]	$1.45 \cdot k_0$	$1.2 \cdot k_0$	$1.175 \cdot k_0$	$1.22 \cdot k_0$
$\Re(10 \cdot \log_{10}(\Pi))$	-36.39	-30.82	-32.01	-33.71
$(k_c)_{imag}$ [rad/m]	$1.0 \cdot k_0$	$1.0 \cdot k_0$	$1.275 \cdot k_0$	$1.02 \cdot k_0$
$\Im(10 \cdot \log_{10}(\Pi))$	83.05	45.40	61.34	31.24

**Table A19.12** Optimum Butterworth filtered double-layer damped beam cut-off frequencies and relative MSE using the IEDI method.

Appendix A20

Figures of Truncated ESPI Displacement and ESPI Measured Vibrational Energy Flow of “Infinite” Beam

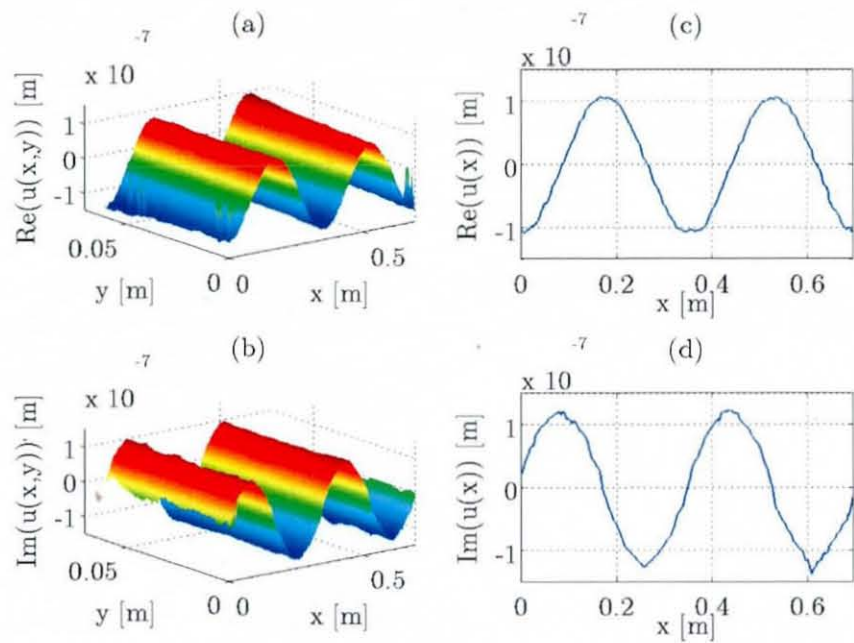


Figure A20.1 ESPI image of the measured beam displacement at 801 Hz: (a) 2D real part, (b) 2D imaginary part, (c) 1D real part, (d) 1D imaginary part.

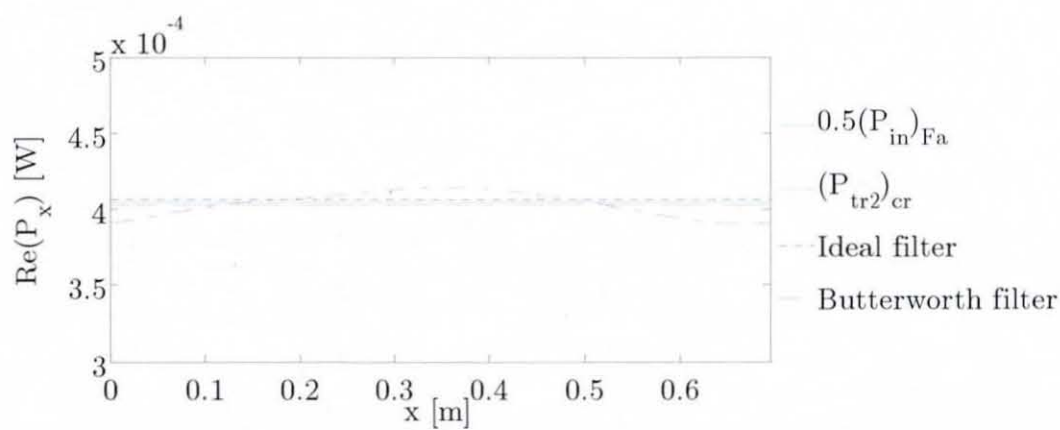
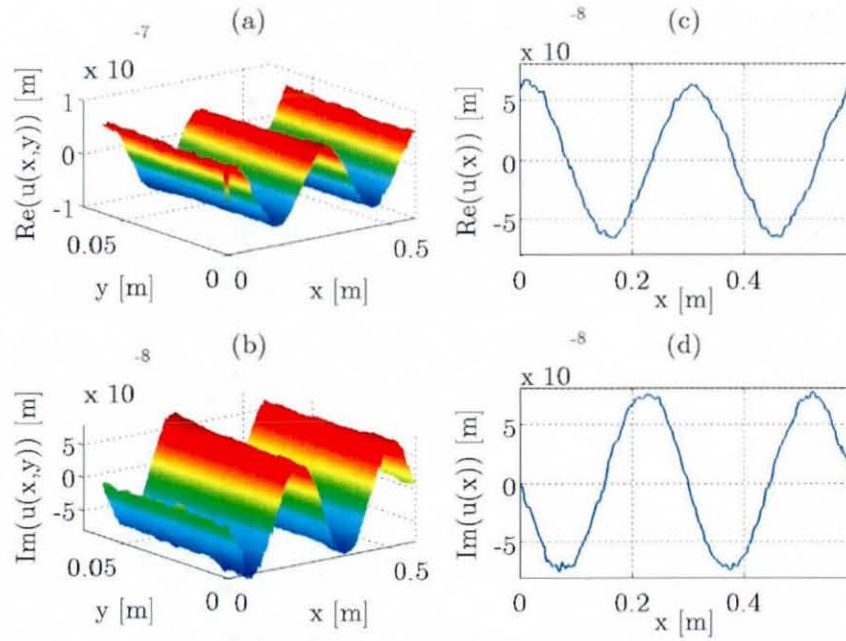
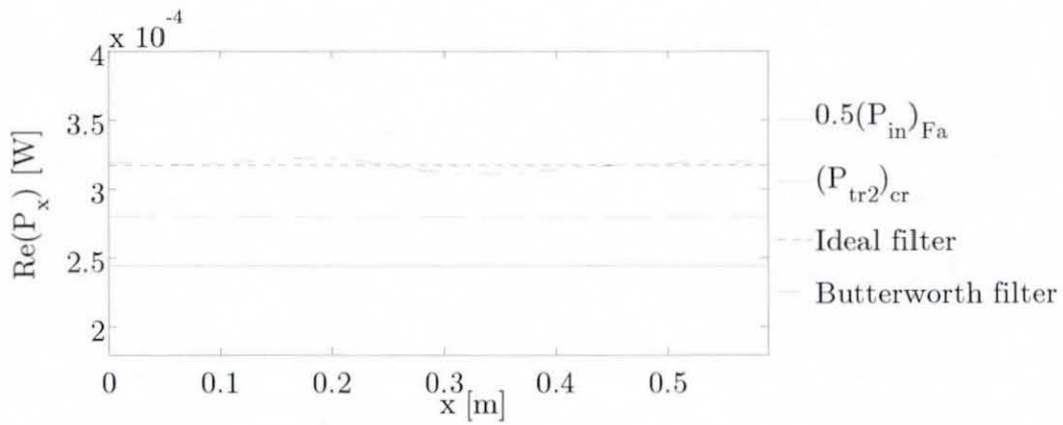


Figure A20.2 Comparison of measured input power  $(P_{in})_{Fa}$ , measured corrected transmitted energy  $(P_{tr2})_{cr}$  and measured ESPI based energy flow at 801 Hz.



**Figure A20.3** ESPI image of the measured beam displacement at 1112 Hz: (a) 2D real part, (b) 2D imaginary part, (c) 1D real part, (d) 1D imaginary part.



**Figure A20.4** Comparison of measured input power  $(P_m)_{Fa}$ , measured corrected transmitted energy  $(P_{tr2})_{cr}$  and measured ESPI based energy flow at 1112 Hz.



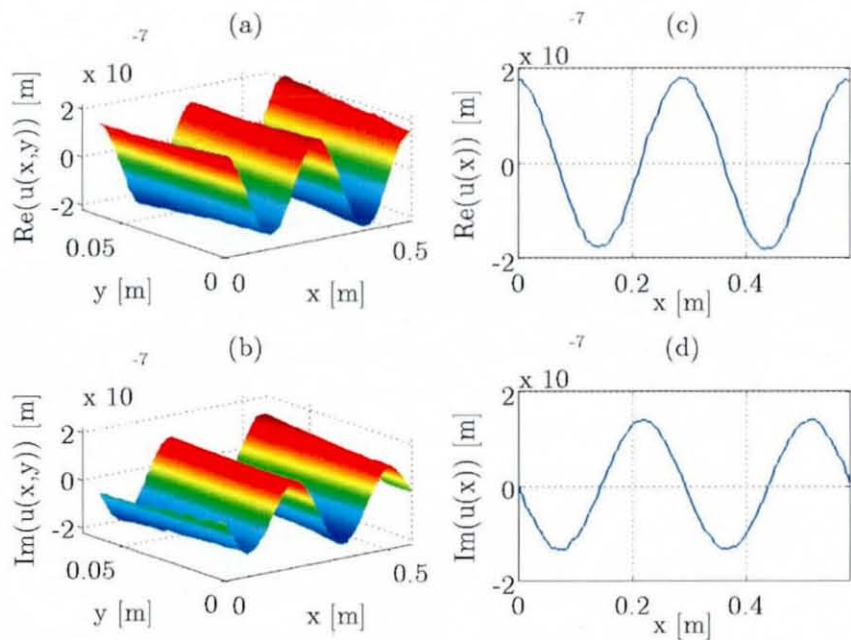


**Figure A20.5** ESPI image of the measured beam displacement at 1146 Hz: (a) 2D real part, (b) 2D imaginary part, (c) 1D real part, (d) 1D imaginary part.

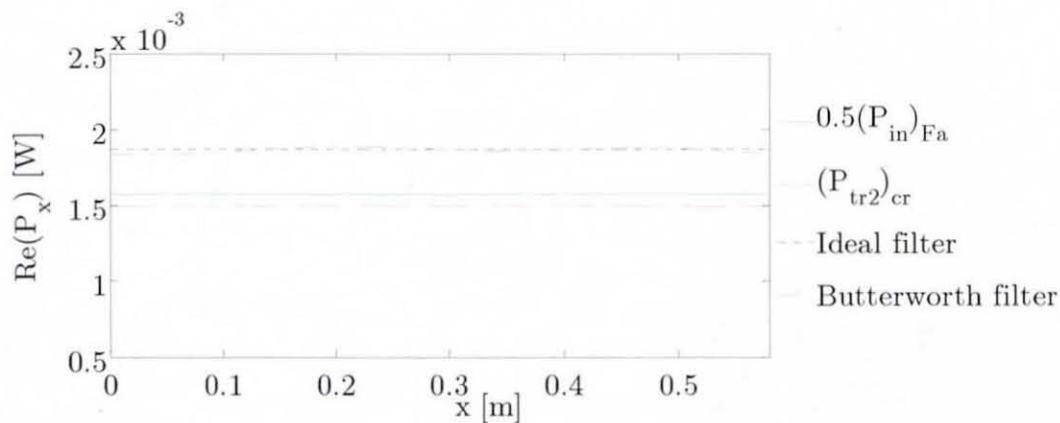


**Figure A20.6** Comparison of measured input power  $(P_{in})_{Fa}$ , measured corrected transmitted energy  $(P_{tr2})_{cr}$  and measured ESPI based energy flow at 1146 Hz.

Here,  $x$  is the beam length and  $y$  is the beam width.

## Appendix A21

### Transducer Measured Vibrational Input Power, Measured Four-Accelerometer and Two-Accelerometer Transmitted Energy of the Simply Supported Beam

Below,  $n$  is mode number,  $f_0$  is the resonant excitation frequency,  $(P_m)_{Fa}$  is the measured VIP,  $(P_{tr_i})$  is the four-accelerometer measured transmitted energy, and  $(P_{tr_j})$  is the two-accelerometer measured transmitted energy to the left and to the right of the excitation location.

$n$	6	8	9	11
$f_0$	857 Hz	1467.5 Hz	1874 Hz	2772 Hz
$(P_m)_{Fa}$	$1.8449 \cdot 10^{-4}$	$3.7349 \cdot 10^{-4}$	$1.3127 \cdot 10^{-4}$	$2.5009 \cdot 10^{-4}$
$(P_{tr_i})_{left}$	$-4.6487 \cdot 10^{-4}$	$-2.1928 \cdot 10^{-4}$	$-2.7560 \cdot 10^{-4}$	$-4.1243 \cdot 10^{-4}$
$(P_{tr_i})_{right}$	$1.1438 \cdot 10^{-4}$	$9.9085 \cdot 10^{-5}$	$1.6196 \cdot 10^{-5}$	$1.1088 \cdot 10^{-4}$
$\Sigma(P_{tr_i})$	$5.7925 \cdot 10^{-4}$	$3.1837 \cdot 10^{-4}$	$2.9180 \cdot 10^{-4}$	$5.2330 \cdot 10^{-4}$

**Table A21.1** Transducer measured input power and measured transmitted energy of the non-layer damped beam (all power values given in units of Watts).

$n$	6	8	9	11
$f_0$	833.5 Hz	1441 Hz	1830.5 Hz	2745 Hz
$(P_m)_{Fa}$	$9.0819 \cdot 10^{-5}$	$2.4778 \cdot 10^{-4}$	$2.0965 \cdot 10^{-4}$	$1.9544 \cdot 10^{-3}$
$(P_{tr_i})_{left}$	$-1.7404 \cdot 10^{-6}$	$-5.5333 \cdot 10^{-11}$	$-3.9034 \cdot 10^{-5}$	$-6.5469 \cdot 10^{-4}$
$(P_{tr_i})_{right}$	$5.5399 \cdot 10^{-5}$	$8.2122 \cdot 10^{-5}$	$6.2524 \cdot 10^{-5}$	$5.9291 \cdot 10^{-4}$
$\Sigma(P_{tr_i})$	$5.7139 \cdot 10^{-5}$	$8.2122 \cdot 10^{-5}$	$1.0156 \cdot 10^{-4}$	$1.2476 \cdot 10^{-3}$

**Table A21.2** Transducer measured input power and measured transmitted energy of the single-layer damped beam (all power values given in units of Watts).

$n$	6	8	9	11
$f_0$	821 Hz	1426 Hz	1797 Hz	2682 Hz
$(P_{in})_{Fa}$	$2.8646 \cdot 10^{-4}$	$1.6653 \cdot 10^{-4}$	$1.8977 \cdot 10^{-4}$	$2.6488 \cdot 10^{-3}$
$(P_{tr_4})_{left}$	$-5.5720 \cdot 10^{-5}$	$-1.4471 \cdot 10^{-4}$	$-9.8116 \cdot 10^{-5}$	$-3.7872 \cdot 10^{-3}$
$(P_{tr_4})_{right}$	$2.2064 \cdot 10^{-4}$	$4.4348 \cdot 10^{-5}$	$1.8676 \cdot 10^{-5}$	$2.2237 \cdot 10^{-3}$
$\Sigma(P_{tr_4})$	$2.7636 \cdot 10^{-4}$	$1.8906 \cdot 10^{-4}$	$1.1679 \cdot 10^{-4}$	$6.0109 \cdot 10^{-3}$

**Table A21.3** Transducer measured input power and measured transmitted energy of the double-layer damped beam (all power values given in units of Watts).

$n$	6	8	9	11
$f_0$	857 Hz	1467.5 Hz	1874 Hz	2772 Hz
$(P_{in})_{Fa}$	$1.8449 \cdot 10^{-4}$	$3.7349 \cdot 10^{-4}$	$1.3127 \cdot 10^{-4}$	$2.5009 \cdot 10^{-4}$
$(P_{tr_2})_{cr-left}$	$-8.4475 \cdot 10^{-5}$	$-7.7153 \cdot 10^{-5}$	$-1.0221 \cdot 10^{-4}$	$-1.7385 \cdot 10^{-4}$
$(P_{tr_2})_{cr-right}$	$1.3379 \cdot 10^{-4}$	$2.1496 \cdot 10^{-4}$	$5.0500 \cdot 10^{-5}$	$1.2318 \cdot 10^{-4}$
$\Sigma(P_{tr_2})_{cr}$	$2.1826 \cdot 10^{-4}$	$2.9211 \cdot 10^{-4}$	$1.5271 \cdot 10^{-4}$	$2.9702 \cdot 10^{-4}$

**Table A21.4** Transducer measured input power and measured transmitted energy of the non-layer damped beam (all power values given in units of Watts).

$n$	6	8	9	11
$f_0$	833.5 Hz	1441 Hz	1830.5 Hz	2745 Hz
$(P_{in})_{Fa}$	$9.0819 \cdot 10^{-5}$	$2.4778 \cdot 10^{-4}$	$2.0965 \cdot 10^{-4}$	$1.9544 \cdot 10^{-3}$
$(P_{tr_2})_{cr-left}$	$-1.7388 \cdot 10^{-5}$	$-8.9068 \cdot 10^{-6}$	$-5.1867 \cdot 10^{-5}$	$-8.2533 \cdot 10^{-4}$
$(P_{tr_2})_{cr-right}$	$5.9086 \cdot 10^{-5}$	$1.6623 \cdot 10^{-4}$	$9.0806 \cdot 10^{-5}$	$7.9381 \cdot 10^{-4}$
$\Sigma(P_{tr_2})_{cr}$	$7.6474 \cdot 10^{-5}$	$1.7513 \cdot 10^{-4}$	$1.4267 \cdot 10^{-4}$	$1.6192 \cdot 10^{-3}$

**Table A21.5** Transducer measured input power and measured transmitted energy of the single-layer damped beam (all power values given in units of Watts).

$n$	6	8	9	11
$f_0$	821 Hz	1426 Hz	1797 Hz	2682 Hz
$(P_{in})_{Fa}$	$2.8646 \cdot 10^{-4}$	$1.6653 \cdot 10^{-4}$	$1.8977 \cdot 10^{-4}$	$2.6488 \cdot 10^{-3}$
$(P_{tr_2})_{cr-left}$	$-4.7323 \cdot 10^{-5}$	$-4.0214 \cdot 10^{-5}$	$-5.4364 \cdot 10^{-5}$	$-2.5924 \cdot 10^{-3}$
$(P_{tr_2})_{cr-right}$	$1.7195 \cdot 10^{-4}$	$1.0172 \cdot 10^{-4}$	$9.3876 \cdot 10^{-5}$	$1.6037 \cdot 10^{-3}$
$\Sigma(P_{tr_2})_{cr}$	$2.1928 \cdot 10^{-4}$	$1.4193 \cdot 10^{-4}$	$1.4824 \cdot 10^{-4}$	$4.1961 \cdot 10^{-3}$

**Table A21.6** Transducer measured input power and measured transmitted energy of the double-layer damped beam (all power values given in units of Watts).

## Appendix A22

# ESPI Measured Vibrational Energy Flow of Experimental Simply Supported Beams Using the VEFESPI Method

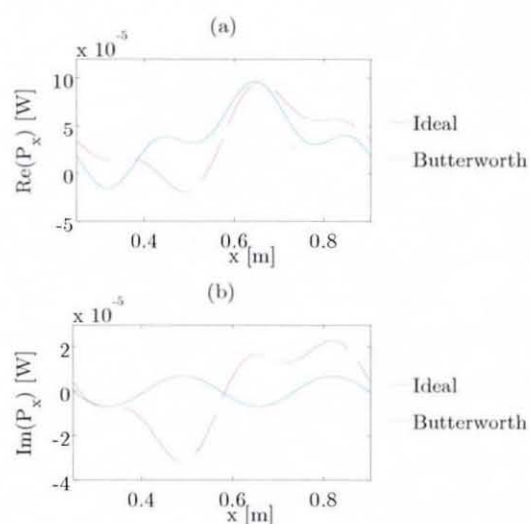


**Figure A22.1** 6<sup>th</sup> mode – no damping layer: (a) active VEF, (b) reactive VEF.

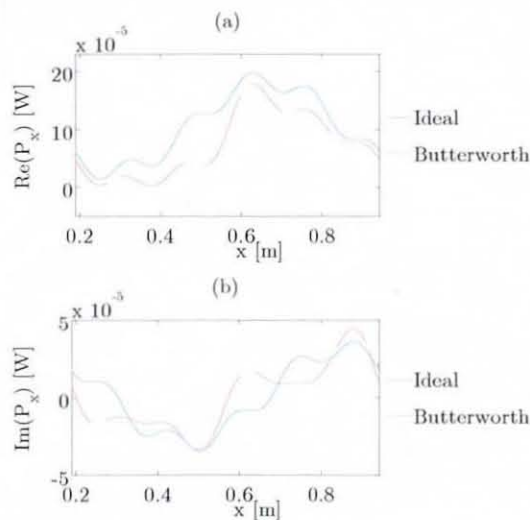


**Figure A22.2** 8<sup>th</sup> mode – no damping layer: (a) active VEF, (b) reactive VEF.

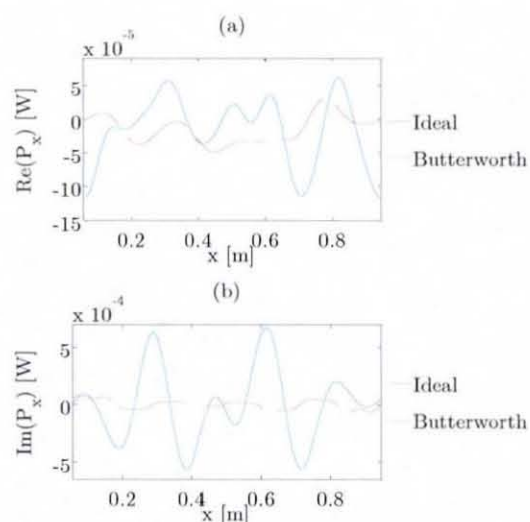


**Figure A22.3** 9<sup>th</sup> mode – no damping layer: (a) active VEF, (b) reactive VEF.

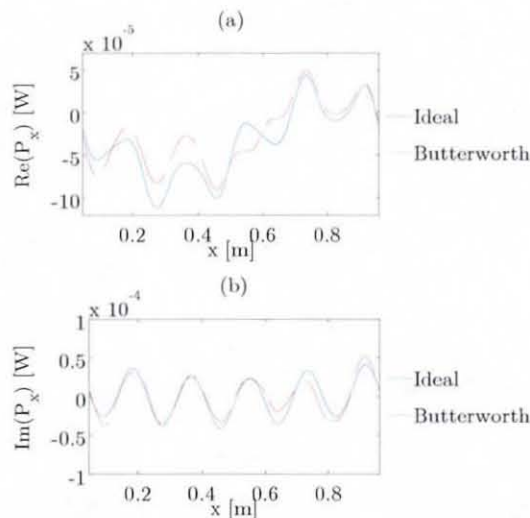


**Figure A22.4** 11<sup>th</sup> mode – no damping layer: (a) active VEF, (b) reactive VEF.



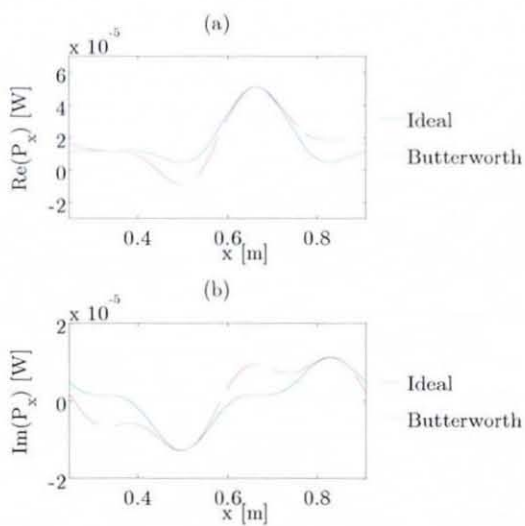


**Figure A22.5** 6<sup>th</sup> mode – single damping layer: (a) active VEF, (b) reactive VEF.

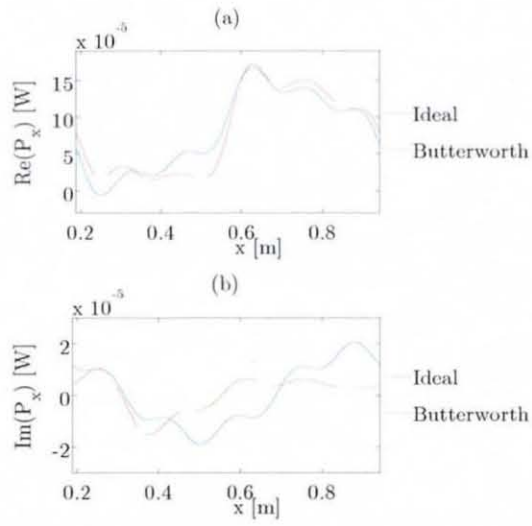


**Figure A22.6** 8<sup>th</sup> mode – single damping layer: (a) active VEF, (b) reactive VEF.

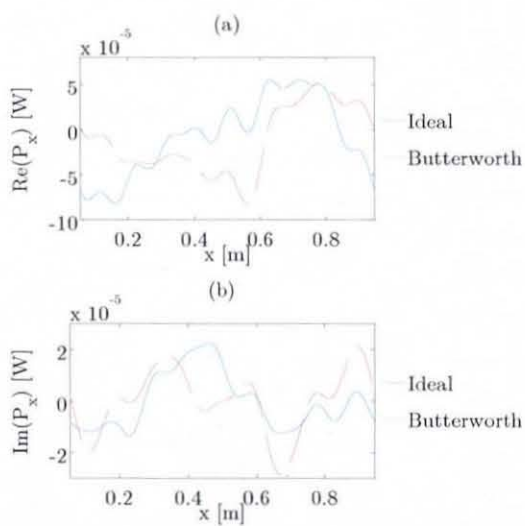


**Figure A22.7** 9<sup>th</sup> mode – single damping layer: (a) active VEF, (b) reactive VEF.

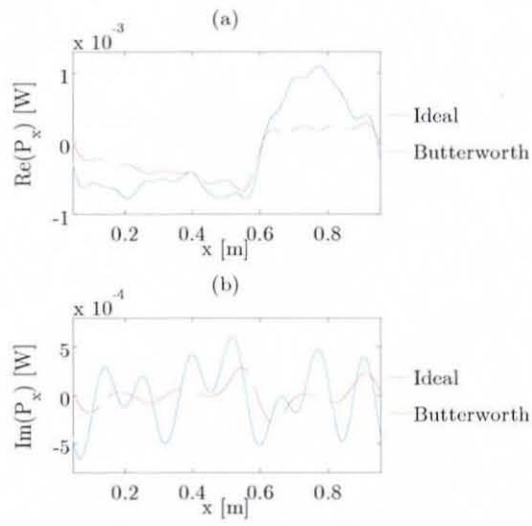


**Figure A22.8** 11<sup>th</sup> mode – single damping layer: (a) active VEF, (b) reactive VEF.

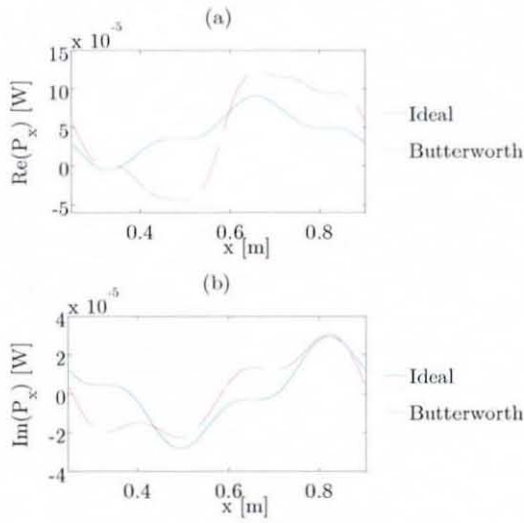


**Figure A22.9** 6<sup>th</sup> mode – double damping layer: (a) active VEF, (b) reactive VEF.

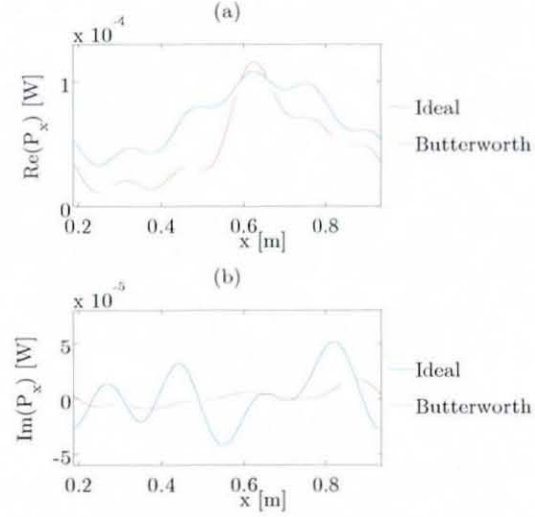


**Figure A22.10** 8<sup>th</sup> mode – double damping layer: (a) active VEF, (b) reactive VEF.

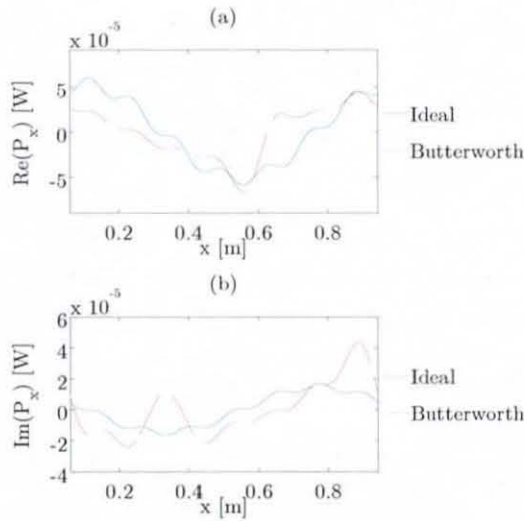


**Figure A22.11** 9<sup>th</sup> mode – double damping layer: (a) active VEF, (b) reactive VEF.

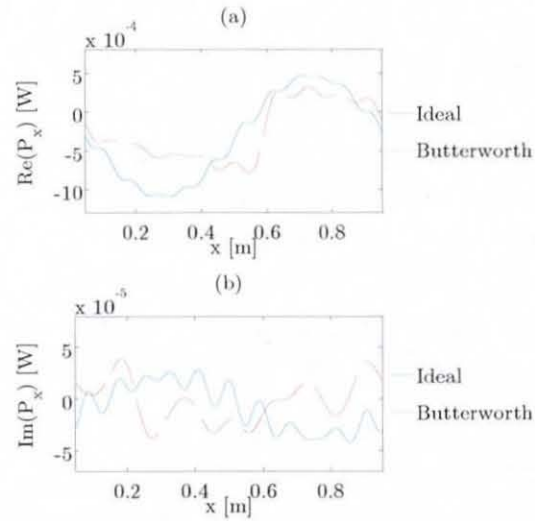


**Figure A22.12** 11<sup>th</sup> mode – double damping layer: (a) active VEF, (b) reactive VEF.

In the above shown figures, the quantity shown on the  $x$ -axis is the beam length  $x$ .

## Appendix A23

### ESPI Measured Vibrational Energy Flow of Experimental Simply Supported Beams Using the Incremental Energy Density Integration Method

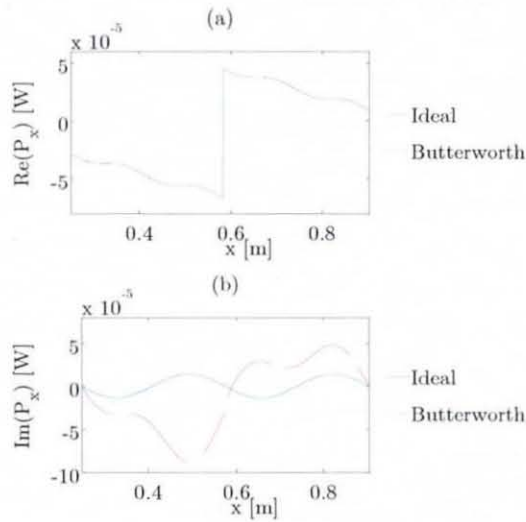


**Figure A23.1** 6<sup>th</sup> mode – no damping layer: (a) active VEF, (b) reactive VEF.

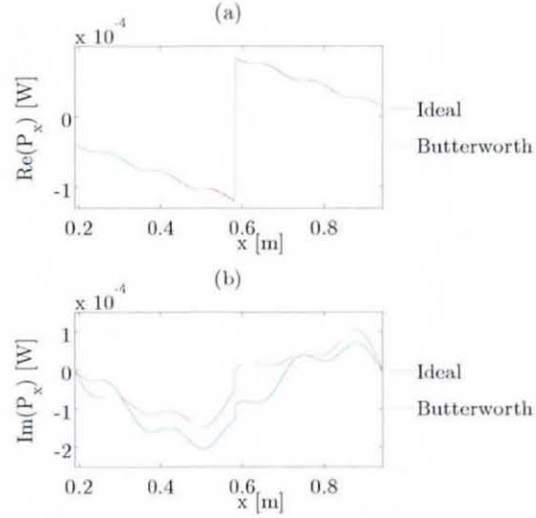


**Figure A23.2** 8<sup>th</sup> mode – no damping layer: (a) active VEF, (b) reactive VEF.

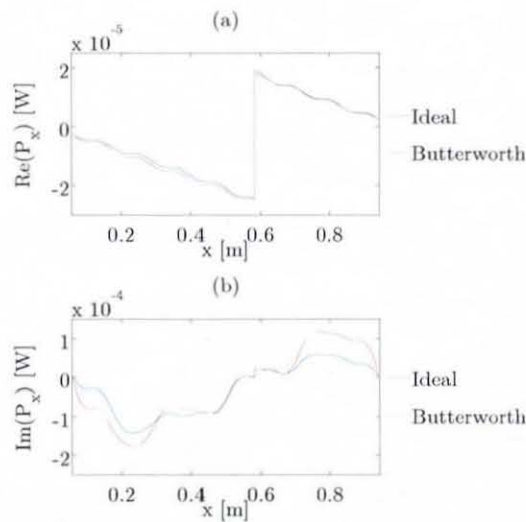


**Figure A23.3** 9<sup>th</sup> mode – no damping layer: (a) active VEF, (b) reactive VEF.

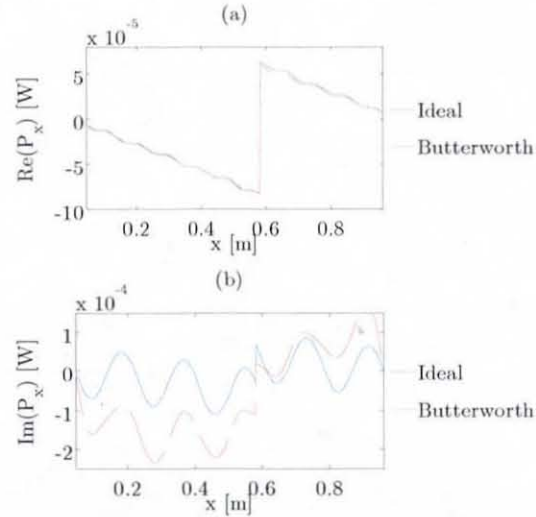


**Figure A23.4** 11<sup>th</sup> mode – no damping layer: (a) active VEF, (b) reactive VEF.



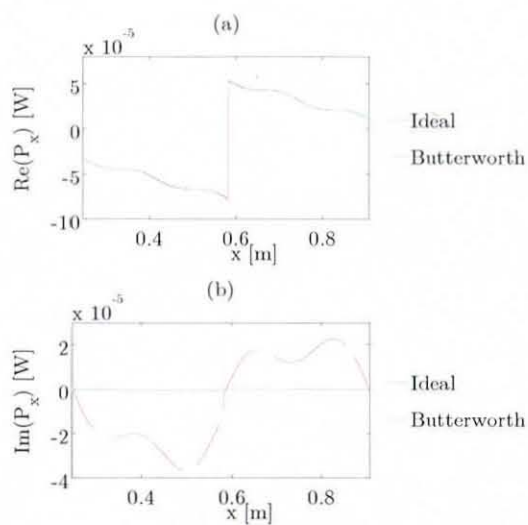


**Figure A23.5** 6<sup>th</sup> mode – single damping layer: (a) active VEF, (b) reactive VEF.

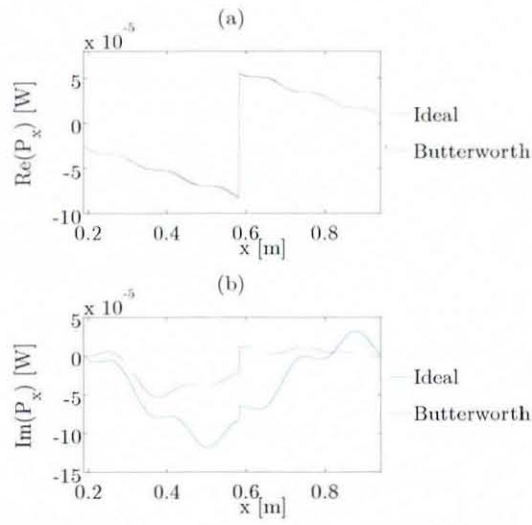


**Figure A23.6** 8<sup>th</sup> mode – single damping layer: (a) active VEF, (b) reactive VEF.

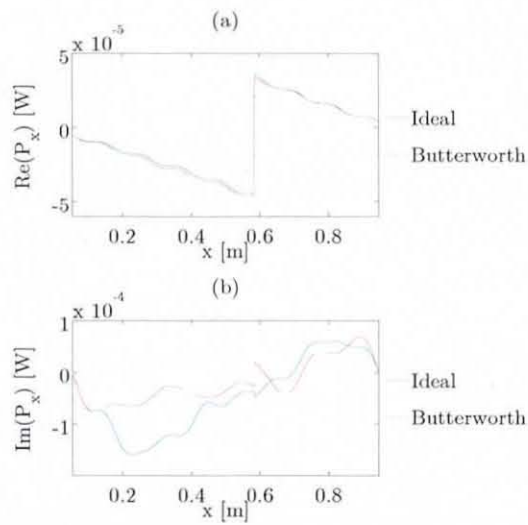


**Figure A23.7** 9<sup>th</sup> mode – single damping layer: (a) active VEF, (b) reactive VEF.

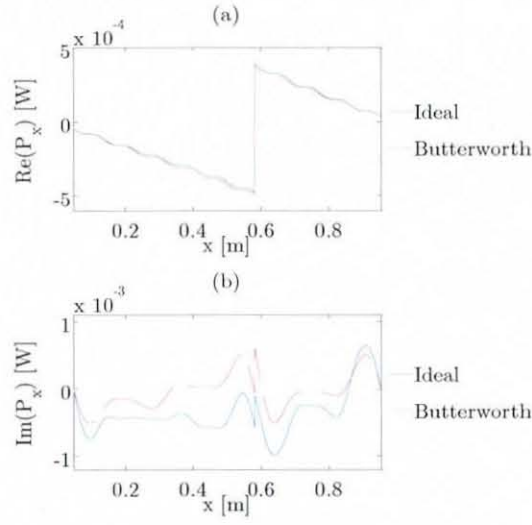


**Figure A23.8** 11<sup>th</sup> mode – single damping layer: (a) active VEF, (b) reactive VEF.

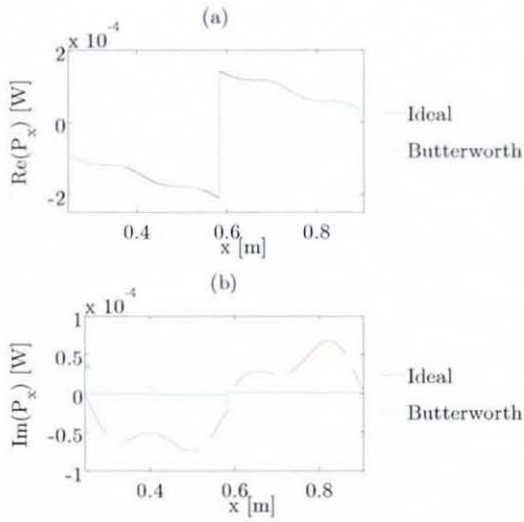


**Figure A23.9** 6<sup>th</sup> mode – double damping layer: (a) active VEF, (b) reactive VEF.

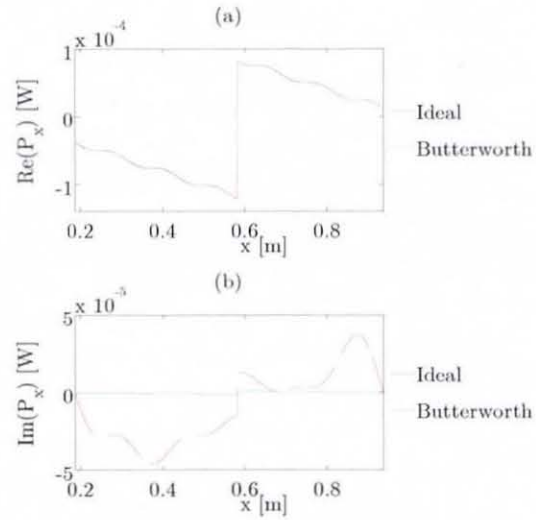


**Figure A23.10** 8<sup>th</sup> mode – double damping layer: (a) active VEF, (b) reactive VEF.

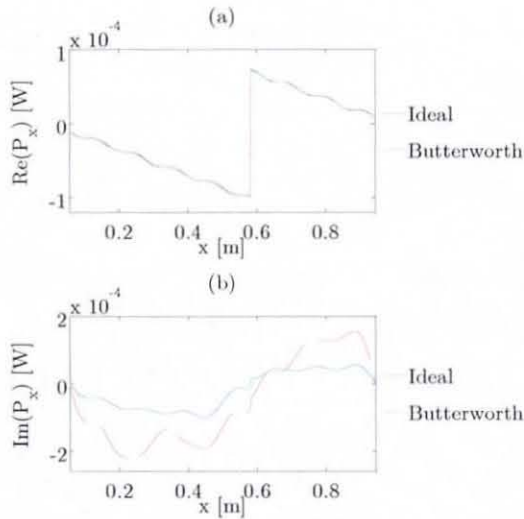


**Figure A23.11** 9<sup>th</sup> mode – double damping layer: (a) active VEF, (b) reactive VEF.

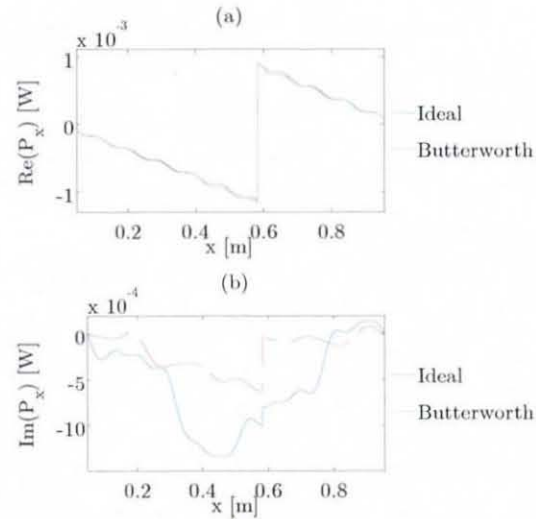


**Figure A23.12** 11<sup>th</sup> mode – double damping layer: (a) active VEF, (b) reactive VEF.

In the above shown figures, the quantity shown on the  $x$ -axis is the beam length  $x$ .

## Appendix A24

### Forced Vibration of an Infinite Plate due to Point Force Excitation

It is assumed herein that the solution of the plate's homogenous partial differential equation of motion is in general form of [18]:

$$w(r, \theta, t) = \Re \left( W_n(r) e^{j(n\theta + \omega t)} \right). \quad (\text{A24.1})$$

Here,  $r$  is the radial distance from the point of excitation,  $\theta$  is the angle between radius and the positive  $x$ -axis,  $w(r, \theta, t)$  is the polar and temporal plate displacement,  $t$  is the variable time and  $n$  is any integer number. If one substitutes equation (A24.1) into the homogenous part of the thin plate's differential equation, as shown in (A3.21), and employs the two-dimensional Laplacian operator  $\nabla^2$  in polar form, as given by equation (3.62), one can divide the 4<sup>th</sup> order differential equation into two 2<sup>nd</sup> order differential equations as [109]:

$$\frac{\partial^2 w}{\partial r^2} + \frac{1}{r} \frac{\partial w}{\partial r} - \left( \frac{n^2}{r^2} \pm k^2 \right) W = 0. \quad (\text{A24.2})$$

It can be noticed that the above displayed differential equation is equivalent to Bessel's differential equation. The general solution of Bessel's differential equation is the Bessel function of the second kind [143]. Taking into account the Sommerfeld radiation condition and the following boundary condition at the excitation location [103]:

$$\frac{\partial w(0, t)}{\partial r} = 0, \quad (\text{A24.3})$$

one can find the solution to the point force excited infinite plate as a combination of two Bessel functions of the third kind. Using a complex

solution, the Hankel function of second kind and zero order can be used to form the infinite plate displacement response as [103]:

$$w(r, \theta, t) = W_0 \left( H_0^{(2)}(kr) - H_0^{(2)}(-jkr) \right) e^{j\omega t}. \quad (\text{A24.4})$$

Here,  $W_0$  is the displacement amplitude at the excitation location and  $H_0^{(2)}(kr)$  is the Hankel function of second kind and zero order ( $n = 0$ ). This part physically represents the farfield of the vibrating plate.  $H_0^{(2)}(-jkr)$  also denotes a Hankel function of second kind and zero order however, represents a decaying nearfield around the excitation location. The unknown displacement amplitude  $W_0$  can be determined from applying the following boundary condition as given by [103]:

$$\int_0^{2\pi} Q(r_0) d\theta = F. \quad (\text{A24.5})$$

Equation (A24.5) states that the integrated radial shear force  $Q(r_0)$  around a small circle of radius  $r_0$  is equal to the excitation force  $F = F_0 e^{j\omega t}$ . The diameter of the circle should be smaller than the wavelength of the flexural wave, generated at the excitation location however, large enough to avoid the singularity of the Hankel function at  $r_0 = 0$ . Solving (A24.5) and taking the circumference  $2\pi r_0$  into account, the displacement of a point force excited infinite plate is given by [103]:

$$w(r, \theta, t) = \frac{F_0}{j8Dk^2} \left( H_0^{(2)}(kr) - H_0^{(2)}(-jkr) \right) e^{j\omega t}. \quad (\text{A24.6})$$

Here,  $D$  is the plate's flexural rigidity as defined by equation (A3.13).

## Appendix A25

### Transmitted Vibrational Energy in an Infinite Plate Using Polar Coordinates

The infinite plate displacement based on the truncated asymptotic expansion for large values of  $|kr|$  is given by [103]:

$$w(r, \theta, t) \approx \frac{F_0}{j8Dk^2} \sqrt{\frac{2}{\pi kr}} \left( e^{-j\left(kr - \frac{\pi}{4}\right)} - je^{-kr} \right) e^{j\omega t}. \quad (10.6)$$

The first exponential term in equation (10.6) represents a travelling wave and the second exponential term in equation (10.6) represents an evanescent wave. If one substitutes the exponential decaying part of equation (10.6) into equation (3.68) (all spatial derivatives in equation (3.69) will be zero), the time-averaged polar shear force VEF due to the evanescent waves can be written as:

$$\left( \overline{P_{rs \text{ evan}}} \right)_{F_\infty} = j \frac{\omega F_0^2 e^{-2kr}}{512D\pi} \left( \frac{5}{k^5 r^4} + \frac{2}{k^4 r^3} + \frac{4}{k^3 r^2} + \frac{8}{k^2 r} \right). \quad (A25.1)$$

Analogously, the time-averaged polar bending moment VEF due to evanescent waves can be found to be:

$$\left( \overline{P_{rb \text{ evan}}} \right)_{F_\infty} = j \frac{\omega F_0^2 e^{-2kr}}{512D\pi} \left( \frac{3}{k^5 r^4} + \frac{10}{k^4 r^3} + \frac{12}{k^3 r^2} + \frac{8}{k^2 r} - \nu \left( \frac{2}{k^5 r^4} + \frac{8}{k^4 r^3} + \frac{8}{k^3 r^2} \right) \right). \quad (A25.2)$$

As mentioned before, due to zero angular displacement variation, the angular twisting moment and, thus, the angular energy transmission is zero.

The total time-averaged polar VEF within the infinite plate due to evanescent waves. i.e.  $(\overline{P}_{r \text{ evan}})_{F_\infty} = (\overline{P}_{rs \text{ evan}})_{F_\infty} - (\overline{P}_{rb \text{ evan}})_{F_\infty}$ , can be defined as:

$$(\overline{P}_{r \text{ evan}})_{F_\infty} = j \frac{\omega F_0^2 e^{-2kr}}{256D\pi} \left( \frac{1+\nu}{k^5 r^4} + 4(\nu-1) \left( \frac{1}{k^4 r^3} + \frac{1}{k^3 r^2} \right) \right). \quad (\text{A25.3})$$

VEF due to travelling wave can be found analogously. If one substitutes the exponential travelling part of equation (10.6) into equation (3.68), the time-averaged polar shear force VEF due to the travelling waves may be written as:

$$(\overline{P}_{rs \text{ trav}})_{F_\infty} = \frac{F_0^2 \omega}{512D\pi} \left( \frac{8}{k^2 r} - \frac{2}{k^4 r^3} + j \left( \frac{5}{k^5 r^4} - \frac{4}{k^3 r^2} \right) \right). \quad (\text{A25.4})$$

Analogously, the time-averaged polar bending moment VEF due to the travelling waves may be found as:

$$(\overline{P}_{rb \text{ trav}})_{F_\infty} = \frac{F_0^2 \omega}{512D\pi} \left( -\frac{8}{k^2 r} + \frac{2}{k^4 r^3} + j \left( \frac{3-2\nu}{k^5 r^4} + \frac{4-8\nu}{k^3 r^2} \right) \right). \quad (\text{A25.5})$$

The total time-averaged polar VEF due to the travelling waves, i.e.  $(\overline{P}_{r \text{ trav}})_{F_\infty} = (\overline{P}_{rs \text{ trav}})_{F_\infty} - (\overline{P}_{rb \text{ trav}})_{F_\infty}$ , is given by:

$$(\overline{P}_{r \text{ trav}})_{F_\infty} = \frac{F_0^2 \omega}{512D\pi} \left( \frac{16}{k^2 r} - \frac{4}{k^4 r^3} + 2j \left( \frac{1+\nu}{k^5 r^4} + \frac{4(\nu-1)}{k^3 r^2} \right) \right). \quad (\text{A25.6})$$



## Appendix A26

### Transmitted Vibrational Energy in an Infinite Plate Using Cartesian Coordinates

The polar infinite plate displacement can be transformed into a Cartesian coordinate based infinite plate displacement by employing the relation  $r^2 = x^2 + y^2$ . If one substitutes this relation into equation (10.6), the Cartesian coordinate based infinite plate displacement of the infinite plate may be written as:

$$w(x, y, t) \approx \frac{F_0}{j8Dk^2} \sqrt{\frac{2}{\pi k(x^2 + y^2)^{\frac{1}{2}}}} \left( e^{-j\left(k(x^2 + y^2)^{\frac{1}{2}} - \frac{\pi}{4}\right)} - je^{-k(x^2 + y^2)^{\frac{1}{2}}} \right) e^{j\omega t}. \quad (10.12)$$

By substituting the evanescent part of equation (10.12) into equation (3.49), the time-averaged shear force VEF due to the evanescent waves of the infinite plate in the  $x$  direction can be found to be:

$$\left( \overline{P}_{x_s \text{ evan}} \right)_{F_\infty} = j \frac{F_0^2 \omega e^{-2k(x^2 + y^2)^{\frac{1}{2}}}}{512Dk^5 \pi (x^2 + y^2)^{\frac{5}{2}}} \left( \begin{aligned} &5x + 2kx(x^2 + y^2)^{\frac{1}{2}} + \\ &4k^2 x(x^2 + y^2) + \\ &8k^3 x(x^2 + y^2)^{\frac{3}{2}} \end{aligned} \right). \quad (A26.1)$$

Analogously, the twisting moment VEF can be found as:

$$\left( \overline{P}_{x_t \text{ evan}} \right)_{F_\infty} = -j \frac{F_0^2 \omega (\nu - 1) e^{-2k(x^2 + y^2)^{\frac{1}{2}}}}{512Dk^5 \pi (x^2 + y^2)^{\frac{5}{2}}} \left( \begin{aligned} &\frac{5xy^2}{(x^2 + y^2)} + 20k^2 xy^2 + \\ &\frac{18kxy^2}{(x^2 + y^2)^{\frac{1}{2}}} + \\ &8k^3 xy^2 (x^2 + y^2)^{\frac{1}{2}} \end{aligned} \right). \quad (A26.2)$$

The bending moment VEF due to the evanescent waves may be written as:

$$\left( \overline{P}_{x_B \text{ evan}} \right)_{F_\infty} = jC_B \left[ \begin{aligned} & \frac{4k^2 x}{(x^2 + y^2)} (x^4 + x^2 y^2 + \nu(x^2 y^2 + y^4)) + \\ & \frac{4kx}{(x^2 + y^2)^{\frac{1}{2}}} (x^2 - y^2 - \nu(x^2 - y^2)) + \\ & \frac{x}{(x^2 + y^2)} (x^2(3 - 2\nu) + y^2(3\nu - 2)) + \\ & \frac{8k^3 x}{(x^2 + y^2)^{\frac{1}{2}}} (x^4 + x^2 y^2 + \nu(x^2 y^2 + y^4)) + \\ & 8k^2 x (x^2 - y^2 - \nu(x^2 - y^2)) + \\ & \frac{2kx}{(x^2 + y^2)^{\frac{1}{2}}} (x^2(3 - 2\nu) + y^2(3\nu - 2)) \end{aligned} \right], \quad (\text{A26.3})$$

with the constant  $C_B$  being defined as:

$$C_B = \frac{F_0^2 \omega e^{-2k(x^2 + y^2)^{\frac{1}{2}}}}{512 D k^5 \pi (x^2 + y^2)^{\frac{5}{2}}}. \quad (\text{A26.4})$$

It can be realised from equation (A26.1) that equation (A26.1) is equal to equation (A25.1). Equation (A25.1) can be obtained, if one substitutes  $r = (x^2 + y^2)^{\frac{1}{2}}$  and  $x = \cos(\theta)r$  with  $\theta = 0$ , into equation (A25.1). The same procedure holds true for the remaining VEF expressions due to bending moment and twisting moment. The total time-averaged Cartesian coordinate based VEF in the  $x$  direction due to evanescent waves, which simply is the difference of all three VEF parts, i.e.  $\left( \overline{P}_{x \text{ evan}} \right)_{F_\infty} = \left( \overline{P}_{x_S \text{ evan}} \right)_{F_\infty} - \left( \overline{P}_{x_B \text{ evan}} \right)_{F_\infty} - \left( \overline{P}_{x_T \text{ evan}} \right)_{F_\infty}$ , is given by:



$$\left(\overline{P}_{x\,evan}\right)_{F_\infty} = j \frac{F_0^2 \omega x e^{-2k(x^2+y^2)^{\frac{1}{2}}}}{256 D k^5 \pi (x^2+y^2)^2} \left[ \frac{4k^2 (x^2+y^2)^{\frac{1}{2}} (\nu-1) +}{4k(\nu-1) + \frac{(\nu+1)}{(x^2+y^2)^{\frac{1}{2}}}} \right]. \quad (A26.5)$$

If one substitutes the travelling part of equation (10.12) into equation (3.49), the Cartesian coordinate based time-averaged shear force VEF can be written as:

$$\left(\overline{P}_{x_s\,trav}\right)_{F_\infty} = \frac{F_0^2 \omega}{512 D k^5 \pi (x^2+y^2)^{\frac{5}{2}}} \left[ \frac{5jx - 2kx(x^2+y^2)^{\frac{1}{2}} -}{4jk^2x(x^2+y^2) + 8k^3x(x^2+y^2)^{\frac{3}{2}}} \right]. \quad (A26.6)$$

The bending moment VEF the  $x$  direction may be written as:

$$\left(\overline{P}_{x_B\,trav}\right)_{F_\infty} = -C_B \left[ \frac{4jk^2x}{(x^2+y^2)} (x^4 + x^2y^2 + \nu(x^2y^2 + y^4)) + \frac{4kx}{(x^2+y^2)^{\frac{1}{2}}} (x^2 - y^2 - \nu(x^2 - y^2)) + \frac{jx}{(x^2+y^2)} (x^2(2\nu-3) + y^2(2-3\nu)) + \frac{8k^3x}{(x^2+y^2)^{\frac{1}{2}}} (x^4 + x^2y^2 + \nu(x^2y^2 + y^4)) - \frac{8jk^2x}{(x^2+y^2)^{\frac{1}{2}}} (x^2 - y^2 - \nu(x^2 - y^2)) + \frac{2kx}{(x^2+y^2)^{\frac{1}{2}}} (x^2(2\nu-3) + y^2(2-3\nu)) \right], \quad (A26.7)$$

with the constant  $C_B$  being defined as:

$$C_B = \frac{F_0^2 \omega (Dk^5 \pi)^{-1}}{512 (x^2 + y^2)^{\frac{5}{2}}}. \quad (\text{A26.8})$$

The twisting moment in the  $x$  direction can be found to be:

$$\left( \overline{P}_{x \text{ trav}} \right)_{F_\infty} = - \frac{F_0^2 \omega (Dk^5 \pi)^{-1} (\nu - 1)}{512 (x^2 + y^2)^{\frac{5}{2}}} \left[ \begin{aligned} & \left( \frac{5jxy^2}{(x^2 + y^2)} + 12jk^2xy^2 + \right. \\ & \left. \frac{2kxy^2}{(x^2 + y^2)^{\frac{1}{2}}} - \right. \\ & \left. 8k^3xy^2(x^2 + y^2)^{\frac{1}{2}} \right). \end{aligned} \right] \quad (\text{A26.9})$$

Shear force, bending moment and twisting moment VEF expression in the  $y$  direction can be found analogously, simply by interchanging  $x$  and  $y$  in the above given equations. The total time-averaged transmitted VEF, i.e.

$\left( \overline{P}_{x \text{ trav}} \right)_{F_\infty} = \left( \overline{P}_{x_s \text{ trav}} \right)_{F_\infty} - \left( \overline{P}_{x_B \text{ trav}} \right)_{F_\infty} - \left( \overline{P}_{x_T \text{ trav}} \right)_{F_\infty}$ , is given by:

$$\left( \overline{P}_{x \text{ trav}} \right)_{F_\infty} = \frac{F_0^2 \omega (Dk^5 \pi)^{-1} x}{256 (x^2 + y^2)^3} \left[ \begin{aligned} & 8k^3 (x^2 + y^2)^2 - 2k (x^2 + y^2) + \\ & j (x^2 + y^2)^{\frac{1}{2}} \left( (\nu + 1) + \right. \\ & \left. 4k^2 (\nu - 1) (x^2 + y^2) \right) \end{aligned} \right]. \quad (\text{A26.10})$$

## Appendix A27

### Transmitted Vibrational Energy in a Simply Supported Plate

The derivation of VEF in a simply supported plate is based on the eigenfunction expansion theorem applied to define the simply supported rectangular plate displacement as given by:

$$w(x, y, t) = \frac{4F_0 e^{j\omega t}}{\rho h L_x L_y} \sum_{m=1}^{\infty} \sum_{n=1}^{\infty} \frac{\sin\left(\frac{m\pi x}{L_x}\right) \sin\left(\frac{n\pi y}{L_y}\right) \sin\left(\frac{m\pi x_0}{L_x}\right) \sin\left(\frac{n\pi y_0}{L_y}\right)}{\omega_{mn}^2 (1 + j\eta) - \omega^2}. \quad (10.25)$$

If one substitutes equation (10.25) into equation (3.49), one may obtain the time-averaged VEF of the shear force, bending moment and twisting moment component in  $x$  the direction separately. The shear force VEF term in the  $x$  direction is then given by:

$$\left(\overline{P}_{x_s}\right)_{F_{ss}} = \frac{j\omega D C^2}{2} \left[ \sum_{m=1}^{\infty} \sum_{n=1}^{\infty} \frac{C_m C_n}{\omega_{mn}^2 (1 + j\eta) - \omega^2} \left( \cos(C_m x) \sin(C_n y) \times \right) \right] \times \left[ \sum_{m=1}^{\infty} \sum_{n=1}^{\infty} \frac{C_m C_n}{\omega_{mn}^2 (1 - j\eta) - \omega^2} \sin(C_m x) \sin(C_n y) \right]. \quad (A27.1)$$

In equation (A27.1) and the following presented VEF expressions, the below listed simplifications are employed:

$$C = \frac{4F_0}{\rho h L_x L_y}, \quad (A27.2)$$

$$C_m = \frac{m\pi}{L_x}, \quad (A27.3)$$

$$C_n = \frac{n\pi}{L_y}, \quad (\text{A27.4})$$

$$C_{n_0} = \sin\left(\frac{m\pi x_0}{L_x}\right), \quad (\text{A27.5})$$

$$C_{n_0} = \sin\left(\frac{n\pi y_0}{L_y}\right). \quad (\text{A27.6})$$

Analogously, the bending moment VEF in the  $x$  direction can be found to be:

$$(\overline{P}_{x_B})_{F_{ss}} = \frac{j\omega DC^2}{2} \left[ \sum_{m=1}^{\infty} \sum_{n=1}^{\infty} \frac{C_{m_0} C_{n_0}}{\omega_{mn}^2 (1+j\eta) - \omega^2} \left( \frac{\sin(C_m x) \sin(C_n y)}{(C_m^2 + \nu C_n^2)} \right) \times \right. \\ \left. \sum_{m=1}^{\infty} \sum_{n=1}^{\infty} \frac{C_{m_0} C_{n_0}}{\omega_{mn}^2 (1-j\eta) - \omega^2} C_m \cos(C_m x) \sin(C_n y) \right]. \quad (\text{A27.7})$$

The twisting moment VEF in the  $x$  direction can be obtained as:

$$(\overline{P}_{x_T})_{F_{ss}} = -\frac{j\omega DC^2}{2} \left[ \sum_{m=1}^{\infty} \sum_{n=1}^{\infty} \frac{C_{m_0} C_{n_0} (1-\nu)}{\omega_{mn}^2 (1+j\eta) - \omega^2} \left( \frac{C_m C_n \times}{\cos(C_m x) \cos(C_n y)} \right) \times \right. \\ \left. \sum_{m=1}^{\infty} \sum_{n=1}^{\infty} \frac{C_{m_0} C_{n_0}}{\omega_{mn}^2 (1-j\eta) - \omega^2} C_n \sin(C_m x) \cos(C_n y) \right]. \quad (\text{A27.8})$$

The transmitted energy in the  $y$  direction can be determined due to symmetry properties simply by interchanging  $x$  and  $y$  as well as  $m$  and  $n$  in equations (A27.1), (A27.7) and A(27.8). Thus, VEF in the simply supported rectangular plate due to the shear force component in  $y$  direction is:

$$(\overline{P}_{y_S})_{F_{ss}} = \frac{j\omega DC^2}{2} \left[ \sum_{m=1}^{\infty} \sum_{n=1}^{\infty} \frac{C_{m_0} C_{n_0}}{\omega_{mn}^2 (1+j\eta) - \omega^2} \left( \frac{\sin(C_m x) \cos(C_n y)}{(C_n^3 + C_n C_m^2)} \right) \times \right. \\ \left. \sum_{m=1}^{\infty} \sum_{n=1}^{\infty} \frac{C_{m_0} C_{n_0}}{\omega_{mn}^2 (1-j\eta) - \omega^2} \sin(C_m x) \sin(C_n y) \right]. \quad (\text{A27.9})$$

Similarly, the bending moment VEF in the  $y$  direction is given by:

$$(\overline{P}_{y_B})_{F_{ss}} = \frac{j\omega DC^2}{2} \left[ \sum_{m=1}^{\infty} \sum_{n=1}^{\infty} \frac{C_{m_0} C_{n_0}}{\omega_{mn}^2 (1+j\eta) - \omega^2} \left( \sin(C_m x) \sin(C_n y) \times \right) \times \right. \\ \left. \sum_{m=1}^{\infty} \sum_{n=1}^{\infty} \frac{C_{m_0} C_{n_0}}{\omega_{mn}^2 (1-j\eta) - \omega^2} C_n \sin(C_m x) \cos(C_n y) \right]. \quad (A27.10)$$

VEF due to the twisting moment component in the  $y$  direction may be written as:

$$(\overline{P}_{y_T})_{F_{ss}} = -\frac{j\omega DC^2}{2} \left[ \sum_{m=1}^{\infty} \sum_{n=1}^{\infty} \frac{C_{m_0} C_{n_0} (1-\nu)}{\omega_{mn}^2 (1+j\eta) - \omega^2} \left( C_m C_n \times \right. \right. \\ \left. \left. \cos(C_m x) \cos(C_n y) \right) \times \right. \\ \left. \sum_{m=1}^{\infty} \sum_{n=1}^{\infty} \frac{C_{m_0} C_{n_0}}{\omega_{mn}^2 (1-j\eta) - \omega^2} C_m \cos(C_m x) \sin(C_n y) \right]. \quad (A27.11)$$

The total VEF due to shear force, bending moment, and twisting moment components can be found by summing up the shear force, bending moment, and twisting moment VEF term, i.e.  $(\overline{P}_x)_{F_{ss}} = (\overline{P}_{x_S})_{F_{ss}} - (\overline{P}_{x_B})_{F_{ss}} - (\overline{P}_{x_T})_{F_{ss}}$ .

Thus, the total VEF in the  $x$  direction can be found to be:

$$(\overline{P}_x)_{F_{ss}} = \frac{j\omega DC^2}{2} \sum_{m=1}^{\infty} \sum_{n=1}^{\infty} \sum_{k=1}^{\infty} \sum_{i=1}^{\infty} \frac{C_{m_0} C_{n_0} C_{k_0} C_{i_0}}{(\omega_{mn}^2 (1+j\eta) - \omega^2)(\omega_{ki}^2 (1-j\eta) - \omega^2)} \times \\ \left[ \cos(C_m x) \sin(C_n y) \sin(C_k x) \sin(C_i y) (C_m^3 + C_m C_n^2) - \right. \\ \left. \sin(C_m x) \sin(C_n y) \cos(C_k x) \sin(C_i y) C_k (C_m^2 + \nu C_n^2) + \right. \\ \left. (1-\nu) \cos(C_m x) \cos(C_n y) \sin(C_k x) \cos(C_i y) C_m C_n C_i \right]. \quad (A27.12)$$

In equation (A27.12) the rule of a product of two double series:

$$\sum_{m=1}^{\infty} \sum_{n=1}^{\infty} A_m B_n \times \sum_{m=1}^{\infty} \sum_{n=1}^{\infty} E_m K_n = \sum_{m=1}^{\infty} \sum_{n=1}^{\infty} \sum_{k=1}^{\infty} \sum_{i=1}^{\infty} A_m B_n E_k K_i, \quad (A27.13)$$

as well as the sum rule of two double series:

$$\sum_{m=1}^{\infty} \sum_{n=1}^{\infty} A_m B_n \pm \sum_{m=1}^{\infty} \sum_{n=1}^{\infty} E_m K_n = \sum_{m=1}^{\infty} \sum_{n=1}^{\infty} (A_m B_n \pm E_m K_n), \quad (\text{A27.14})$$

were taken into account in order to form a fourfold series expression. Analogously, the total VEF in the  $y$  direction can be found simply by interchanging  $x$  and  $y$ ,  $m$  and  $n$  as well as  $k$  and  $i$  and, thus:

$$\begin{aligned} (\overline{P}_y)_{F_u} = & \frac{j\omega DC^2}{2} \sum_{m=1}^{\infty} \sum_{n=1}^{\infty} \sum_{k=1}^{\infty} \sum_{i=1}^{\infty} \frac{C_{m_0} C_{n_0} C_{k_0} C_{i_0}}{(\omega_{mn}^2 (1 + j\eta) - \omega^2)(\omega_{ki}^2 (1 - j\eta) - \omega^2)} \times \\ & \left( \sin(C_m x) \cos(C_n y) \sin(C_k x) \sin(C_i y) (C_n^3 + C_n C_m^2) - \right. \\ & \left. \sin(C_m x) \sin(C_n y) \sin(C_k x) \cos(C_i y) C_i (C_n^2 + \nu C_m^2) + \right. \\ & \left. (1 - \nu) \cos(C_m x) \cos(C_n y) \cos(C_k x) \sin(C_i y) C_m C_n C_k \right). \quad (\text{A27.15}) \end{aligned}$$

Equations (A27.12) and (A27.15) display the total VEF within a simply supported plate in the  $x$  and  $y$  direction, respectively. These expressions can be simplified further, by using the cotangent function. If one takes into account that  $\cot(x) = \cos(x)/\sin(x)$ , equation (A27.12) can also be written as:

$$\begin{aligned} (\overline{P}_x)_{F_u} = & \frac{j\omega DC^2}{2} \sum_{m=1}^{\infty} \sum_{n=1}^{\infty} \sum_{k=1}^{\infty} \sum_{i=1}^{\infty} \frac{C_{m_0} C_{n_0} C_{k_0} C_{i_0}}{(\omega_{mn}^2 (1 + j\eta) - \omega^2)(\omega_{ki}^2 (1 - j\eta) - \omega^2)} \times \\ & \sin(C_m x) \sin(C_n y) \sin(C_k x) \sin(C_i y) \times \\ & \left( \cot(C_m x) (C_m^3 + C_m C_n^2) - \cot(C_k x) C_k (C_m^2 + \nu C_n^2) + \right. \\ & \left. (1 - \nu) \cot(C_m x) \cot(C_n y) \cot(C_i y) C_m C_n C_i \right). \quad (\text{A27.16}) \end{aligned}$$

By interchanging  $x$  and  $y$ ,  $m$  and  $n$  as well as  $k$  and  $i$ , the VEF within a simply supported rectangular plate in the  $y$  direction can be defined as:

$$(\overline{P}_y)_{F_s} = \frac{j\omega DC^2}{2} \sum_{m=1}^{\infty} \sum_{n=1}^{\infty} \sum_{k=1}^{\infty} \sum_{i=1}^{\infty} \frac{C_{m_0} C_{n_0} C_{k_0} C_{i_0}}{(\omega_{mn}^2 (1 + j\eta) - \omega^2)(\omega_{ki}^2 (1 - j\eta) - \omega^2)} \times \\ \sin(C_m x) \sin(C_n y) \sin(C_k x) \sin(C_i y) \times \\ \left( \cot(C_n y) (C_n^3 + C_n C_m^2) - \cot(C_i y) C_i (C_n^2 + \nu C_m^2) + \right. \\ \left. (1 - \nu) \cot(C_m x) \cot(C_n y) \cot(C_k x) C_m C_n C_k \right). \quad (\text{A27.17})$$

Note, the constants  $C_{k_0}$  and  $C_{i_0}$  as well as  $C_k$  and  $C_i$  can be found by substituting the integer variable  $k$  and  $i$  into equations (A27.3) to (A27.6) accordingly.

## Appendix A28

### Unconstrained Layer Damping of Plates

The attachment of a damping layer, as shown in Figure 10.2, causes a shift of the neutral axis of bending away from the plate's middle plane towards the attached layer. Due to the layer attachment, the original flexural rigidity of the plate changes. If one considers that the resultant normal force on the transverse cross-section due to the bending stress  $\sigma_x$  must be zero, i.e.  $\int \sigma_x dz = 0$ , the following definition may be formulated as:

$$\int_{-(h_p - z_N)}^{z_N} \sigma_{x_P} dz + \int_{z_N}^{(h_D + z_N)} \sigma_{x_D} dz = 0. \quad (\text{A28.1})$$

Herein, the subscript  $P$  denotes plate properties and the subscript  $D$  denotes damping layer properties. If one substitutes the plate and damping layer bending stress in the  $x$  direction, as given by equation (A3.7), into equation (A28.1), one may find the shifting distance  $z_N$  to be:

$$z_N = \frac{\underline{E}_P h_P^2 - \underline{E}_D h_D^2}{2(\underline{E}_P h_P + \underline{E}_D h_D)} = \frac{h_P (1 - e_{DP} H_{DP}^2)}{2(1 + e_{DP} H_{DP})}. \quad (\text{A28.2})$$

Here,  $h_P$  is the plate's thickness,  $h_D$  is the damping layer thickness,  $e_{DP} = \underline{E}_D / \underline{E}_P$  and  $H_{DP} = h_D / h_P$ . The under-bar denotes complex quantities. As it can be seen in equation (A28.2), a complex Young's modulus is employed to take structural damping into account. The respective complex Young's modulus is given as:

$$\underline{E}_P = E_P (1 + j\eta_P), \quad (\text{A28.3})$$

$$\underline{E}_D = E_D (1 + j\eta_D), \quad (\text{A17.3})$$



where  $\eta$  is the respective linear hysteretic loss factor. To simplify the definition of the neutral axis offset  $z_N$ , it was assumed in equation (A28.2) that Poisson's ratio of both materials is approximately the same thus,  $\nu_P \approx \nu_D$ . The complex, combined, flexural rigidity,  $\underline{D}_{PD} = \underline{D}_P + \underline{D}_D$ , in general obtained using equations (3.7) and (3.10), may be given by:

$$\underline{D}_{PD} = \frac{\underline{E}_P}{1 - \nu_P^2} \int_{-(h_P - z_N)}^{z_N} z^2 dz + \frac{\underline{E}_D}{1 - \nu_D^2} \int_{z_N}^{(h_D + z_N)} z^2 dz. \quad (\text{A28.4})$$

It can be seen from equation (A28.4) that the combined flexural rigidity is the sum of the plate's and damping layer rigidity. However, in equation (A28.4) the offset of the neutral axis of bending is taken into account. If one substitutes equation (A28.2) into (A28.4), the plate rigidity due to neutral axis offset can be defined as:

$$\underline{D}_P = \frac{\underline{E}_P h_P^3}{12(1 - \nu_P^2)} \left( 4 + \frac{e_{DP} (3H_{DP}^4 + 6H_{DP}^3) - 3e_{PD} - 6H_{DP}}{2H_{DP} + e_{PD} + e_{DP} H_{DP}^2} \right). \quad (\text{A28.5})$$

Analogously, the damping layer flexural rigidity due to neutral axis offset may be written as:

$$\underline{D}_D = \frac{\underline{E}_D h_D^3}{12(1 - \nu_D^2)} \left( 4 + \frac{e_{PD} (3H_{PD}^2 + 6H_{PD}) - 3e_{DP} H_{DP}^2 - 6H_{DP}}{2H_{DP} + e_{PD} + e_{DP} H_{DP}^2} \right). \quad (\text{A28.6})$$

Herein  $e_{PD} = (e_{DP})^{-1}$  and  $H_{PD} = (H_{DP})^{-1}$ . It can be seen from equations (A28.5) and (A28.6) that both definitions are complex fractions. If one substitutes equations (A28.3) and (A17.3) into equation (A28.5), the complex, flexural plate rigidity can be found to be:

$$\underline{D}_P = \frac{\underline{E}_P h_P^3}{12(1 - \nu_P^2)} (1 + j\eta_P) \left( 4 + \frac{A_P + jB_P}{C_{PD}} \right). \quad (\text{A28.7})$$

Herein  $A_P$ ,  $B_P$  and  $C_P$  are defined as:

$$A_P = \left[ \begin{aligned} &E_{DP}F_P(6H_{DP}^5 + 12H_{DP}^4 - 6H_{DP}^3) - 12E_{PD}F_DH_{DP} + \\ &E_{DP}^2(F_P^2 + K_P^2)(3H_{DP}^6 + 6H_{DP}^5) - 3E_{PD}^2(F_D^2 + K_D^2) + \\ &(F_PF_D + K_PK_D)(3H_{DP}^4 + 6H_{DP}^3 - 3H_{DP}^2) - 12H_{DP}^2 \end{aligned} \right], \quad (A28.8)$$

$$B_P = \left[ \begin{aligned} &E_{DP}K_P(6H_{DP}^5 + 12H_{DP}^4 + 6H_{DP}^3) + \\ &(K_PF_D - K_DF_P)(3H_{DP}^4 + 6H_{DP}^3 + 3H_{DP}^2) \end{aligned} \right], \quad (A28.9)$$

$$C_{PD} = (2H_{DP} + E_{PD}F_D + E_{DP}F_PH_{DP}^2)^2 + (E_{PD}K_D + E_{DP}K_PH_{DP}^2)^2. \quad (A28.10)$$

In the above shown expressions, the following abbreviations were used:

$$F_P = \frac{1 + \eta_P\eta_D}{1 + \eta_P^2}, \quad (A28.11)$$

$$F_D = \frac{1 + \eta_P\eta_D}{1 + \eta_D^2}, \quad (A28.12)$$

$$K_P = \frac{\eta_D - \eta_P}{1 + \eta_P^2}, \quad (A28.13)$$

$$K_D = \frac{\eta_P - \eta_D}{1 + \eta_D^2}. \quad (A28.14)$$

Similarly, the flexural rigidity of the attached layer can be written as:

$$\underline{D}_D = \frac{E_D h_D^3}{12(1 - \nu_D^2)} (1 + j\eta_D) \left( 4 + \frac{A_D + jB_D}{C_{PD}} \right). \quad (A28.15)$$

Herein,  $A_D$  and  $B_D$  are defined as:

$$A_D = \left[ \begin{aligned} &-12E_{DP}F_P H_{DP}^3 + E_{PD}F_D (6H_{PD} + 12 - 6H_{DP}) + \\ &E_{PD}^2 (F_D^2 + K_D^2) (3H_{PD}^2 + 6H_{PD}) - 3E_{DP}^2 H_{DP}^4 (F_P^2 + K_P^2) + \\ &(F_P F_D + K_P K_D) (3 + 6H_{DP} - 3H_{DP}^2) - 12H_{DP}^2 \end{aligned} \right], \quad (\text{A28.16})$$

$$B_D = \left[ \begin{aligned} &E_{PD}K_D (6H_{PD} + 12 + 6H_{DP}) + \\ &(K_D F_P - K_P F_D) (3H_{DP}^2 + 3 + 6H_{DP}) \end{aligned} \right]. \quad (\text{A28.17})$$

It can be seen from equations (A28.7) and (A28.15) that in both expressions the respective Poisson ratio is employed. Adding both terms will yield to a rather extensive expression. However, if one assumes again that  $\nu_P \approx \nu_D$ , the combined flexural rigidity  $\underline{D}_{PD}$  can be written as:

$$\underline{D}_{PD} = \frac{A_{PD}}{12C_{PD}(1-\nu^2)} \left( 1 + j \frac{B_{PD}}{A_{PD}} \right). \quad (\text{A28.18})$$

It can be noticed from equation (A28.18) that this expression is in form of  $\underline{D}_{PD} = D_{PD}(1+j\eta_{PD})$ , where  $\eta_{PD}$  is the combined loss factor. Here,  $A_{PD}$ ,  $B_{PD}$  and  $C_{PD}$  are given as:

$$A_{PD} = \left[ \begin{aligned} &B_{Eh} (A_{Eh} + E_P^2 h_P^4 + E_D^2 h_D^4) + \\ &2\eta_P \eta_D (E_P^2 h_P^4 E_D h_D + E_D^2 h_D^4 E_P h_P) + \\ &\eta_P^2 E_P h_P (A_{Eh} + 2E_P^2 h_P^4 - E_P h_P^3 B_{Eh}) + \\ &\eta_D^2 E_D h_D (A_{Eh} + 2E_D^2 h_D^4 - E_D h_D^3 B_{Eh}) \end{aligned} \right], \quad (\text{A28.19})$$

$$B_{PD} = \begin{pmatrix} \eta_P^2 \eta_D E_P h_P (A_{Eh} + E_P h_P^3 E_D h_D) + \\ \eta_P (E_D h_D (A_{Eh} - E_D h_D^3 E_P h_P) - E_P^2 h_P^4 (E_P h_P - 2B_{Eh})) + \\ \eta_D (E_P h_P (A_{Eh} - E_P h_P^3 E_D h_D) - E_D^2 h_D^4 (E_D h_D - 2B_{Eh})) + \\ \eta_P \eta_D^2 E_D h_D (A_{Eh} + E_D h_D^3 E_P h_P) + \eta_P^3 E_P^3 h_P^5 + \eta_D^3 E_D^3 h_D^5 \end{pmatrix}, \quad (A28.20)$$

$$C_{PD} = B_{Eh}^2 + (E_P h_P \eta_P + E_D h_D \eta_D)^2. \quad (A28.21)$$

In equations (A28.19), (A28.20) and (A28.21) the following abbreviations are used:

$$A_{Eh} = 2E_P h_P E_D h_D (2h_P^2 + 2h_D^2 + 3h_P h_D), \quad (A28.22)$$

$$B_{Eh} = E_P h_P + E_D h_D. \quad (A28.23)$$

Using equations (A28.19), (A28.20), (A28.22) and (A28.23), the hysteretic loss factor  $\eta_{PD} = B_{PD}/A_{PD}$  of the plate-layer compound is given by:

$$\eta_{PD} = \frac{\begin{pmatrix} \eta_P^2 \eta_D E_P h_P (A_{Eh} + E_P h_P^3 E_D h_D) + \\ \eta_P (E_D h_D (A_{Eh} - E_D h_D^3 E_P h_P) - E_P^2 h_P^4 (E_P h_P - 2B_{Eh})) + \\ \eta_D (E_P h_P (A_{Eh} - E_P h_P^3 E_D h_D) - E_D^2 h_D^4 (E_D h_D - 2B_{Eh})) + \\ \eta_P \eta_D^2 E_D h_D (A_{Eh} + E_D h_D^3 E_P h_P) + \eta_P^3 E_P^3 h_P^5 + \eta_D^3 E_D^3 h_D^5 \end{pmatrix}}{\begin{pmatrix} B_{Eh} (A_{Eh} + E_P^2 h_P^4 + E_D^2 h_D^4) + \\ 2\eta_P \eta_D (E_P^2 h_P^4 E_D h_D + E_D^2 h_D^4 E_P h_P) + \\ \eta_P^2 E_P h_P (A_{Eh} + 2E_P^2 h_P^4 - E_P h_P^3 B_{Eh}) + \\ \eta_D^2 E_D h_D (A_{Eh} + 2E_D^2 h_D^4 - E_D h_D^3 B_{Eh}) \end{pmatrix}}. \quad (A28.24)$$

## Appendix A29

### Tables of Predicted Cut-Off Points and Relative Mean Square Error of Three Differently Damped Simply Supported Plate Structures Using Extracted ESPI Noise and Measured Force Magnitude

Due to brevity reasons the following abbreviations are employed in the columns in the tables below:

- A    % of max  $|Amplitude|_x$  of real displacement
- B     $10 \cdot \log_{10}(\Re(II_x))$
- C    % of max  $|Amplitude|_y$  of real displacement
- D     $10 \cdot \log_{10}(\Re(II_y))$
- E    % of max  $|Amplitude|_x$  of imaginary displacement
- F     $10 \cdot \log_{10}(\Im(II_x))$
- G    % of max  $|Amplitude|_y$  of imaginary displacement
- H     $10 \cdot \log_{10}(\Im(II_y))$

mode	$f_{m,n}$ [Hz]	A [%]	B	C [%]	D	E [%]	F	G [%]	H
(3,3)	428.7	6.8	0.99	4.4	15.75	6.4	8.54	5.8	19.86
(5,3)	711.6	6.2	-6.63	6.2	0.87	7.2	13.74	3.6	7.16
(1,5)	766.7	6.2	-1.44	3.8	-11.41	1.6	-11.78	8.2	43.99
(7,1)	896.2	6.2	28.43	6.2	-1.46	7.6	33.36	2.2	-11.89
(5,5)	1190.9	4.6	0.33	7.8	-7.29	7.2	3.00	7.8	18.71
(9,1)	1461.9	2.8	-6.57	3.2	10.48	4.8	28.83	5.6	-8.32
(7,5)	1615.2	4.8	1.32	6.0	19.69	5.6	5.49	9.6	24.72
(9,5)	2180.9	7.4	-2.72	6.8	10.09	6.6	4.67	8.2	-0.98

**Table A29.1** Optimum, ideal filtered, non-layer damped plate cut-off points and relative MSE using the VEFESPI method.

mode	$f_{m,n}$ [Hz]	A [%]	B	C [%]	D	E[%]	F	G[%]	H
(3,3)	398.1	6.8	19.15	6.8	6.60	4.2	7.8	6	19.87
(5,3)	660.7	6.8	-6.83	6.8	-3.33	6.8	16.0	5.4	12.12
(7,1)	832.1	3.4	10.68	9.2	-6.27	6.8	20.41	6.6	-4.33
(5,5)	1105.7	4.6	-6.19	4.8	-7.78	7.8	12.0	4.0	32.74
(9,1)	1357.3	4.8	-21.20	3.8	2.46	6.6	16.23	4.8	-10.17
(7,5)	1499.6	8.8	-6.85	5.0	2.80	4.0	9.52	8.8	-0.67
(5,7)	1773.3	5.2	-7.27	5.6	-19.98	7.4	-2.96	7.4	13.18
(11,1)	2013.8	4.8	-9.45	7.0	-8.03	4.6	5.34	5.2	10.98

**Table A29.2** Optimum, ideal filtered, single-layer damped plate cut-off points and relative MSE using the VEFESPI method.

mode	$f_{m,n}$ [Hz]	A [%]	B	C [%]	D	E[%]	F	G[%]	H
(3,3)	412.1	7.4	2.25	7.4	2.99	3.8	4.41	3.6	17.35
(5,3)	684.0	6.4	-6.69	6.4	-1.73	7.2	14.23	4.6	9.85
(7,1)	861.4	3.4	29.88	8.2	-1.72	8.2	23.32	6.4	-6.02
(5,5)	1144.7	3.2	-2.08	4.2	-7.85	7.2	3.01	9.4	22.41
(9,1)	1405.2	4.8	-11.77	4.8	22.50	9.8	26.15	5.8	-5.66
(7,5)	1552.6	9	-7.30	4.6	0.07	7.0	11.0	9.0	-0.84
(5,7)	1835.9	4.8	-7.90	4.6	-18.32	7.4	-0.01	7.2	9.03
(9,5)	2096.3	4.6	-18.9	5.8	-5.58	3.4	17.45	9.6	-0.08

**Table A29.3** Optimum, ideal filtered, checkerboard-layer damped plate cut-off points and relative MSE using the VEFESPI method.

mode	$f_{m,n}$ [Hz]	A [%]	B	C [%]	D	E[%]	F	G[%]	H
(3,3)	428.7	3.0	5.05	3.0	61.94	2.0	-24.79	1.0	-16.06
(5,3)	711.6	2.2	3.42	3.4	-3.76	1.4	-19.65	1	-9.53
(1,5)	766.7	-	-	-	-	-	-	-	-
(7,1)	896.2	-	-	-	-	-	-	-	-
(5,5)	1190.9	2.6	20.95	2.2	-13.98	1.6	-11.57	1.4	1.95
(9,1)	1461.9	-	-	-	-	-	-	-	-
(7,5)	1615.2	1.4	18.32	5.6	7.62	4.4	20.14	3.4	-3.91
(9,5)	2180.9	6.2	-9.03	8.8	4.6	6.2	8.97	6.6	5.26

**Table A29.4** Optimum, ideal filtered, non-layer damped plate cut-off points and relative MSE of integer-wave truncated simply supported plate displacement using the VEFESPI method.

mode	$f_{m,n}$ [Hz]	A [%]	B	C [%]	D	E[%]	F	G[%]	H
(3,3)	398.1	2.8	-2.96	2.2	38.03	4.0	-26.37	4.0	-23.40
(5,3)	660.7	2.4	-4.80	3.8	-7.67	4.4	-20.04	5.2	-17.98
(7,1)	832.1	-	-	-	-	-	-	-	-
(5,5)	1105.7	1.4	2.54	2.4	-15.04	1.4	-3.44	2.2	6.08
(9,1)	1357.3	-	-	-	-	-	-	-	-
(7,5)	1499.6	3.0	-13.70	2.2	-6.58	4.0	-1.84	1.6	-1.80
(5,7)	1773.3	1.8	-12.83	3.4	-19.63	1.8	-1.38	2.4	-1.42
(11,1)	2013.8	-	-	-	-	-	-	-	-

**Table A29.5** Optimum, ideal filtered, single-layer damped plate cut-off points and relative MSE of integer-wave truncated simply supported plate displacement using the VEFESPI method.

mode	$f_{m,n}$ [Hz]	A [%]	B	C [%]	D	E[%]	F	G[%]	H
(3,3)	412.1	2.6	-7.12	2.0	36.25	3.2	-16.51	7.0	-22.44
(5,3)	684.0	2.0	-9.40	1.8	-1.00	2.4	-5.39	1.0	-6.36
(7,1)	861.4	-	-	-	-	-	-	-	-
(5,5)	1144.7	3.0	38.83	2.8	-14.13	8.0	-27.03	8.0	16.64
(9,1)	1405.2	-	-	-	-	-	-	-	-
(7,5)	1552.6	7.6	-14.38	4.4	1.53	1.6	2.94	2.6	-6.36
(5,7)	1835.9	3.2	-8.49	2.8	-21.28	2.8	-12.53	2.4	0.22
(9,5)	2096.3	4.2	-13.36	6.6	26.85	6.6	-10.68	4.0	-4.54

**Table A29.6** Optimum, ideal filtered, checkerboard-layer damped plate cut-off points and relative MSE of integer-wave truncated simply supported plate displacement using the VEFESPI method.

$$\text{I} \quad (k_{c_x} / k_x)_{real}$$

$$\text{J} \quad (k_{c_y} / k_y)_{real}$$

$$\text{K} \quad (k_{c_x} / k_x)_{imag}$$

$$\text{L} \quad (k_{c_y} / k_y)_{imag}$$

mode	$f_{m,n}$ [Hz]	I	B	J	D	K	F	L	H
(3,3)	428.7	2.6492	3.95	2.7134	12.42	3.6681	4.02	3.6527	22.14
(5,3)	711.6	2.2099	-9.04	2.1018	16.23	2.052	16.63	2.9102	13.10
(1,5)	766.7	2.0505	-4.27	1.5402	-14.74	2.0505	-9.73	1.2602	24.18
(7,1)	896.2	2.3107	9.01	1.3017	-5.56	1.2709	22.49	1.8934	-10.4
(5,5)	1190.9	1.5284	-6.73	2.0664	-7.13	2.0175	3.99	2.0038	7.83
(9,1)	1461.9	1.8340	-14.8	2.5047	29.0	1.2227	25.12	2.4003	-10.2
(7,5)	1615.2	1.3950	-4.59	1.9581	24.12	1.7051	1.62	1.6935	-0.05
(9,5)	2180.9	1.5949	-12.5	1.6335	-4.52	2.0505	7.09	2.0069	14.78

**Table A29.7** Optimum, Butterworth filtered, non-layer damped plate cut-off points and relative MSE using the VEFESPI method.



mode	$f_{m,n}$ [Hz]	I	B	J	D	K	F	L	H
(3,3)	398.1	2.7511	2.18	2.7178	12.77	3.6681	4.64	3.8614	16.18
(5,3)	660.7	2.2888	-9.18	2.1018	15.79	2.1310	16.40	2.9910	8.39
(7,1)	832.1	1.7330	7.21	2.6034	-6.30	1.2709	38.80	2.4850	-4.44
(5,5)	1105.7	2.3843	-8.04	2.0038	-8.21	2.0175	2.59	2.0038	9.90
(9,1)	1357.3	1.7322	-19.5	2.4003	-3.61	1.4265	14.99	1.8785	-10.3
(7,5)	1499.6	1.9634	-6.04	1.4289	-7.74	2.0667	16.22	2.0110	32.78
(5,7)	1773.3	2.1184	-13.1	1.5347	-7.88	1.7567	-1.92	2.0110	6.50
(11,1)	2013.8	1.6590	-10.4	2.7376	-16.4	2.6728	28.45	2.3600	9.44

**Table A29.8** Optimum, Butterworth filtered, single-layer damped plate cut-off points and relative MSE using the VEFESPI method.

mode	$f_{m,n}$ [Hz]	I	B	J	D	K	F	L	H
(3,3)	412.1	2.7511	2.97	1.9829	8.20	3.6681	4.00	3.7570	17.61
(5,3)	684.0	2.2888	-8.74	2.1018	13.58	1.9731	14.10	2.9910	12.30
(7,1)	861.4	1.7330	10.95	1.7750	-6.73	1.1553	13.36	2.6034	-6.59
(5,5)	1144.7	1.5284	-6.72	2.0664	-7.03	1.9563	3.27	1.6280	0.81
(9,1)	1405.2	1.6303	-11.5	2.1916	37.8	1.4265	31.9	1.7742	-12.1
(7,5)	1552.6	1.3950	-5.65	1.4289	-7.31	1.7051	22.89	1.5347	30.17
(5,7)	1835.9	2.0667	-13.4	1.5347	-7.68	1.8084	-0.66	1.6935	0.56
(9,5)	2096.3	1.4126	-18.5	1.6335	-10.8	1.8227	5.68	1.5869	11.04

**Table A29.9** Optimum, Butterworth filtered, checkerboard-layer damped plate cut-off points and relative MSE using the VEFESPI method.

mode	$f_{m,n}$ [Hz]	I	B	J	D	K	F	L	H
(3,3)	428.7	2.1614	-9.18	2.1174	46.32	2.1614	-25.29	3.1055	-16.3
(5,3)	711.6	1.8348	7.67	1.8488	-8.35	1.6513	-20.58	3.9151	-15.0
(1,5)	766.7	-	-	-	-	-	-	-	-
(7,1)	896.2	-	-	-	-	-	-	-	-
(5,5)	1190.9	2.1684	7.34	1.9563	-12.8	1.8793	-19.6	3.1441	-6.05
(9,1)	1461.9	-	-	-	-	-	-	-	-
(7,5)	1615.2	1.5004	13.19	1.5741	-2.12	1.5004	-2.28	2.0404	-6.84
(9,5)	2180.9	1.4433	-9.89	1.4691	-2.59	1.6839	-2.52	1.9098	-4.20

**Table A29.10** Optimum, Butterworth filtered, non-layer damped plate cut-off points and relative MSE of integer-wave truncated simply supported plate displacement using the VEFESPI method.

mode	$f_{m,n}$ [Hz]	I	B	J	D	K	F	L	H
(3,3)	398.1	2.4199	-12.63	2.4128	45.19	2.2775	-28.5	1.5612	-21.1
(5,3)	660.7	1.7431	-10.56	1.8588	-6.0	1.6513	-20.7	1.5308	-18.0
(7,1)	832.1	-	-	-	-	-	-	-	-
(5,5)	1105.7	2.6207	-4.62	1.9651	-15.0	2.5499	-10.4	2.1756	6.75
(9,1)	1357.3	-	-	-	-	-	-	-	-
(7,5)	1499.6	1.6217	-12.6	2.2153	-5.51	1.6776	-1.61	2.7400	-1.05
(5,7)	1773.3	2.3625	-16.33	1.8289	-19.2	2.3035	-0.32	1.8844	-0.61
(11,1)	2013.8	-	-	-	-	-	-	-	-

**Table A29.11** Optimum, Butterworth filtered, single-layer damped plate cut-off points and relative MSE of integer-wave truncated simply supported plate displacement using the VEFESPI method.

mode	$f_{m,n}$ [Hz]	I	B	J	D	K	F	L	H
(3,3)	412.1	2.2596	-6.09	2.1289	12.01	1.5535	-16.61	1.7031	-21.9
(5,3)	684.0	1.6402	-9.0	1.8394	-5.28	1.6402	-10.0	3.2461	-2.58
(7,1)	861.4	-	-	-	-	-	-	-	-
(5,5)	1144.7	1.9318	16.0	1.9563	-13.8	1.6456	-25.8	3.0742	-2.51
(9,1)	1405.2	-	-	-	-	-	-	-	-
(7,5)	1552.6	1.6418	-13.0	1.5806	-5.16	1.6418	4.48	2.1661	-6.24
(5,7)	1835.9	1.6107	-8.50	1.6557	-20.8	2.0879	-15.46	2.4284	-4.95
(9,5)	2096.3	1.4870	-14.9	1.5095	12.48	2.3984	-7.31	2.0127	-7.25

**Table A29.12** Optimum, Butterworth filtered, checkerboard-layer damped plate cut-off points and relative MSE of integer-wave truncated simply supported plate displacement using the VEFESPI method.

## Appendix A30

### Figures of Truncated ESPI Displacement and ESPI Measured Vibrational Energy Flow of “Infinite” Plate

This section presents the ESPI amplitude and ESPI phase plots recorded during the experimental “infinite” plate experiment for all five excitation frequencies. Furthermore, the truncated displacements and its top view images are shown. Also, the filtered active and reactive energy flow maps determined from the prior displayed and truncated ESPI plate displacements are presented. In addition, the total transmitted vibrational energy (TTVE) through a numerous number of square contours about the excitation location is shown in comparison to the vibrational input power (VIP) injected into the plate. Finally, the relative difference between the TTVE and the VIP in percent is displayed.

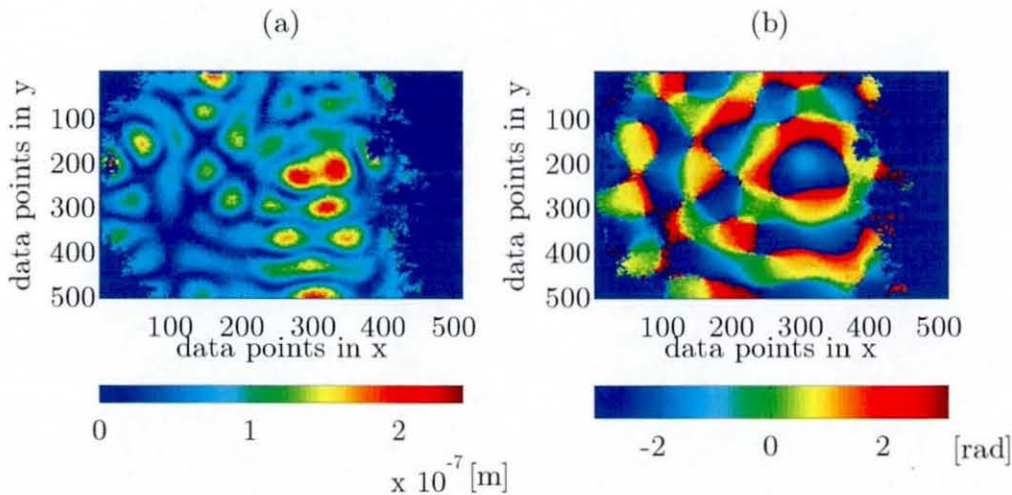


**Figure A30.1** ESPI image of the measured “infinite” plate displacement at 569.7 Hz: (a) amplitude, (b) phase.

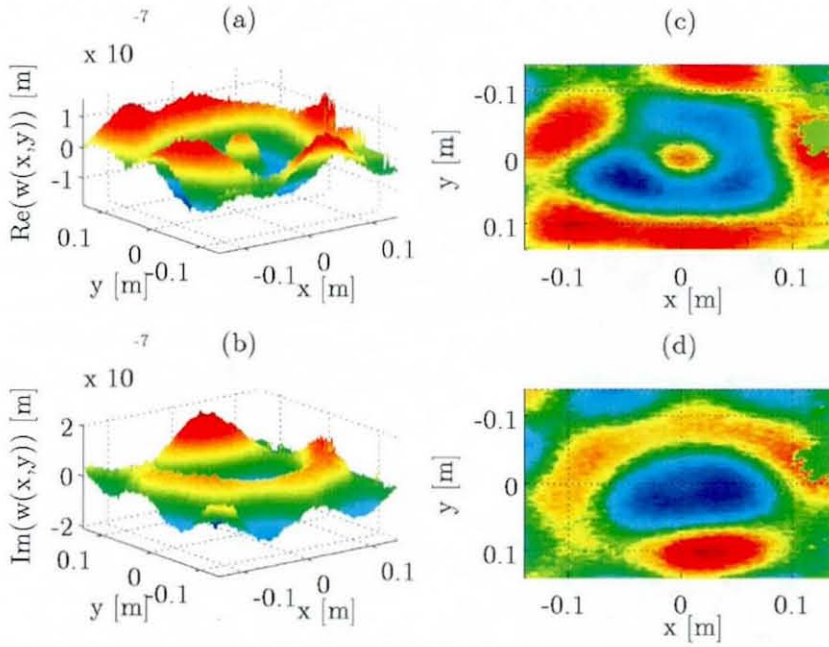


**Figure A30.2** ESPI image of the measured and truncated “infinite” plate displacement at 569.7 Hz: (a) 2D real part, (b) 2D imaginary part, (c) real part image, (d) imaginary part image.

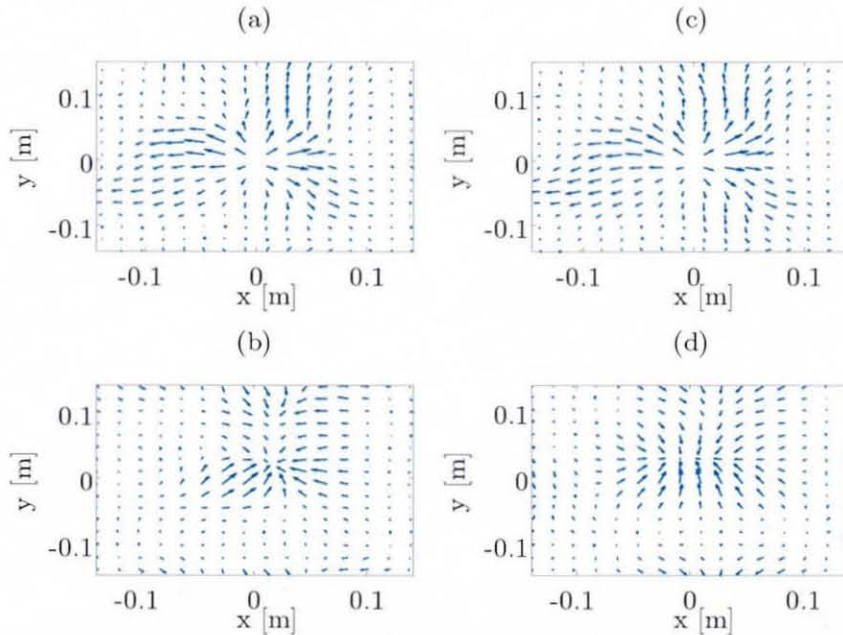


**Figure A30.3** Filtered VEF maps from the “infinite” plate displacement at 569.7 Hz: (a) active VEF – ideal filter, (b) reactive VEF – ideal filter, (c) active VEF – Butterworth filter, (d) reactive VEF – Butterworth filter.

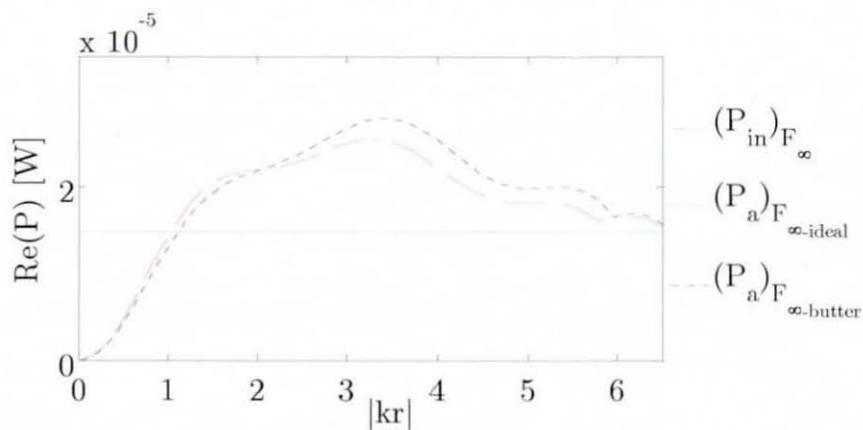


**Figure A30.4** Comparison of ESPI measured active TTVE and transducer measured VIP at 569.7 Hz.

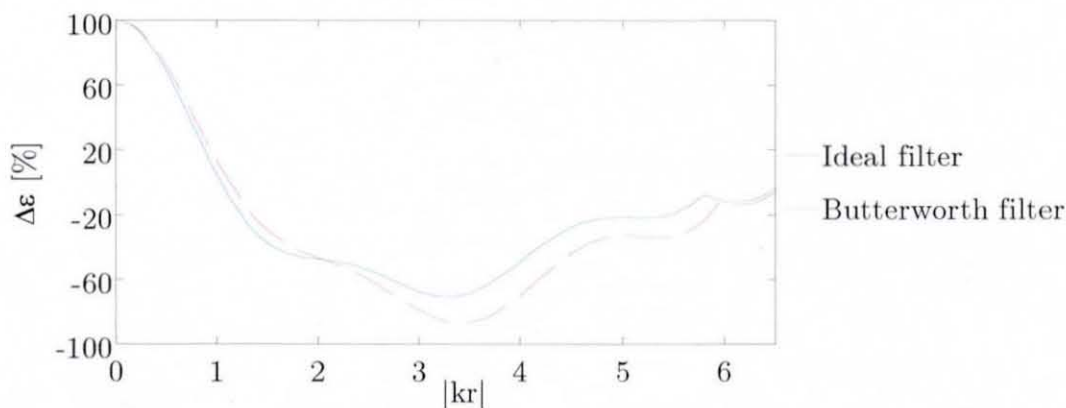


**Figure A30.5** Relative difference in percent between ESPI measured active TTVE and transducer measured VIP at 569.7 Hz.



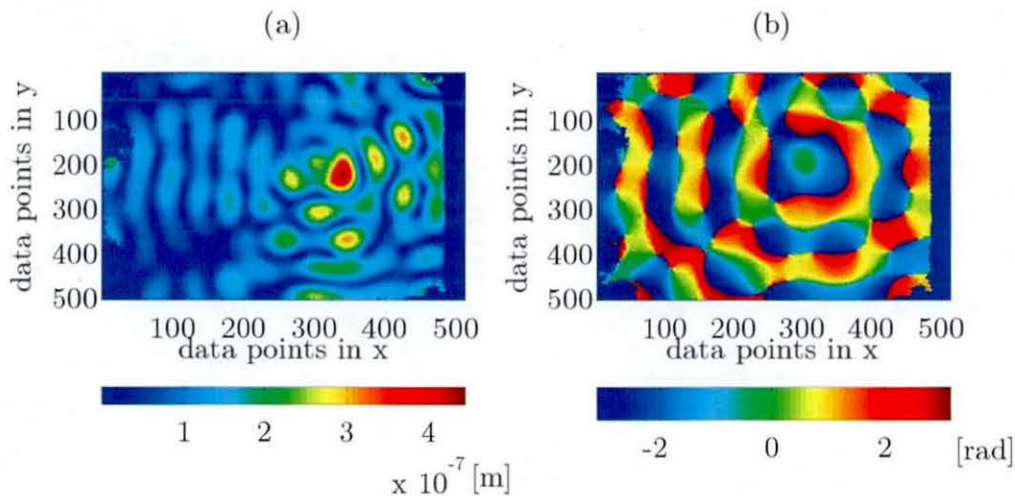


**Figure A30.6** ESPI image of the measured “infinite” plate displacement at 605.6 Hz: (a) amplitude, (b) phase.

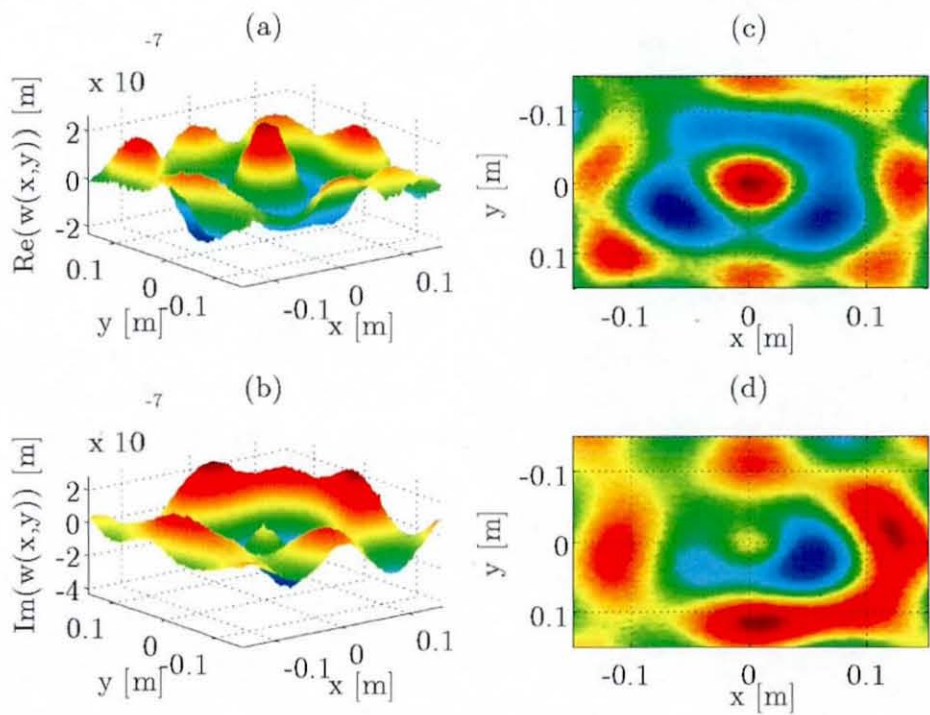


**Figure A30.7** ESPI image of the measured and truncated “infinite” plate displacement at 605.6 Hz: (a) 2D real part, (b) 2D imaginary part, (c) real part image, (d) imaginary part image.

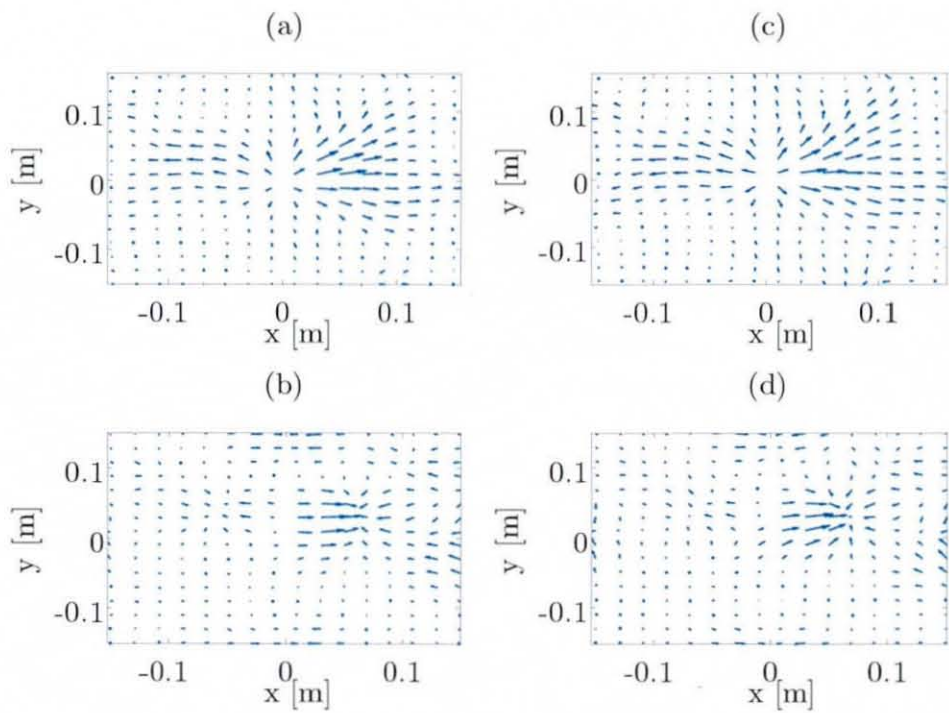


**Figure A30.8** Filtered VEF maps from the “infinite” plate displacement at 605.6 Hz: (a) active VEF – ideal filter, (b) reactive VEF – ideal filter, (c) active VEF – Butterworth filter, (d) reactive VEF – Butterworth filter.

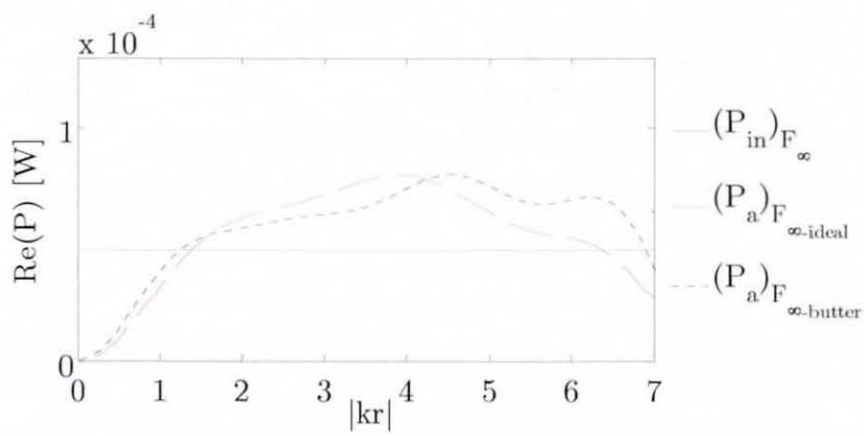


**Figure A30.9** Comparison of ESPI measured active TTVE and transducer measured VIP at 605.6 Hz.



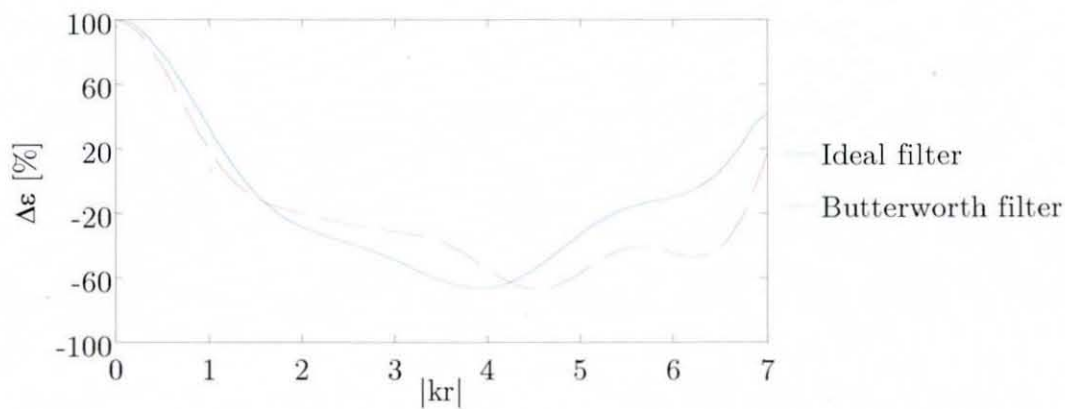


**Figure A30.10** Relative difference in percent between ESPI measured active TTVE and transducer measured VIP at 605.6 Hz.

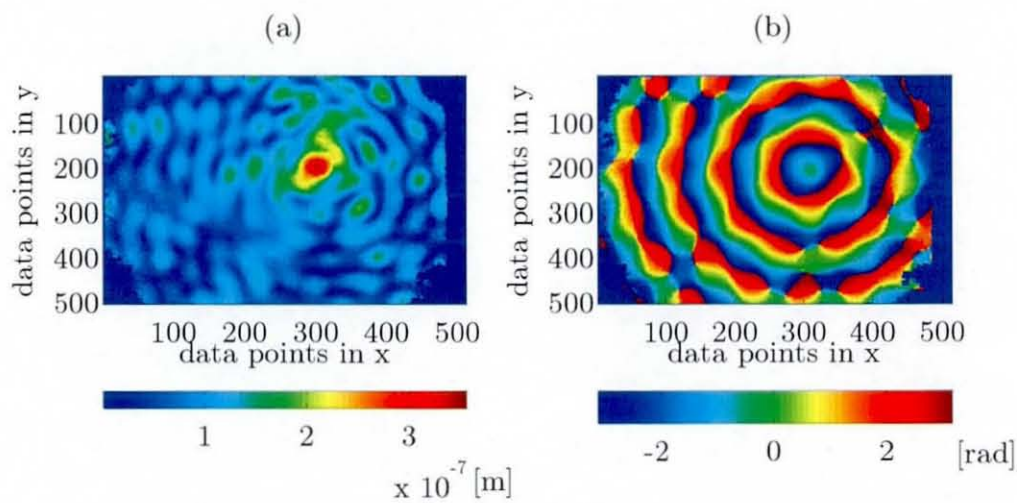


**Figure A30.11** ESPI image of the measured “infinite” plate displacement at 899.5 Hz: (a) amplitude, (b) phase.

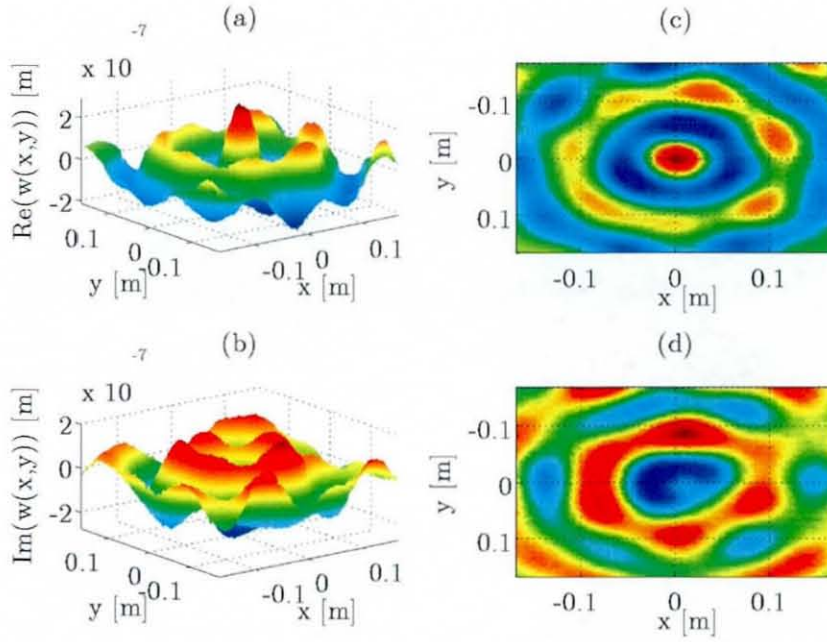


**Figure A30.12** ESPI image of the measured and truncated “infinite” plate displacement at 899.5 Hz: (a) 2D real part, (b) 2D imaginary part, (c) real part image, (d) imaginary part image.

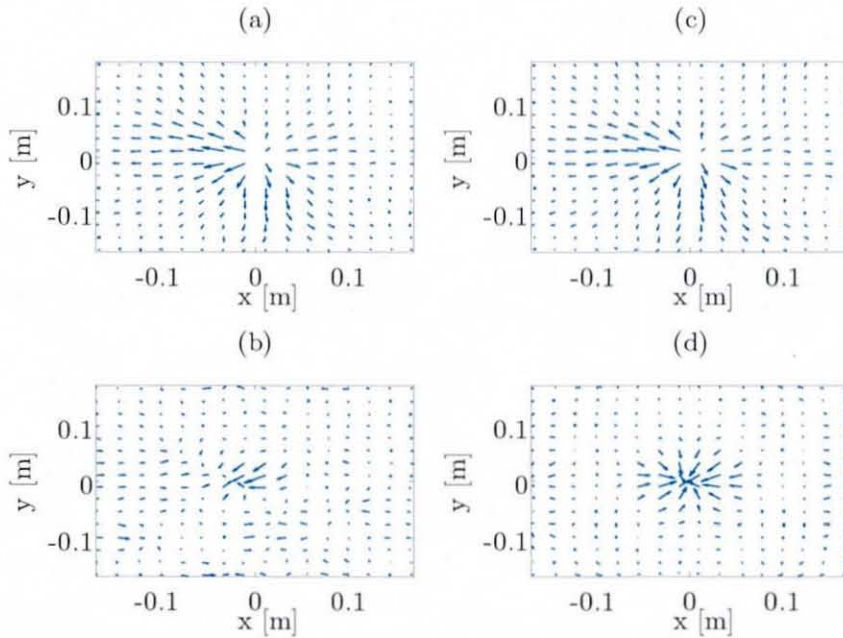


**Figure A30.13** Filtered VEF maps from the “infinite” plate displacement at 899.5 Hz: (a) active VEF – ideal filter, (b) reactive VEF – ideal filter, (c) active VEF – Butterworth filter, (d) reactive VEF – Butterworth filter.

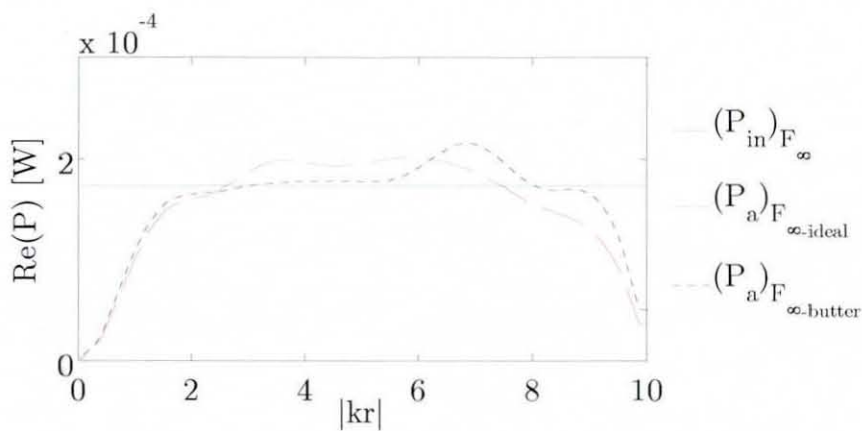


**Figure A30.14** Comparison of ESPI measured active TTVE and transducer measured VIP at 899.5 Hz.

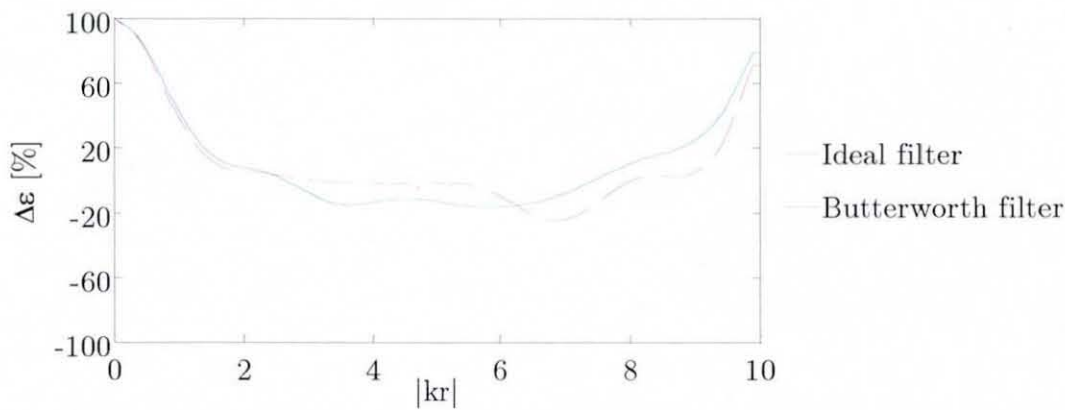


**Figure A30.15** Relative difference in percent between ESPI measured active TTVE and transducer measured VIP at 899.5 Hz.

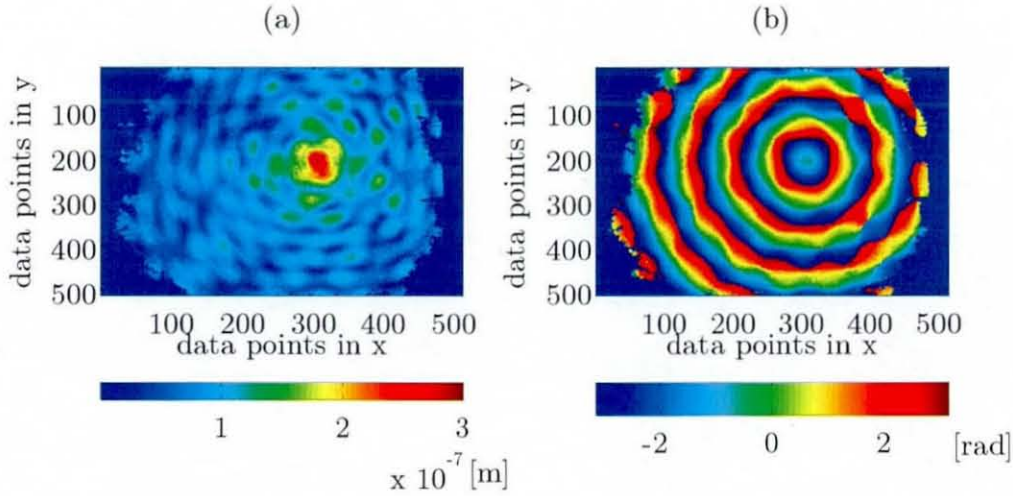


**Figure A30.16** ESPI image of the measured "infinite" plate displacement at 1194.4 Hz: (a) amplitude, (b) phase.

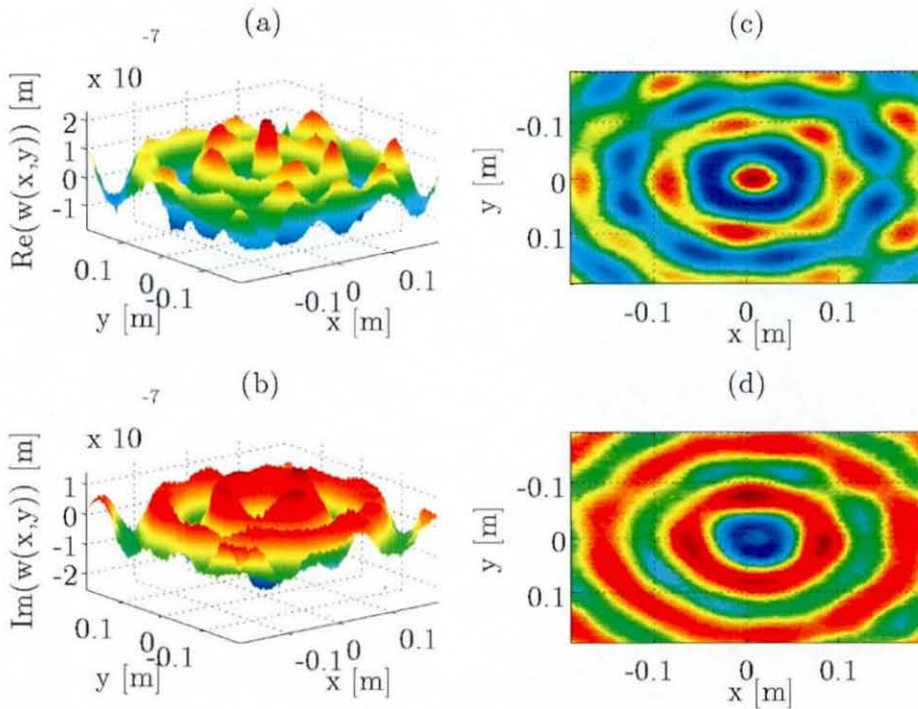


**Figure A30.17** ESPI image of the measured and truncated "infinite" plate displacement at 1194.4 Hz: (a) 2D real part, (b) 2D imaginary part, (c) real part image, (d) imaginary part image.



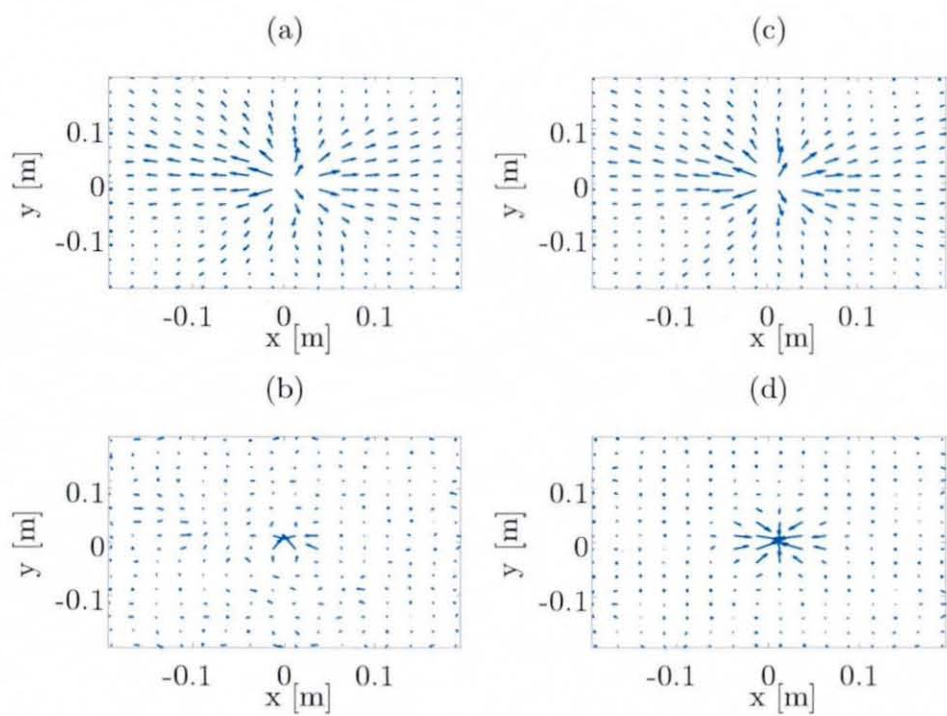


**Figure A30.18** Filtered VEF maps from the “infinite” plate displacement at 1194.4 Hz: (a) active VEF – ideal filter, (b) reactive VEF – ideal filter, (c) active VEF – Butterworth filter, (d) reactive VEF – Butterworth filter.

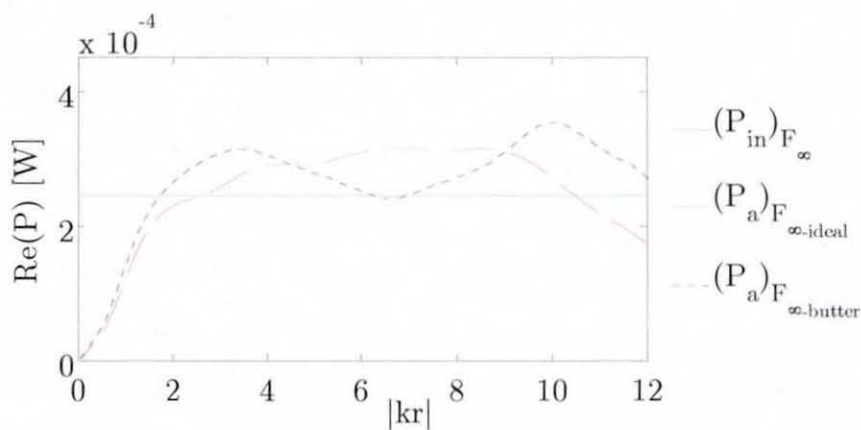


**Figure A30.19** Comparison of ESPI measured active TTVE and transducer measured VIP at 1194.4 Hz.

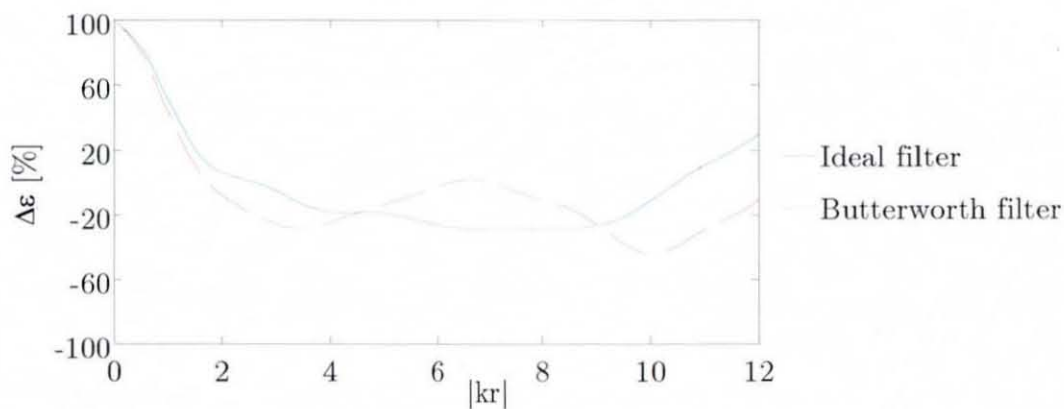


**Figure A30.20** Relative difference in percent between ESPI measured active TTVE and transducer measured VIP at 1194.4 Hz.

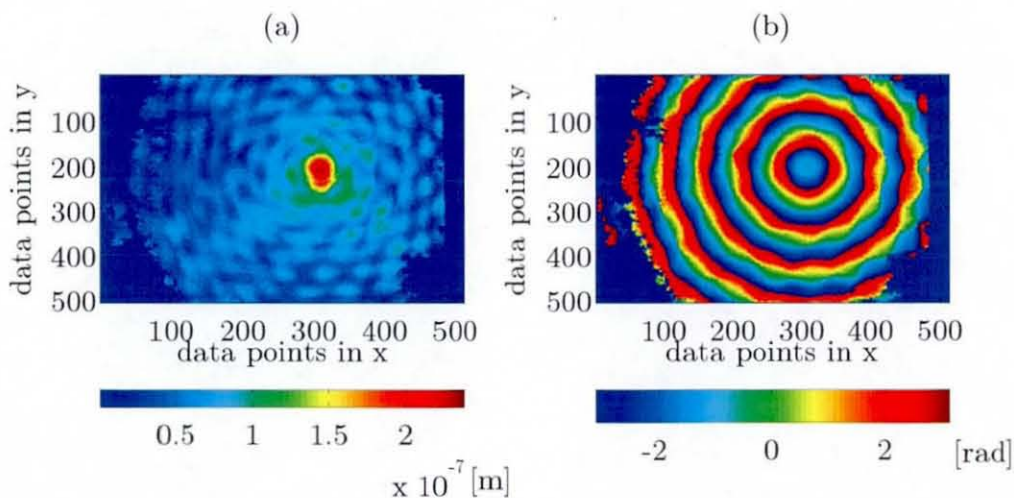


**Figure A30.21** ESPI image of the measured “infinite” plate displacement at 1503.2 Hz: (a) amplitude, (b) phase.

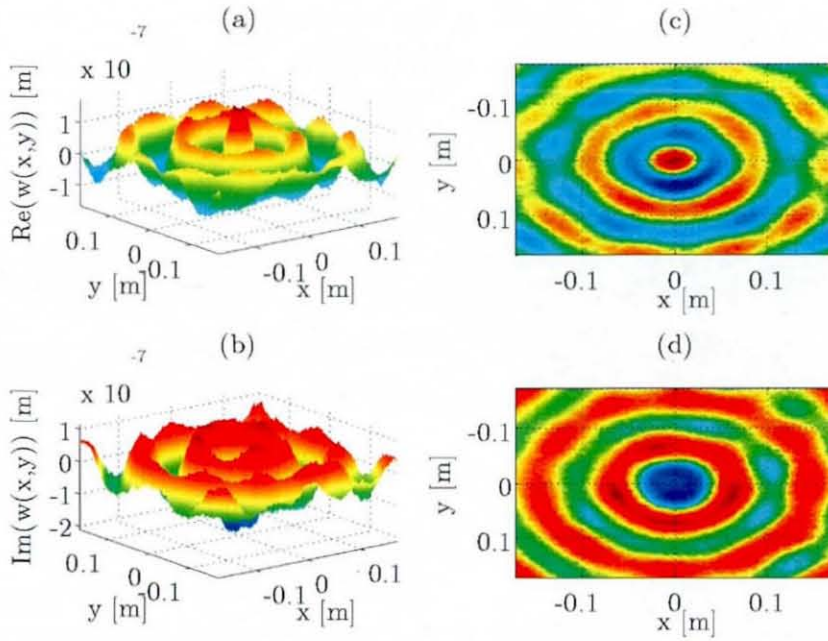


**Figure A30.22** ESPI image of the measured and truncated “infinite” plate displacement at 1503.2 Hz: (a) 2D real part, (b) 2D imaginary part, (c) real part image, (d) imaginary part image.

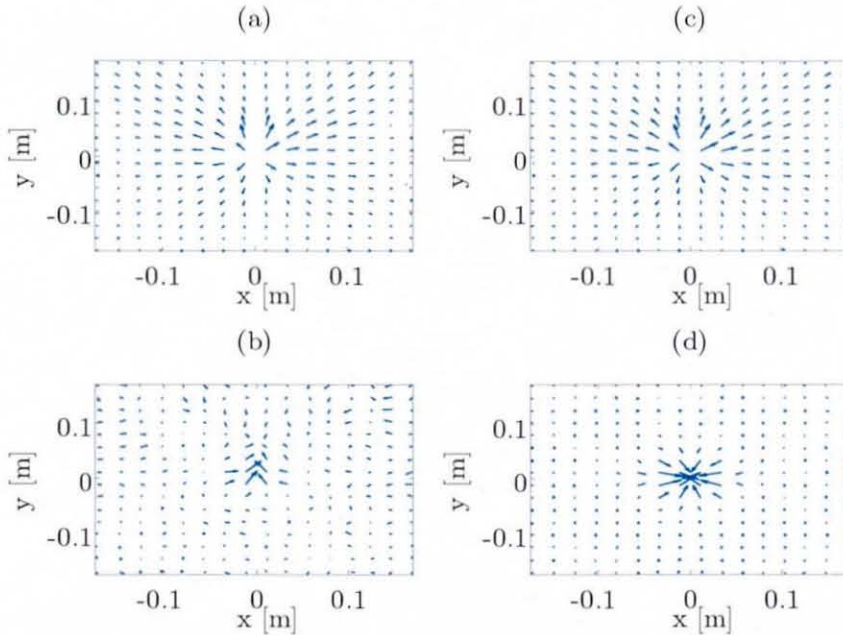


**Figure A30.23** Filtered VEF maps from the “infinite” plate displacement at 1503.2 Hz: (a) active VEF – ideal filter, (b) reactive VEF – ideal filter, (c) active VEF – Butterworth filter, (d) reactive VEF – Butterworth filter.

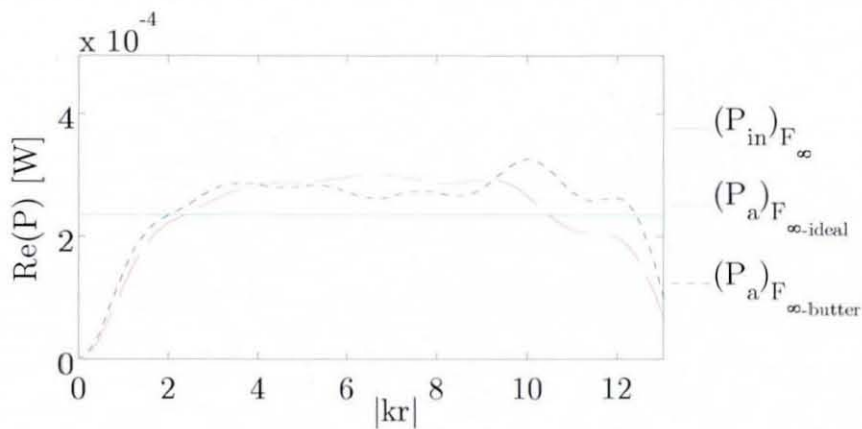


**Figure A30.24** Comparison of ESPI measured active TTVE and transducer measured VIP at 1503.2 Hz.

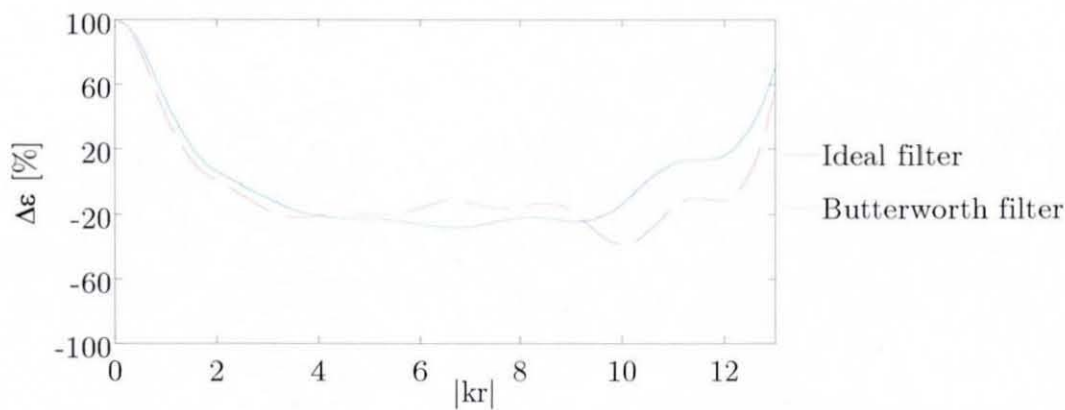


**Figure A30.25** Relative difference in percent between ESPI measured active TTVE and transducer measured VIP at 1503.2 Hz.



## Appendix A31

### Measured Vibrational Input Power of the Experimental Simply Supported Plates

mode	$(P_{in})_{Fa}$ [W]
(3,3)	$1.3930 \cdot 10^{-5}$
(5,3)	$4.7663 \cdot 10^{-5}$
(1,5)	0
(7,1)	$9.3091 \cdot 10^{-5}$
(5,5)	$1.3710 \cdot 10^{-4}$
(9,1)	$1.9988 \cdot 10^{-4}$
(7,5)	$4.3866 \cdot 10^{-4}$
(9,5)	$9.2169 \cdot 10^{-4}$

**Table A31.1** Transducer measured vibrational input power of the experimental non-layer damped simply supported plate.

mode	$(P_{in})_{Fa}$ [W]
(3,3)	$1.0766 \cdot 10^{-4}$
(5,3)	$1.8218 \cdot 10^{-4}$
(7,1)	$3.4381 \cdot 10^{-4}$
(5,5)	$7.7383 \cdot 10^{-4}$
(9,1)	$8.6997 \cdot 10^{-4}$
(7,5)	$7.9213 \cdot 10^{-4}$
(5,7)	$1.4015 \cdot 10^{-3}$
(11,1)	$1.8334 \cdot 10^{-3}$

**Table A31.2** Transducer measured vibrational input power of the experimental single-layer damped simply supported plate.

mode	$(P_{in})_{Fa}$ [W]
(3,3)	$4.8013 \cdot 10^{-5}$
(5,3)	$1.6354 \cdot 10^{-4}$
(7,1)	$7.0699 \cdot 10^{-5}$
(5,5)	$2.9489 \cdot 10^{-4}$
(9,1)	$2.0285 \cdot 10^{-4}$
(7,5)	$7.5562 \cdot 10^{-4}$
(5,7)	$4.5899 \cdot 10^{-4}$
(9,5)	$1.7498 \cdot 10^{-3}$

**Table A31.3** Transducer measured vibrational input power of the experimental checkerboard pattern layer-damped simply supported plate.

## Appendix A32

### Measured Vibrational Energy Flow Maps of the Experimental Simply Supported Plates Using the VEFESPI Method

The VEF maps shown in this section were computed from the periodically truncated and ESPI measured simply supported plates displacements. Further, in the figures shown below  $x$  is the plate length and  $y$  is the plate width.

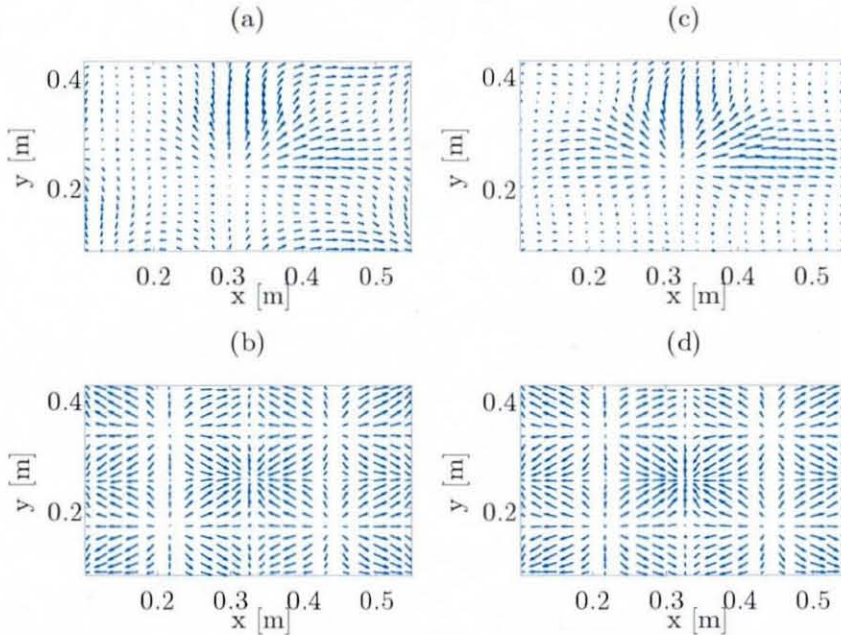


**Figure A32.1** Filtered VEF maps of the experimental, non-layer damped, simply supported plate at 422.5 Hz & mode (3,3): (a) active ideal filtered, (b) reactive ideal filtered, (c) active Butterworth filtered, (d) reactive Butterworth filtered.

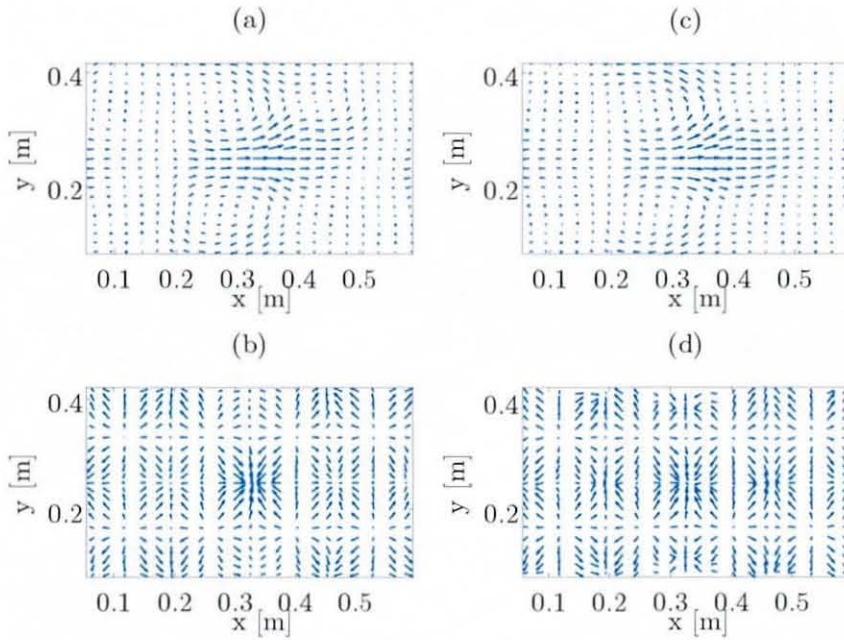


**Figure A32.2** Filtered VEF maps of the experimental non-layer damped, simply supported plate at 689 Hz & mode (5,3): (a) active ideal filtered, (b) reactive ideal filtered, (c) active Butterworth filtered, (d) reactive Butterworth filtered.

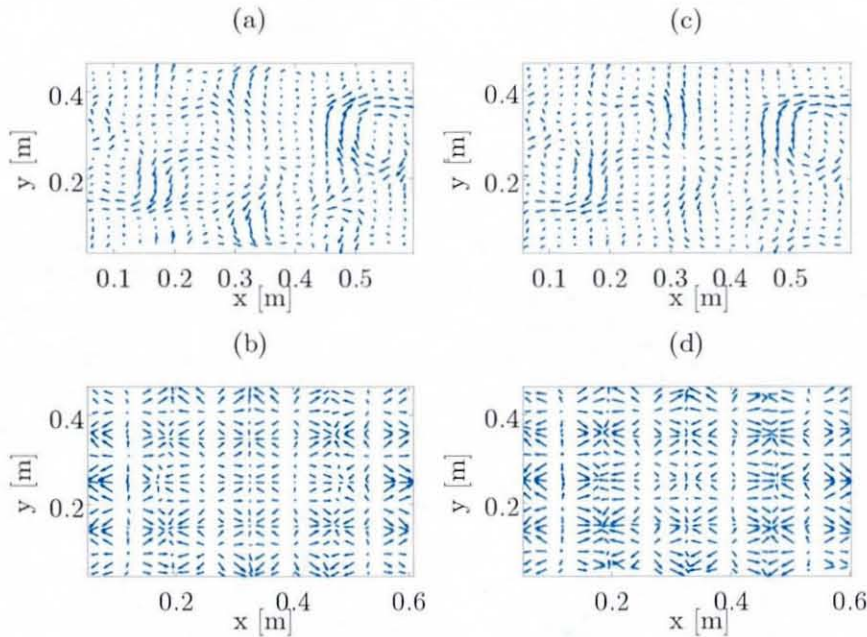


**Figure A32.3** Filtered VEF maps of the experimental, non-layer damped, simply supported plate at 1139 Hz & mode (5,5): (a) active ideal filtered, (b) reactive ideal filtered, (c) active Butterworth filtered, (d) reactive Butterworth filtered.



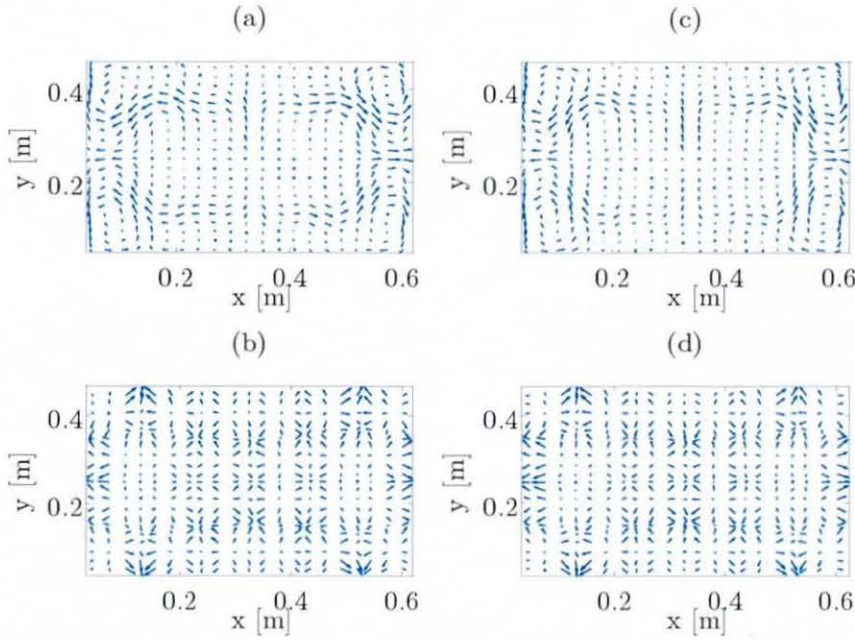


**Figure A32.4** Filtered VEF maps of the experimental non-layer damped, simply supported plate at 1536 Hz & mode (7,5): (a) active ideal filtered, (b) reactive ideal filtered, (c) active Butterworth filtered, (d) reactive Butterworth filtered.

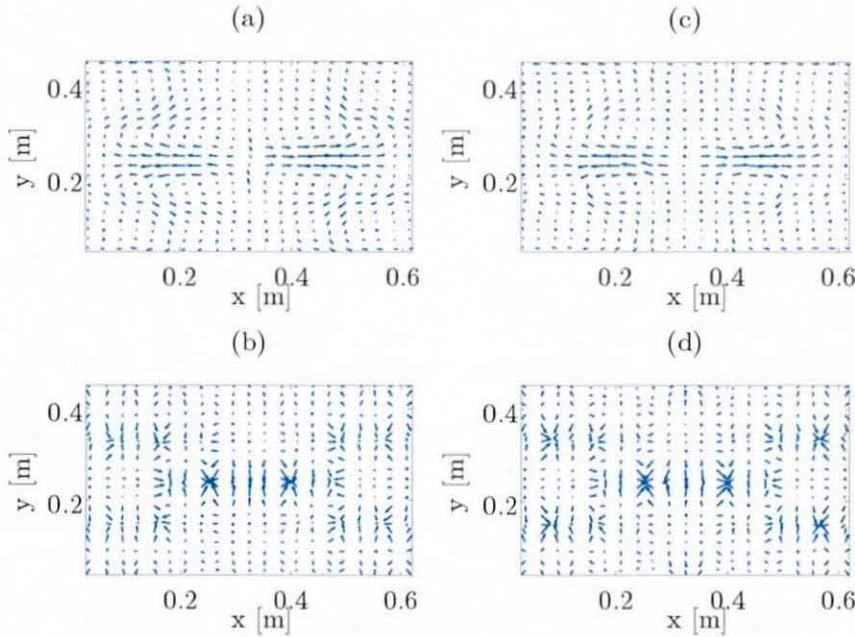


**Figure A32.5** Filtered VEF maps of the experimental, non-layer damped, simply supported plate at 2040.5 Hz & mode (9,5): (a) active ideal filtered, (b) reactive ideal filtered, (c) active Butterworth filtered, (d) reactive Butterworth filtered.

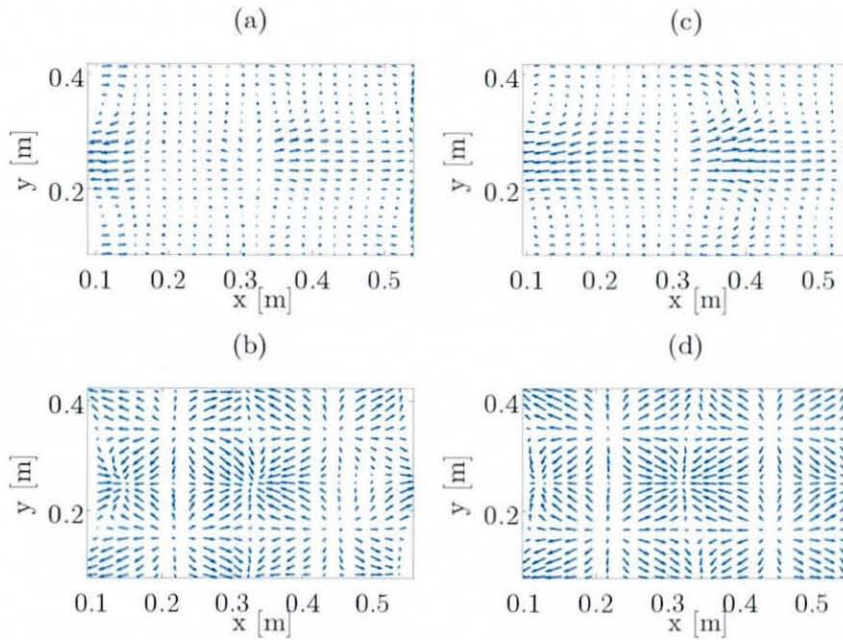


**Figure A32.6** Filtered VEF maps of the experimental single-layer damped, simply supported plate at 402 Hz & mode (3,3): (a) active ideal filtered, (b) reactive ideal filtered, (c) active Butterworth filtered, (d) reactive Butterworth filtered.

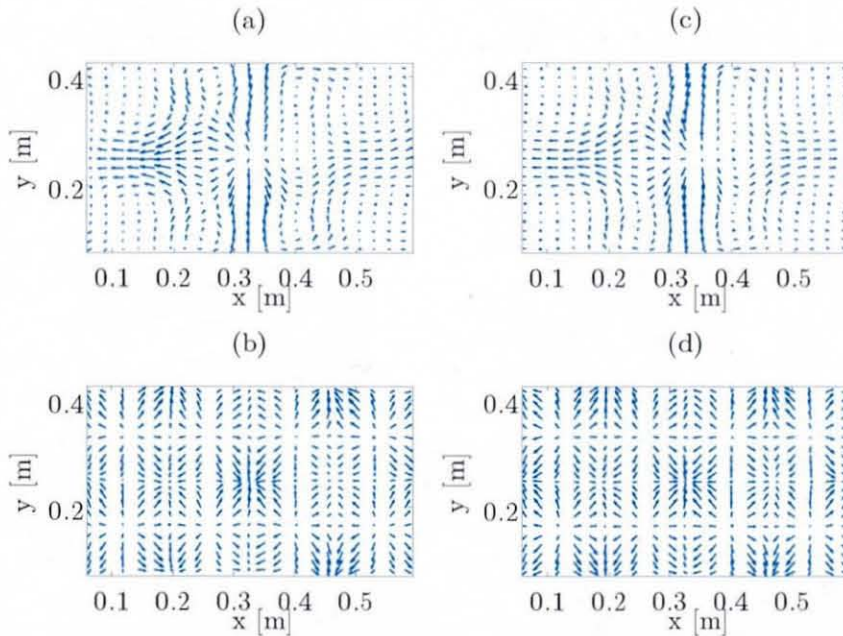


**Figure A32.7** Filtered VEF maps of the experimental, single-layer damped, simply supported plate at 658 Hz & mode (5,3): (a) active ideal filtered, (b) reactive ideal filtered, (c) active Butterworth filtered, (d) reactive Butterworth filtered.



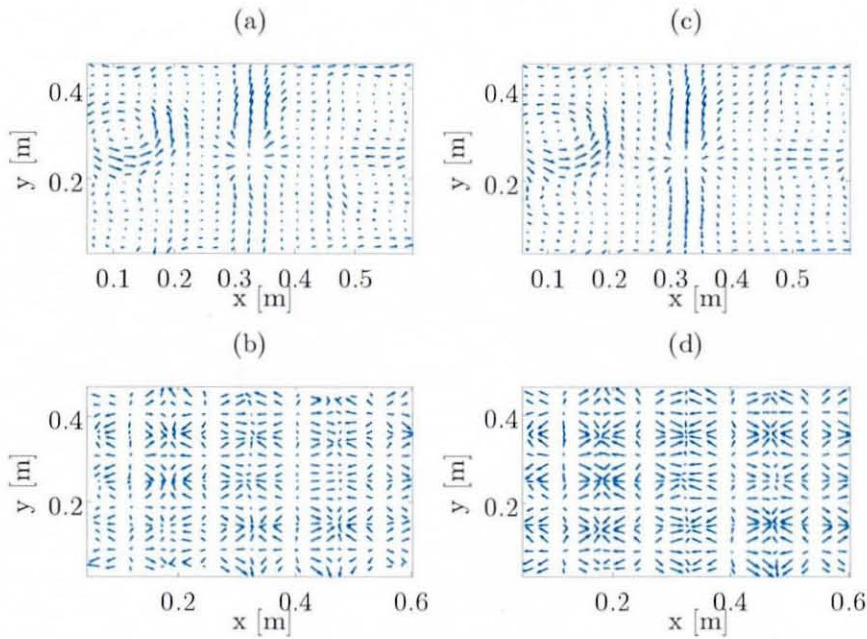


**Figure A32.8** Filtered VEF maps of the experimental single-layer damped, simply supported plate at 1086 Hz & mode (5,5): (a) active ideal filtered, (b) reactive ideal filtered, (c) active Butterworth filtered, (d) reactive Butterworth filtered.

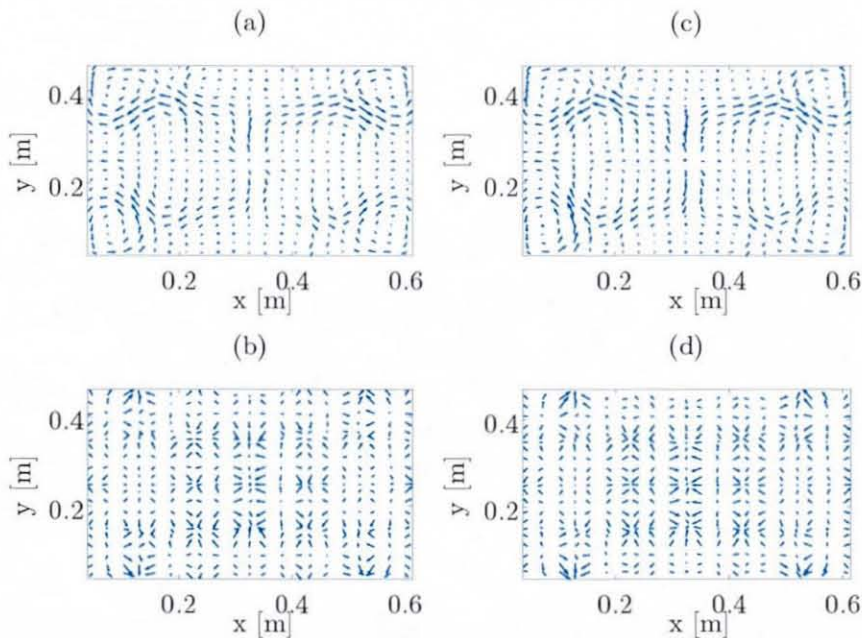


**Figure A32.9** Filtered VEF maps of the experimental, single-layer damped, simply supported plate at 1459 Hz & mode (7,5): (a) active ideal filtered, (b) reactive ideal filtered, (c) active Butterworth filtered, (d) reactive Butterworth filtered.

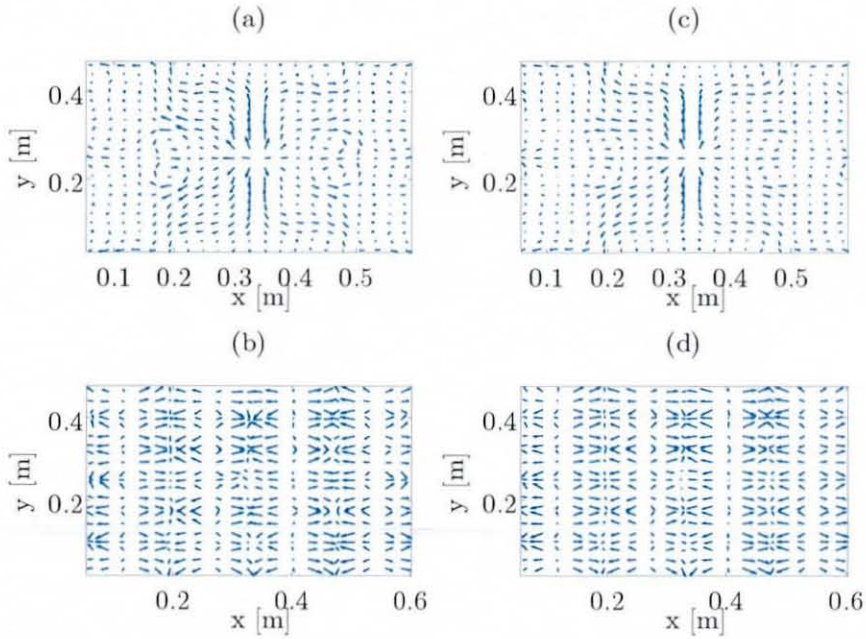


**Figure A32.10** Filtered VEF maps of the experimental single-layer damped, simply supported plate at 1716 Hz & mode (5,7): (a) active ideal filtered, (b) reactive ideal filtered, (c) active Butterworth filtered, (d) reactive Butterworth filtered.

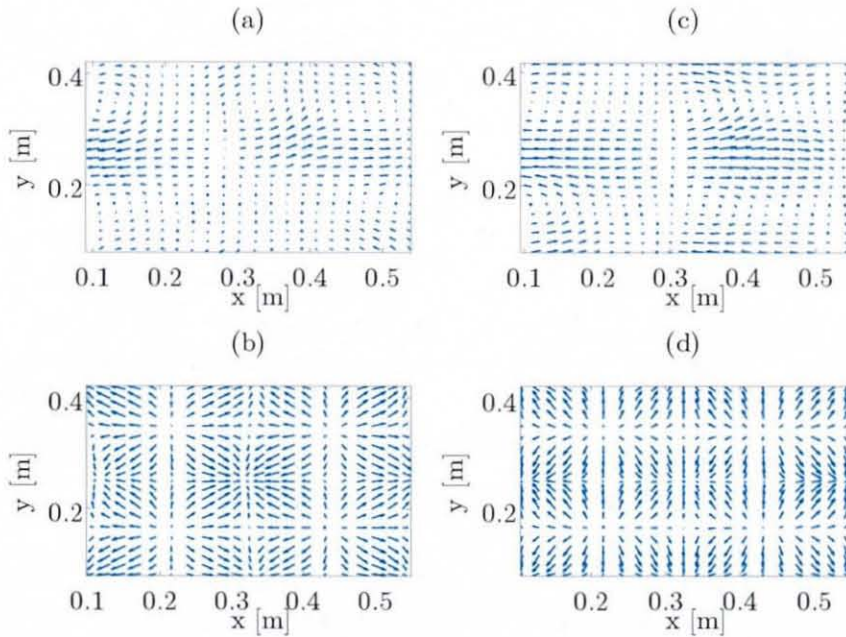


**Figure A32.11** VEF maps of the experimental, checkerboard-layer damped, simply supported plate at 404.5 Hz & mode (3,3): (a) active ideal filtered, (b) reactive ideal filtered, (c) active Butterworth filtered, (d) reactive Butterworth filtered.



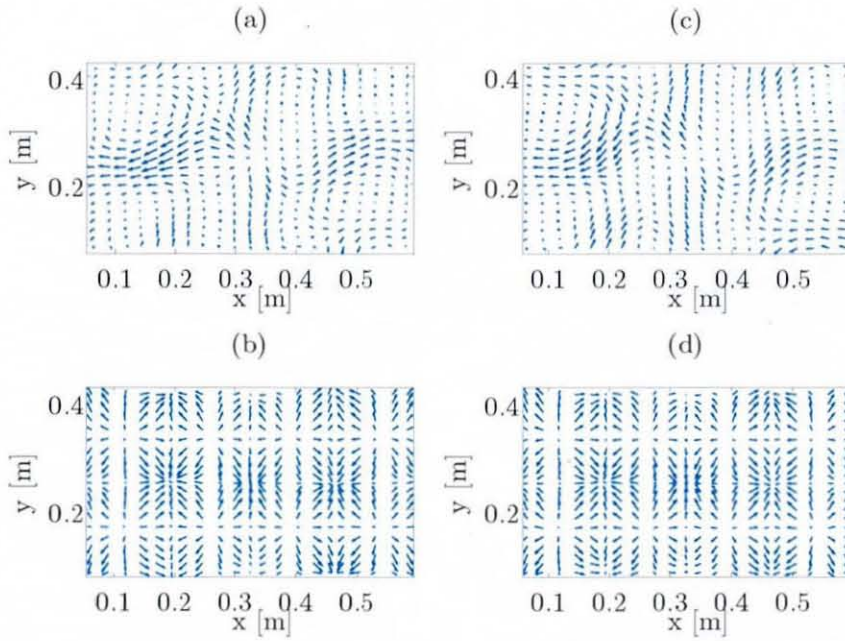


**Figure A32.12** VEF maps of the experimental, checkerboard-layer damped, simply supported plate at 669 Hz & mode (5,3): (a) active ideal filtered, (b) reactive ideal filtered, (c) active Butterworth filtered, (d) reactive Butterworth filtered.

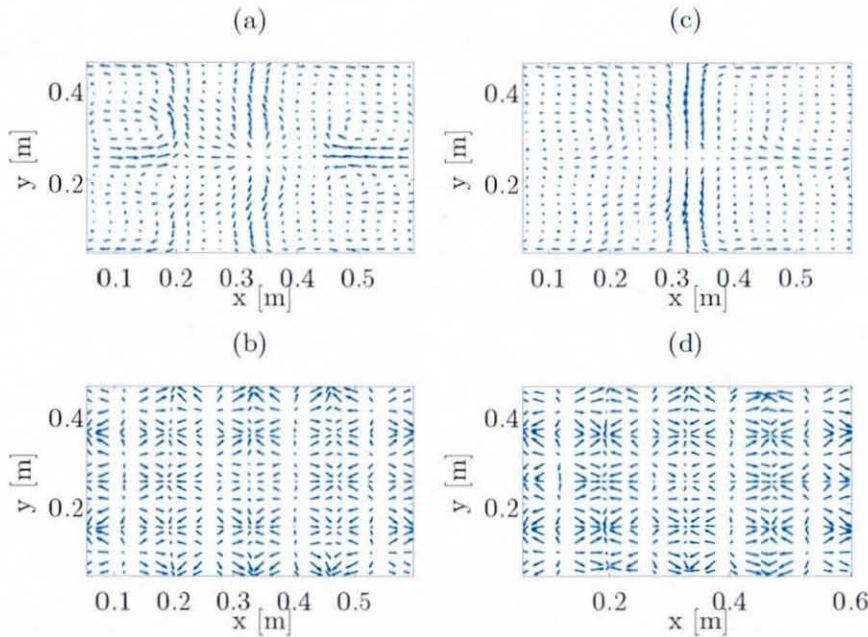


**Figure A32.13** VEF maps of the experimental, checkerboard-layer damped, simply supported plate at 1111.5 Hz & mode (5,5): (a) active ideal filtered, (b) reactive ideal filtered, (c) active Butterworth filtered, (d) reactive Butterworth filtered.

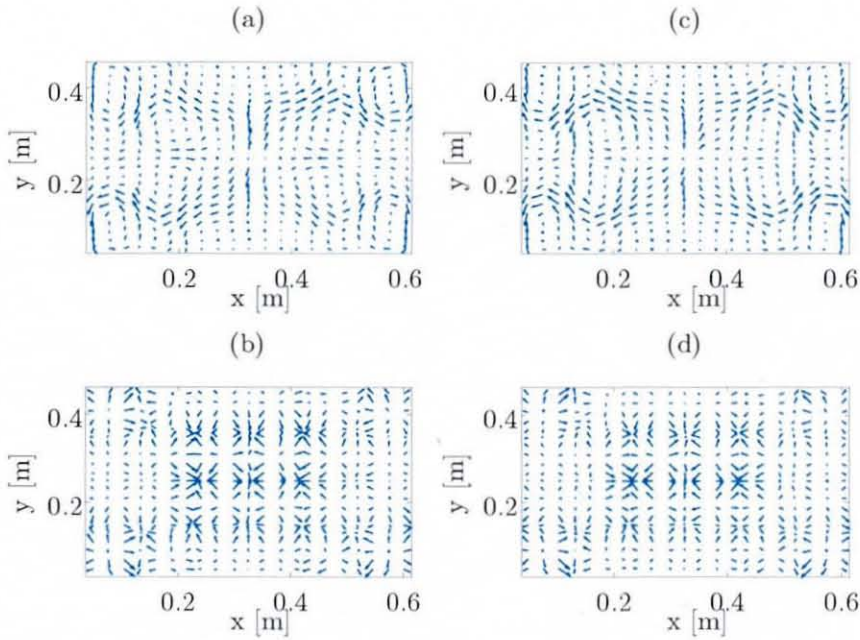


**Figure A32.14** VEF maps of the experimental, checkerboard-layer damped, simply supported plate at 1486.5 Hz & mode (7,5): (a) active ideal filtered, (b) reactive ideal filtered, (c) active Butterworth filtered, (d) reactive Butterworth filtered.

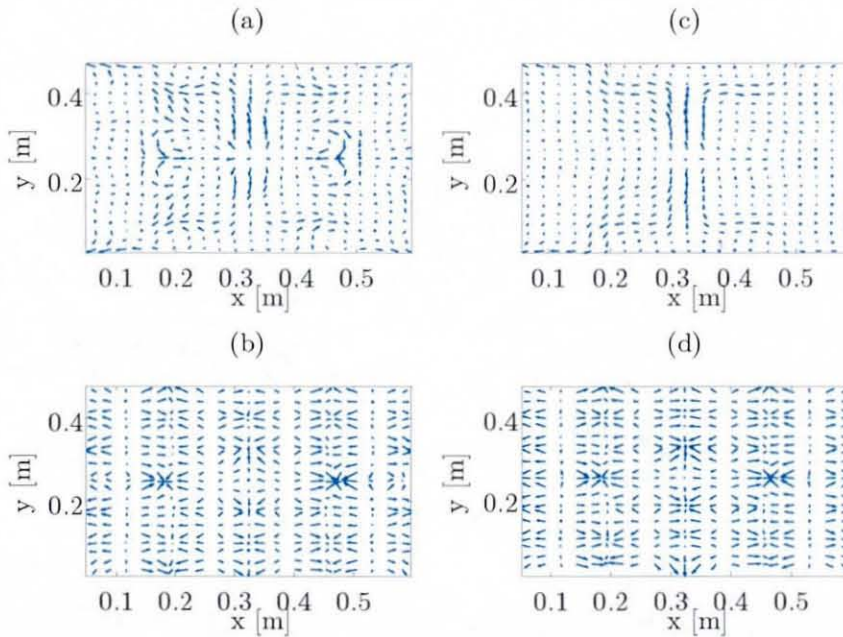


**Figure A32.15** VEF maps of the experimental, checkerboard-layer damped, simply supported plate at 1750 Hz & mode (5,7): (a) active ideal filtered, (b) reactive ideal filtered, (c) active Butterworth filtered, (d) reactive Butterworth filtered.

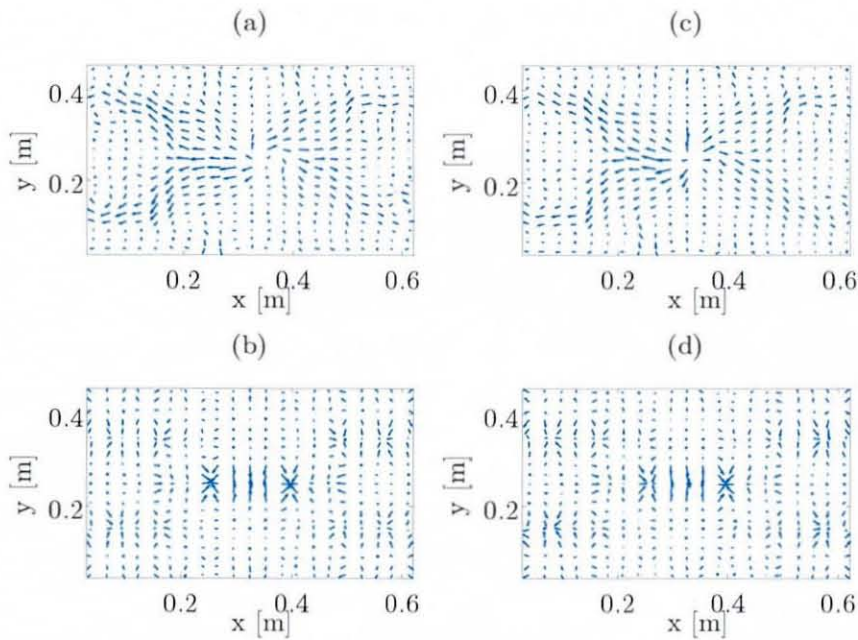


**Figure A32.16** VEF maps of the experimental, checkerboard-layer damped, simply supported plate at 2005.5 Hz & mode (9,5): (a) active ideal filtered, (b) reactive ideal filtered, (c) active Butterworth filtered, (d) reactive Butterworth filtered.



## Appendix A33

## Analytical Vibrational Energy Flow Maps of Simply Supported Plate

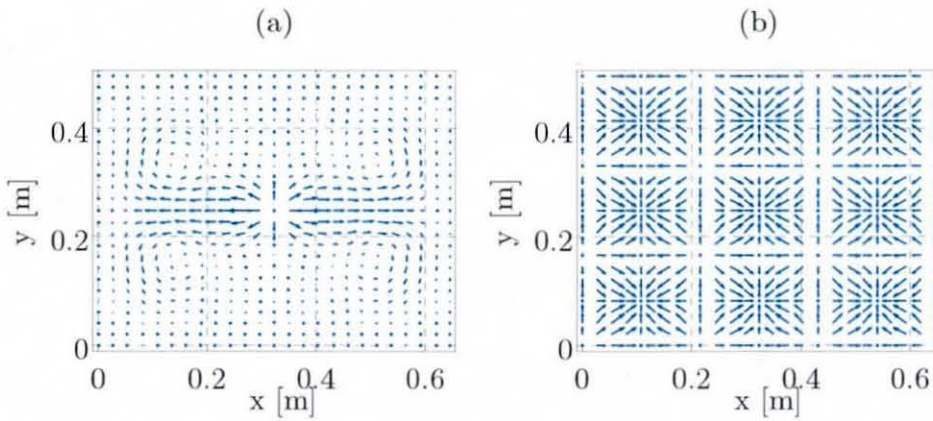


**Figure A33.1** Analytical VEF maps of the simply supported plate excited at mode (3,3): (a) active VEF, (b) reactive VEF.

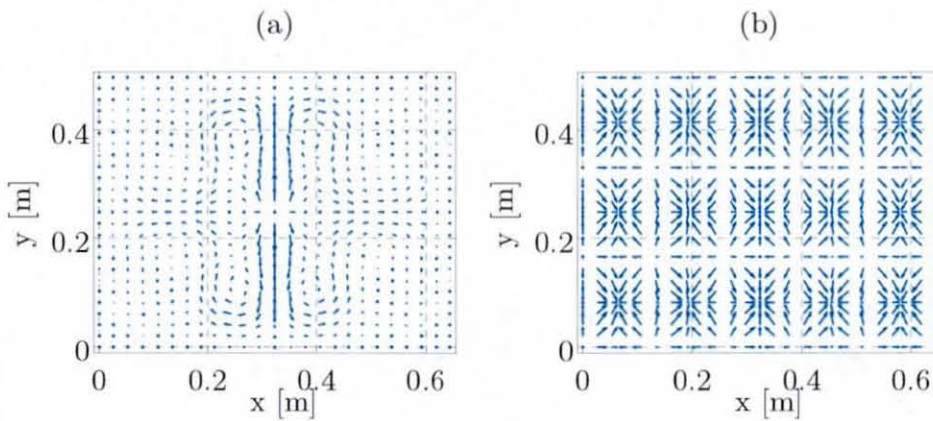


**Figure A33.2** Analytical VEF maps of the simply supported plate excited at mode (5,3): (a) active VEF, (b) reactive VEF.

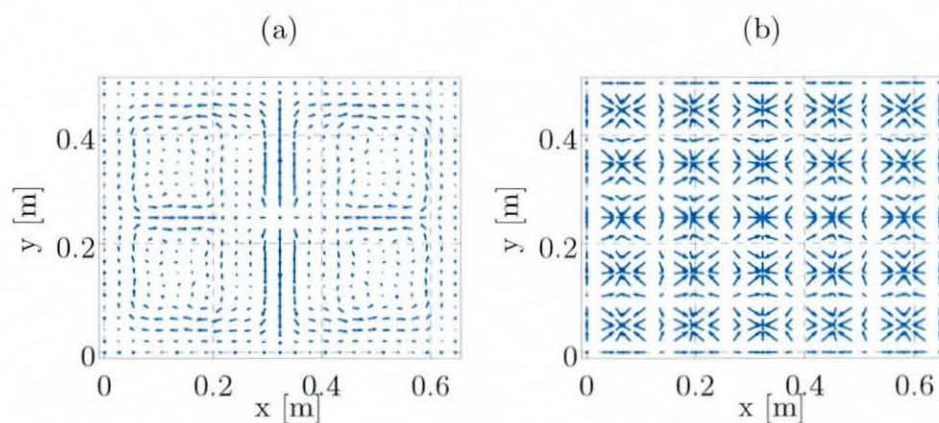


**Figure A33.3** Analytical VEF maps of the simply supported plate excited at mode (5,5): (a) active VEF, (b) reactive VEF.

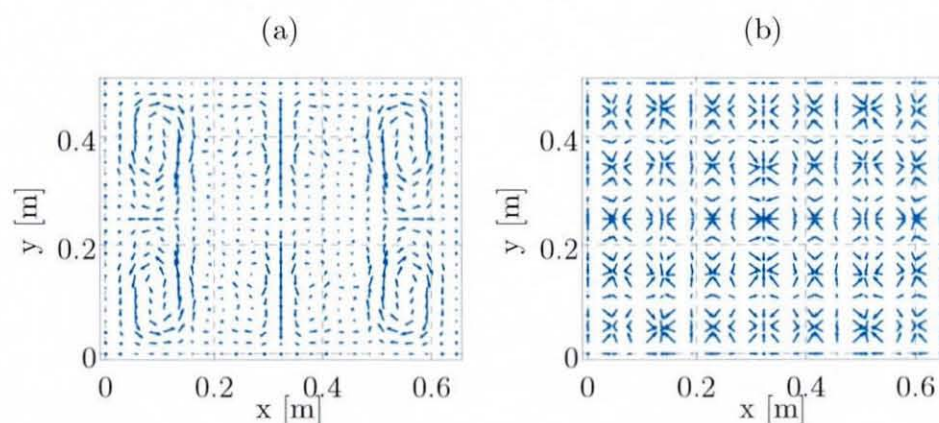


**Figure A33.4** Analytical VEF maps of the simply supported plate excited at mode (7,5): (a) active VEF, (b) reactive VEF.

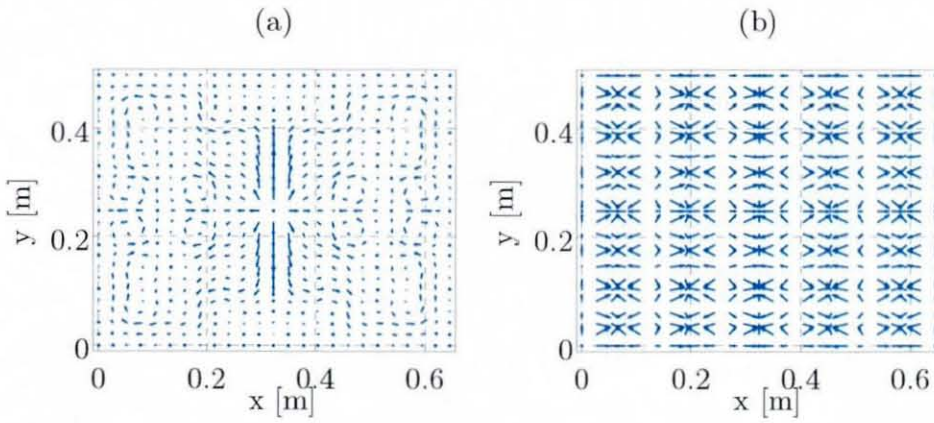


**Figure A33.5** Analytical VEF maps of the simply supported plate excited at mode (5,7): (a) active VEF, (b) reactive VEF.

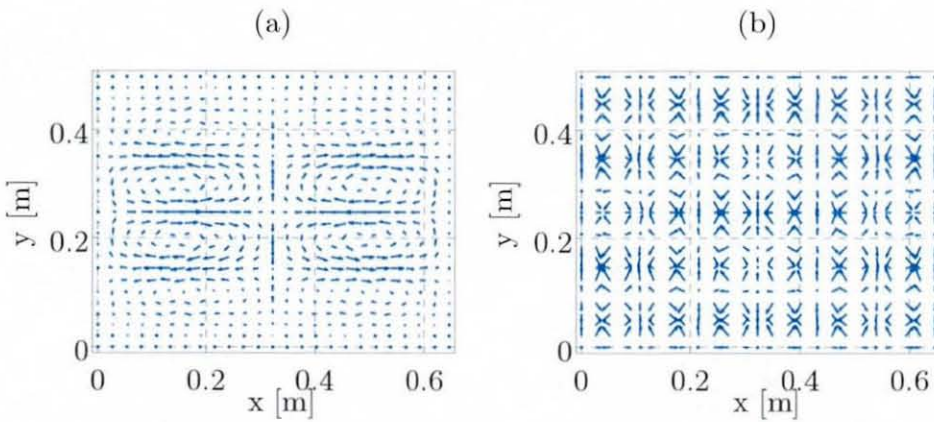


**Figure A33.6** Analytical VEF maps of the simply supported plate excited at mode (9,5): (a) active VEF, (b) reactive VEF.

